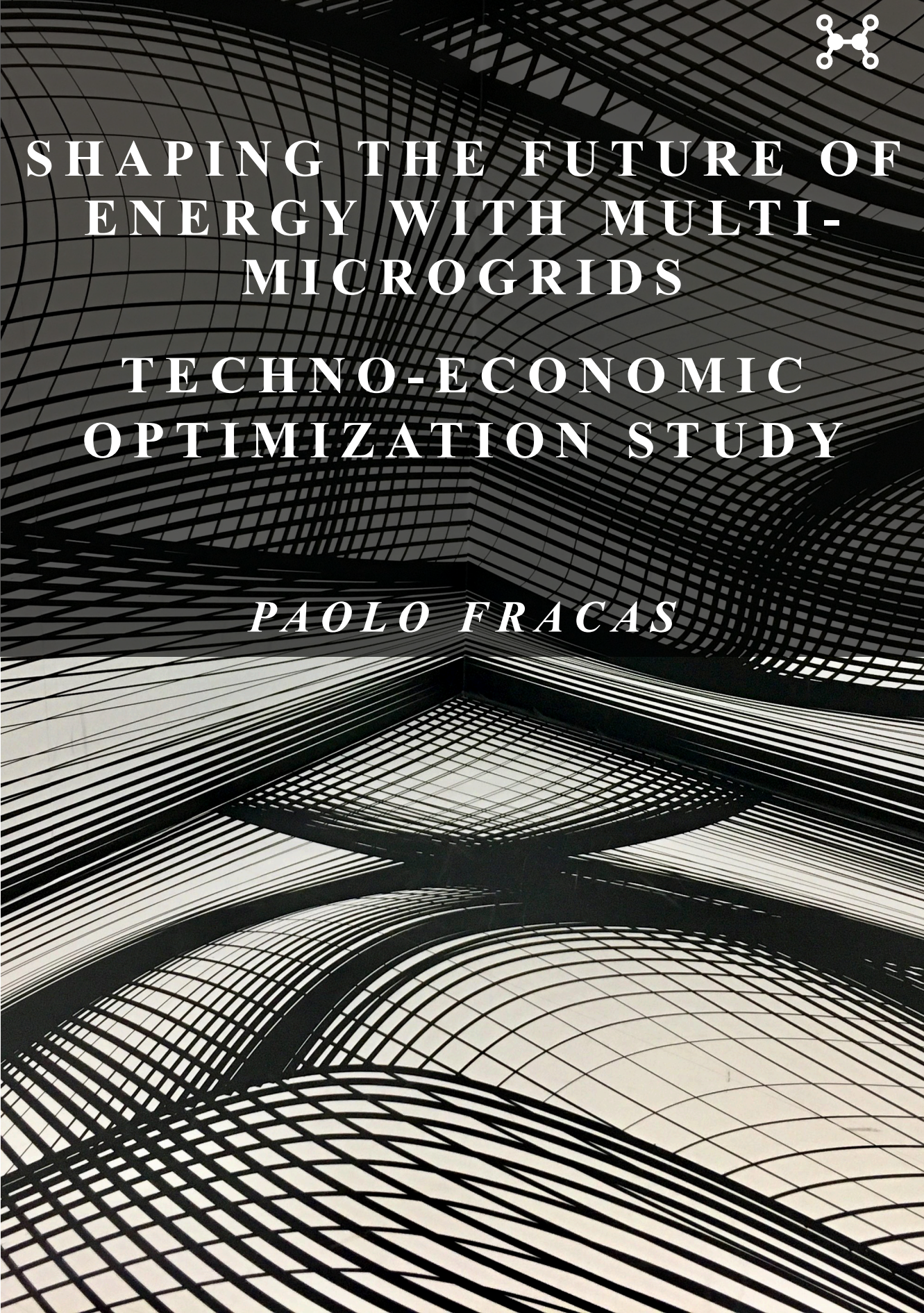

SHAPING THE FUTURE OF ENERGY WITH MULTI-MICROGRIDS

TECHNO-ECONOMIC OPTIMIZATION STUDY

PAOLO FRACAS

SHAPING THE FUTURE OF ENERGY WITH MULTI-MICROGRIDS

TECHNO-ECONOMIC OPTIMIZATION STUDY

DISSERTATION

to obtain
the degree of doctor at the Universiteit Twente,
on the authority of the rector magnificus,
prof. dr. ir. A. Veldkamp,
on account of the decision of the Doctorate Board
to be publicly defended
on Wednesday 23 February 2022 at 16.45 hours

by

Paolo Fracas

born on the 18th of November, 1964

in Genova, Italy

This dissertation has been approved by:

Supervisors

Prof. dr. ir. E. Zondervan

Prof. dr. ing. M.B. Franke

Cover design: Armand Khoury
Printed by: Gildeprint – The Netherlands
Lay-out: Paolo Fracas
ISBN: 978-90-365-5321-6
DOI: https://doi.org/10.3990/1.9789036553216

Graduation Committee:

Chairman/secretary:

Prof. dr. J.L. Herek

Supervisors:

Prof. dr. ir. E. Zondervan

Prof. dr. ing. M.B. Franke

Members:

Prof. dr. S.R.A. Kersten

Prof. dr. J.L. Hurink

Prof. J.G. Slootweg (Technische Universiteit Eindhoven)

Prof. K.V. Camarda (The University of Kansas)

Prof. Antonio Frisoli (Scuola Superiore Sant'Anna)

In whatever way we may define the concept of probability, or whatever axiomatic formulations we choose, probability statements will not be falsifiable.

Karl Popper, Logik der Forschung, 1935

Table of Contents

Summary

The world is currently facing massive energy- and dramatic environment challenges caused by global warming and increase in energy demand. The Intergovernmental Panel on Climate Change (IPCC) assessed in December 2019 that human activities have already caused approximately a global temperature increase of 1.0°C above the pre-industrial levels. A 1.5°C warmer world is more likely between 2030 and 2052, if business models and energy policies are not changing. Limiting global warming is mandatory to keep future health, livelihoods, food availability, water supply, human security, and economic growth and to reduce the risk of pandemics.

Through a tight integration of highly intermittent renewable distributed energy resources, the microgrid is the technology of choice to deliver the expected impacts, making clean energy affordable. The focus of this work lies on the techno-economic analysis of optimal combined heat and power multi-microgrids (CHP-MMG); a novel distribution system architecture with two interconnected microgrids. These are complex energy systems that have been only partially investigated. High computational resources are needed to find their optimal siting, design, and operations fitting the climate conditions of a geographical area. To this aim, a novel two-layer optimization framework is proposed to simultaneously solve the problem of finding their optimal design, sizing and siting (hereinafter referred as the setting of CHP-MMG) while the energy dispatch balance is achieved with minimal operational costs and highest revenues. At a lower level, a sequential least squares programming (SLSQP) method ensures that the stochastic generation and consumption of energy deriving from each CHP-MMG trial setting are balanced at each time-step. At the upper level, two novel multi-objective self-adaptive evolutionary algorithms are proposed to search the setting that returns the highest internal rate of return (IRR) and the lowest levelized cost of energy (LCOE) among the trial CHP-MMG settings. In the self-adaptive differential evolution (ADE) method, the trial setting is obtained by perturbing the target individual with the difference of random set of other individuals. To improve the search space, the values of the mutant and crossover factors are adapted based on the gradient of the fitness value. In the self-adaptive artificial immune evolutionary algorithm (AIE), the mutant is generated with a normal random distribution, driven by the diversity of population and fitness convergence. The crossover recombines genes of the mutant with pieces of external genotypes and of target setting by means of horizontal/vertical gene

transfer techniques. The test results demonstrate that AIE returns best-so-far fitness values (BSF) over 70% better than the original Differential Evolution (DE) algorithm.

The search of the best setting for a CHP-MMG is a stochastic problem. The two-layer optimization algorithm returns clusters of optima of similar quality. To find the best configuration, the optimization must be repeated until the distribution of fitness measures reaches the desired target. The solution associated to the lowest fitness value can be assumed as the candidate of being the best probabilistic solution. To verify whether the latter returns the best-expected performance over all the uncertain scenarios, the sample average approximation method is used.

The computing performance of the two-layer optimization tool has been further improved with multiple numerical approaches to reduce the overall time required for the computation tasks. The processing of the individuals has been distributed into computing elements working in parallel. Moreover, SLSQP optimization has been implemented to slice of datasets. Lastly, a machine learning algorithm based on linear regression and deep neural network methods replaced the analytical techno-economic model for preliminary optimal searches.

Finally, the optimization algorithm has been used to investigate different scenarios for in Northern and Southern Europe. The impact of price policies, cost of fuels on IRR, LCOE, and quality of energy has been analyzed. The hydrogen cost fixed at 3 €/kg makes fuel cells the main choice of electricity. Whenever the cost rises, the main grid turns into the principal supplier of heat. High fuel costs cause a substantial increment of the wind turbines (WT) followed by photovoltaic panels (PV). In Northern Europe where wind conditions are favorables, an optimal CHP-MMG comprises a WT coupled with fuel cells (FC), making energy at low cost and the return of the investment attractive with the delivery of energy services to the main grid. Thermal energy is generated with heat pumps and exchanged between the CHP-MMG. Similarly, in Southern Europe the best configurations are obtained with PV combined with WT, FC and the main grid. The latter is used to provide energy services. The techno-economic scenarios dealing with off-grid supply have demonstrated that optimal CHP-MMG configurations still return an attractive IRR (i.e., 24%) with electricity tariff similar to those applied today by the utility. Further optimizations have considered on-site blue-hydrogen generation by thermal plasma methane decomposition. The outcomes have shown that this bridging technology can still make CHP-MMG profitable. Moreover, the

simulations have brought out a scheme of collaboration among CHP-MMG (i.e.,'swarm effect') that improves the overall efficiency and response to the uncertainty of renewable energy.

This work demonstrates the versatility of CHP-MMG technology. The results show that at each latitude and longitude, with different input settings, there are always optimal configurations to supply good quality of energy and provide attractive financial performances.

To conclude, the innovation contents of the thesis comprise:

- A novel simulation-optimization tool designed to simultaneously determine under realistic operating conditions: 1) the design, 2) the sizing, 3) the siting, 4) the operation optimizations of two interconnected heat and power microgrids (appendix C).
- A two-layer optimization algorithm combining a novel evolutionary computing method with SLSQP to improve the quality of the results and the solution space search (Chapters 1,2,4).
- A method to find global solutions over the most probable scenarios (Chapters 4,5).
- Four different approaches based on an analytical technical-economic and complementary machine learning models to describe the stochastic problem (Chapters 2,3).

The latter have addressed the need of the high computing resource required to investigate:

- How the new small energy system framework comprising two interconnected heat and power microgrids fulfill energy demand of both thermal and electric loads, provides energy services to utility grids with different price policies, cost and type of hydrogen (Chapters 2,4,6).
- The beneficial effect induced by the collaboration scheme between the two interconnected heat and power microgrids (i.e., swarm effect) fostering: 1) the overall efficiency, 2) the response to uncertainty, and consequently 3) the best financial performances over the most probable scenarios (Chapters 1,2,4,6).

Acknowledgements

The idea for this scientific work arises in the mature stage of my professional life.

The PhD gave me the opportunity to experiment how to combine ‘knowledge by facts’ with rigorous ‘scientific method’ for overcoming uncertain complex situations.

Before applying, I was not completely confident that I could afford this challenge. To turn back in the role of being a student is not easy at all. Since the first meeting, I understood that I could rely on Prof. dr. ir. Edwin Zondervan. Our meeting and conversations where we shared ideas, discussed results, contributed not only to enrich my knowledge but also to provide invaluable insights. I wish to deeply thank him for the confidence in me and for his invaluable support. He has fundamentally changed my thinking about science.

I am grateful to Prof. dr. ing. Meik Franke for accepting the supervision in the latest phase of the thesis. His advices have been very valuable to strengthen the work. I also want to thank Prof. Kyle V. Camarda, for our brief but fruitful discussions about optimizations at ESCAPE 2019 in Eindhoven. Our conversations during launch-break have been inspirational in many ways.

I wish to deeply thank Prof. Antonio Frisoli of the Scuola Superiore Sant’Anna for his support and valuable suggestions in the final rephrasing of the Thesis and Prof. Remo Proietti Zaccaria of the Italian Institute of Technology. Our long and fruitful collaboration in research projects and the Chinese experience was further enriched by his advice in this work.

This journey would not have been possible without the dedicated support of my wife, Michela. Her tireless and care for the family over the past three years has made this endeavor possible. Her encouragement has been once again determinant. She contributed with a different but equally valuable humanistic perspective to my work. I dedicate this work also to my daughter Emma, my son Filippo.

Finally, I would like to remember my beloved brother ing. Serafino Fracas for his continuous support during the last mile of his life.

CHAPTER 1: Introduction

As energy and environmental sustainability is becoming increasingly prominent, achieving a low-carbon economy is the global priority. The current energy system is economically inefficient to deliver a climate-neutral economy and too rigid for a massive penetration of renewables. Fortunately, cost-effective IT infrastructures and communication technologies, are boosting the connectivity of distributed renewable energy resources into peer-to-peer power systems. A new paradigm of energy produced in small and smart independent energy networks is now emerging, namely the microgrid. This energy system integrates the generation, transmission, distribution and consumption of energy as a whole, providing an intelligent optimal interaction among all nodes of the system. The microgrid is a groundbreaking technology that enables scalable and thus, more economic and affordable financial investments. Combined heat and power multi-microgrids strengthen the distributed technology concept with a tight, more effective integration of energy devices. This chapter introduces the multi-microgrid technology and the challenges to achieve a competitive design and optimized operation. A review of the state-of-art related to the simulation and optimization tools is provided. The rational for the use and development of computer-based tools is discussed. The chapter ends with the research topics undertaken in this work for the optimal design and operations of combined heat and power interconnected microgrids.

1.1 The microgrids

In his famous book published in 2019, J. Rifkin [1] addressed the need for urgently setting a new agenda to confront the climate change, to transform the economy, and to create a green post-fossil fuel culture. One year earlier (2018), K. Kotilainen et al. [2] analyzed the new energy contest and the drivers that are profoundly changing the way energy is produced and delivered.
Further economic studies [3] revealed a new emerging actor within the business community that in forthcoming years will shake the very foundation of the global economy, leading to a revolution in the energy sector: the prosumer.

The prosumer is defined as a sort of consumer that: 1) actively participates in the efficient, sustainable peer-to-peer production, 2) uses renewable energy, and 3) delivers demand response services [4] through small-scale distributed energy systems. The integration of renewable energy systems (RES) such as wind turbine and solar panels, distributed generation (DG) together with energy storage can potentially reduce the carbon emissions, improve the power reliability, and the energy efficiency. However, the peer-to-peer matching of unpredictable load variation with the large degree of intermittency caused by weather, day-night cycles and seasons of renewable energy is a new challenge for grid operation and control. This challenge can be effectively addressed by microgrids (MG).

The definition of a MG depends on the perspective. According to the U.S. Department of Energy (DoE) a microgrid represents “a group of interconnected loads and distributed energy resources (DER) within clearly defined electrical boundaries that acts as a single controllable entity with respect to the grid” and “can connect and disconnect from the grid to operate either in grid-connected or island-mode.” A remote microgrid is a variation of a microgrid that operates in islanded conditions.

Among the new technology for energy production and harvesting, microgrids are unanimously recognized as a key technology capable of boosting the new paradigm of energy, once favorable policies for distributed energy systems are set, legal obstructions and transaction costs for peer-to-peer are removed and coproduction is fostered [5].

The core component of a microgrid is the DG, a small electric- and thermal power generator independent of traditional utility grids, which is located at the end-user side to meet his/her unique demand.

The other important component of a microgrid is the so-called distributed resource (DR) which refers to a combined DG and energy storage system (ES). In multi-microgrid architectures forming a grid of microgrids, DR are also the devices for the electrical (ITCEL) and thermal interconnection (ITCTH) between nearby MG, or to a utility grid (GRID) to which prosumers can sell surplus power. As shown in Figure 1.1,

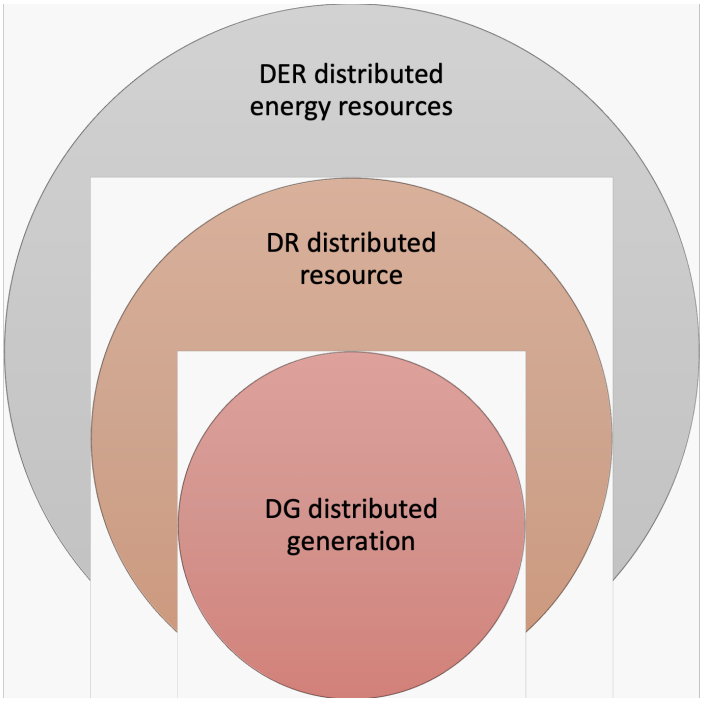

Figure 1.1 *Subsets of DER in a microgrid*

it can be inferred that the DG is a subset of the DR, which is then a subset of the DER.

The DG and ES are usually directly connected to the user side in parallel and are managed by the microgrid control center (MGCC). The microgrid control center is the core of the MG control system. In addition to the supervision, the MGCC optimizes the control strategy based on the actual operating conditions to ensure smooth transfer between grid connection, islanding, shutdown, and startup of DG. In grid-connected operation, MGCC also provides the microgrid and the best DR performance. In islanded mode, it adjusts the DG outputs and load consumption to secure stable, safe operation of the microgrid, at the most economic conditions.

When thermal and electric DER are both incorporated in the same MG, it becomes a combined heat and power microgrid (CHP-MG). The latter can be interconnected to make a cluster of microgrids, in which each system benefits from this cooperation during grid-connected and islanded modes. Clusters of hybrid microgrids are hereafter indicated as: combined heat and power multi-microgrid (CHP-MMG). Figure 1.2 shows the general layout of a cluster made by two CHP-MMG.

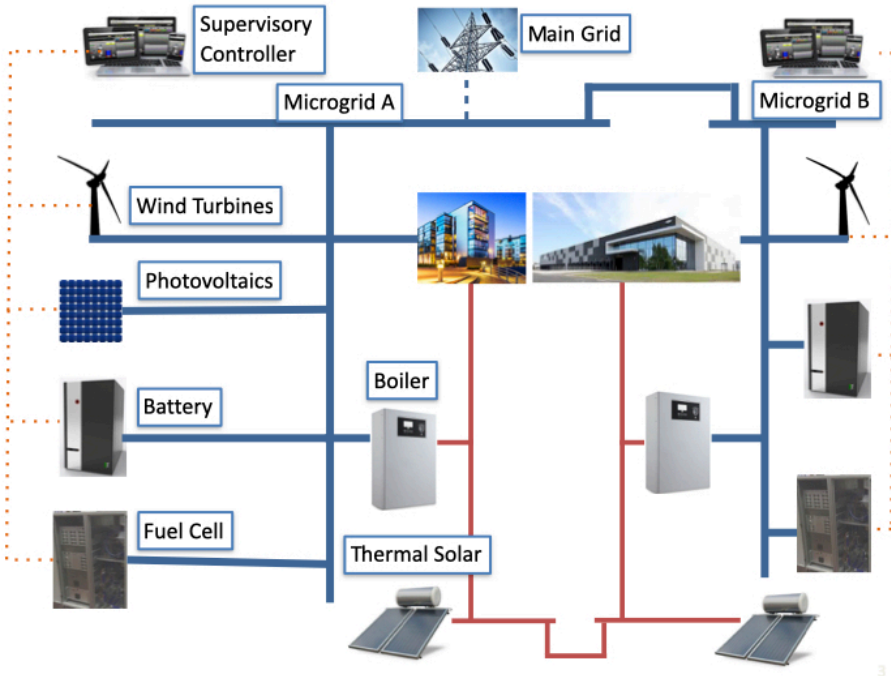

Figure 1.2 *Layout of two interconnected heat and power microgrids*

MG are capable of autonomous control, protection, and management. MG can operate either in parallel with the utility grid (on-grid) or in an intentional islanded mode (off-grid). While centralized traditional power generation systems bring energy flow only in one direction (from large synchronous generators through a transmission/ distribution network to end-users), the MG is a small electric power system that incorporates peer-to-peer nodes with distributed generation, transmission, and distribution at a single layer.

MG can achieve power balance and optimal energy allocation over a given area and act as a virtual power source in a distribution network. Compared with traditional

vertical transmission- and distribution networks, MG has a much more flexible structure. It can be defined more generally as a medium-or low distribution grid. Based on the type of source that is managed, MG can be classified as 1) direct current line (DC), 2) alternating current line (AC), or 3) hybrid (AD/DC) as shown in Figure 1.3.

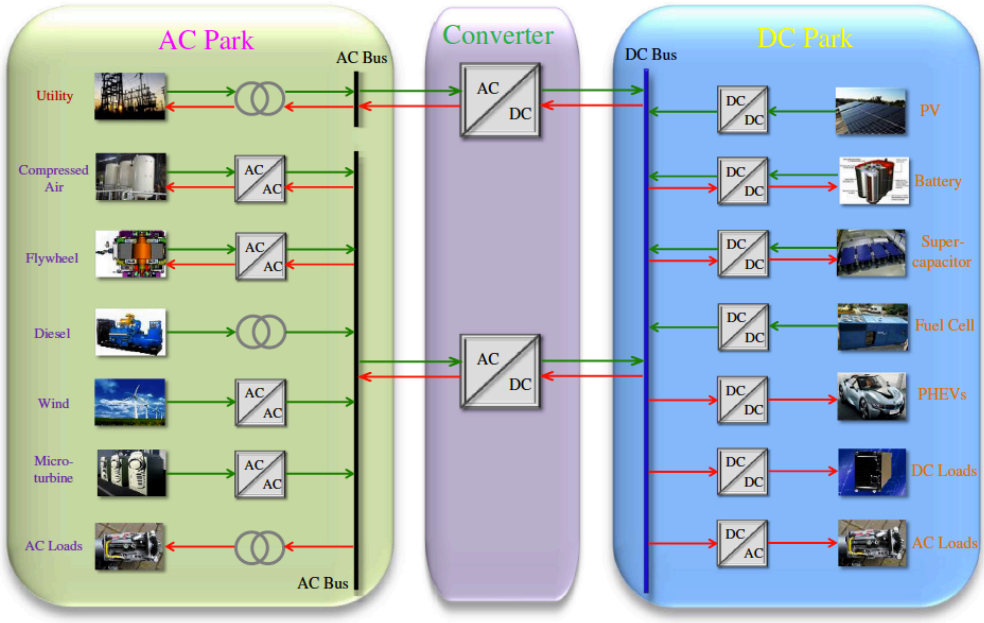

Figure 1.3 *Typical layout of a microgrid incorporating both AC and DC DER*

In a microgrid, it is essential to continuously balance the power supply with the demand, because the generation of the intermittent distributed sources is difficult to precisely predict and the actual available power fluctuates significantly, depending on the availability of the primary sources (solar irradiation and wind).

The balancing of supply and demand becomes even more critical in an islanding microgrid, as only the internal supply is available to balance the demand.

1.1.2 Clusters of microgrids

The concept of MG can be extended to a larger scale, in which two or more MG operate interconnected with each other to form a cluster of controllable MG. To mitigate the unstable operation of individual MG during islanded operation the interconnection of multiple MG (MMG) has been proposed as a viable solution providing numerous

economic benefits to both the utility grid and the MG systems participating in the network.

Interconnected MG can take advantage of the increased reliability and stability, enhanced security and reduced costs associated with the cooperation of multiple MG. During a blackout of the utility grid, individual MG may fail to deliver a reliable and stable power supply to the critical loads due to the high penetration of non-controllable and weather-dependent RES. This can be overcome by interconnecting multiple MG systems and enabling them to support each other by sharing resources.

An enhanced solution of clusters of microgrids is represented by CHP-MMG. In such hybrid configuration, the MG have several options for an optimal management of the abundant energy that is available in a certain time: 1) it can storage the abundant energy (e.g., electricity with batteries, heat with tanks of water, hydrogen with pressurized canisters) 2) it can supply their excess of energy to the loads of the nearby MG lacking in generation 3) it can convert abundant energy (e.g., electricity to heat with heat pumps, hydrogen with electrolyzers), 4) it can exchange the abundant energy (e.g., to the utility grid or to another MG for delivering demand response services).

However, the coupling of multiple systems on both grid-connected and islanded MG requires accurate techno-economic investigations to search the optimal: 1) architectures; 2) size of the distributed energy resources; 3) siting; 4) energy-management strategies 5) energy-trading techniques, ensuring a cost effective, reliable operation.

Currently, the study of microgrid clustering architecture and control strategies were mostly oriented to a few electrical configurations [6]. The “Parallel Connected Microgrids” (PCM) with an external grid layout, that is represented in Figure 1.4(a), refers to a structure in which all microgrids are connected to the same external grid, where each microgrid has only one point of common coupling (PCC). These points are the interconnections with other grids.

In the "Grid of Series of Interconnected Microgrids” (GSIM), which is shown in Figure 1.4(b), the microgrids are interconnected forming a grid, where the interconnections are based on the point-to-point structure.

The management of MG clustering frameworks has been extensively discussed and several energy-management frameworks have been proposed in the literature [7].

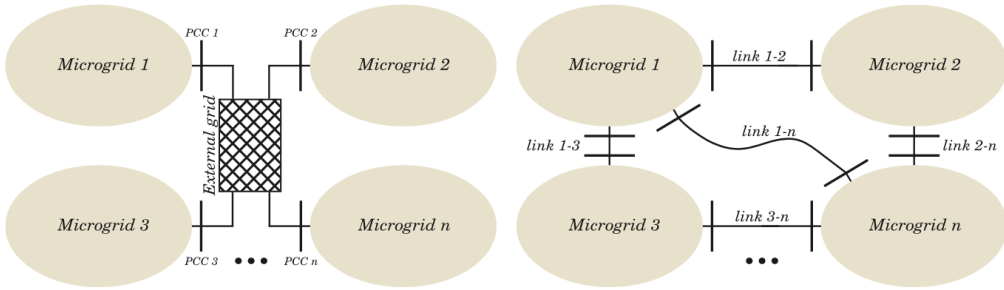

Figure 1.4 *Example of microgrids architectures: a) Parallel connect microgrid with an external grid; b) Grid of series of interconnected microgrid (Bullich-Massagué, Díaz-González et al. 2018).*

However, the research presented in the literature mainly focuses on the control and energy management of MG clusters, with various control strategies and algorithms being proposed to guarantee the optimal operation and economic feasibility of the system. These control strategies can follow centralized, decentralized, and distributed architectures or can be implemented in layers with different tasks and goals through a hierarchical architecture.

Multi-agent technology and system-of-systems structures have also been proposed in the literature for the control and energy management of multiple MG systems. The study carried out by F. Bandeiras et al. in 2020 [8] has addressed the cooperation of five industrial MG operating in islanded mode. An algorithm has been developed to evaluate the cooperation among these MG and coordinate their hourly energy trade through three distinct market models with market clearing price/quantity in asymmetric pool.

Studies and works that treat in detail the overall optimal best design, sizing, and siting of CHP-MMG in combination with optimal management however, are still missing.

1.1.3 Applications of microgrids

Community, industry, commerce, military, remote off-grid units, and university campuses are typical applications of MG, where the aggregation of on-site generation with multiple loads displaced in tight geography allow the owner to determine how to manage them.

In the first quarter of 2020, Guidehouse Insights identified 6610 MG projects which have been proposed, planned, and deployed around the world, representing a combined installed power capacity of around 31.8 GW [9].

Microgrids are becoming increasingly popular in North America where about 34% of the current world's microgrid installations are located. Here, the drivers for this rapid growth include the aging mega grid and the end-user's increasing desire for greater security and reliability (A. Wilson et al., 2017) [10]. Besides the North America, microgrid projects are expanding rapidly to other regions of the world, especially in Asia Pacific region, which takes about 40% of the world total microgrid capacity.

Various policies drive microgrid development in different countries and regions. In the EU, microgrid development is accompanied by a comprehensive R&D effort that is supported by a series of EU's Framework Programs (J.Romankiewicz et al., 2013) [11]. Here, demonstration projects are executed with focus on island and remote microgrid systems, utility scale multi-microgrids, and microgrid control and operation.

In Asia, Japan is a leader in microgrid research. The New Energy and Industrial Technology Development Organization (NEDO) has funded many microgrid research and demonstration projects around the world (T. S. Ustun et al., 2011) [12]. The goals of these demonstration projects are often related with alternative new energy solutions, new technologies, and controls for better reliability and resilience. Japan's demonstration projects show excellent performance during natural disasters, particularly the successful operation the Sendai Microgrid after the "3-11 Great Easter Japan Sumani" (K. Hirose (2013) [13].

China started its microgrid development through the 12th Five Year Plan (FYP, from 2011 to 2015). The primary goal was to find a distributed clean energy way which could relieve China's dependence on centralized coal power and provide low emission and good air quality to the atmosphere. Chinese central government had a target to build 30 MG pilots projects in the 12th five-years plan (FYP) and this work is further extended to

the 13th FYP (from 2015 to 2020). MG Pilots was turning towards integrating renewable energy and energy storage on the demand-side or on the grid side, in many cases linked to electric vehicle charging. In China MG are distinguished in island, remote and city microgrids. For each category, applicable energy system configurations are recommended [14]. China views MG infrastructure as a strategic evolution of the power sector. MG is expected to be an integral aspect of the 14th FYP for energy [15].

1.1.4 Current challenges in modeling and optimization of microgrids

A strategic interest of the stakeholders involved in the energy value chain is the choice of the optimal combination of technologies, operations, location of MG that are best suited to provide the energy services needed at the most economic conditions.

Finding a solution to this challenge - for investors - means to determine the capital expenditures, operational costs, and revenues streams returning the most attractive payback and return of investment (e.g., IRR) over different options and scenarios. Users desire to satisfy their energy demand with inexpensive and reliable services. Energy providers (e.g., producers and distributors) aim to predict and correctly balance the energy demand and fulfill the users at lowest cost. Simulation and optimization tools are essential to find best solutions to these requests.

There are further issues that must be considered in the design of MG; the long lifetime of installations (typically more than 20 years) may cause lock-in situations due to high exit barriers; the rapid development of novel technologies can have far-reaching impacts on the system, so possible effects should be anticipated.

A large number of simulation and optimization tools have been developed by the scientific community over the previous decades due to the complexity of MG and the multiple challenging requirements.

The choice of type and size of DER and their geographical site have a great impact on the economic and technical performance of MG (e.g., MG in a windy island of North Europe with only PV as primary energy generator, will probably bring higher cost and less reliability than MG based on WT as primary energy generator). The minimum cost of energy, the highest profitability, the highest power quality must be achieved by matching the uncertainty of RES availability, the variability of the load profile.

The type of DG impacts on the MG's operation, lifetime and efficiency. An example of this is when the energy demand of a household is fulfilled by a PV that is interconnected uniquely with an ES. The latter will be cycled frequently and consequently its lifetime will be affected. Moreover, a power outage may occur if the ES is not properly sized or combined with a genset.

The same load profile can be met by integrating different combinations of DER. Since the energy flows of each configuration are different, the operating costs will be different and consequently the financial performance will be affected.

To identify the configuration that delivers the best value, it is necessary to calculate the energy flows involved among DG and the loads. Lastly, the total cost of ownership can be estimated. This computational analysis must be accomplished for each MG configuration. Via such calculations, the quality of the energy balance, the amount of the total cost of ownership (sum of initial costs and operating costs) can be determined. Hence, the configuration which satisfies the requirements will be identified. In case of 20 years of installation, the energy balance equations, and the subsequent financial models, need to be solved 175200 times (i.e., 20 times 8760 time-step/year). If 1000 different combinations of DER are analyzed, more than 170 million calculations are required. A computer-based simulator can reproduce the behaviour of MG using mathematical models. The latter can solve the energy balance equations and perform a cost analysis for long times period and a large number of combinations of DER units precisely in a very short time. This is the most effective approach to predict complex scenarios and identify the optimal one.

1.2 State of the art

1.2.1 State-of-art of simulation and optimization tools

Modeling, simulation and optimization of energy system have different scopes – both conceptually and computationally. In modeling the corresponding sets of inputs (e.g., size of DER) and outputs are known (e.g., total cost of ownership of energy generated by DER), and a relationship is sought that delivers the correct output for each known input. The latter is a system identification problem.

In simulation, the system model inputs are known, and in relation to these, the outputs are computed (e.g., simulate the energy flows each time-step). Each component of the energy system is represented in the model, and the scope of the simulation is to analyze the throughput of the system. In optimization, the model is known, together with the desired output, and the task is to find the input(s) leading to this output so that a given objective is minimized or maximized (e.g., find the best set of DER to obtain full energy balance at minimum costs). Optimization and modeling problems can be seen as search methods, but this is not the case for simulation problems. This view naturally leads to the concept of a search space, being the collection of all objects of interest including the solution we are seeking. The search space consists of all possible inputs to a model (optimization problems), or all possible computational models that describe the phenomenon we are studying (modeling problems). In simulation, there is no overall objective, as optimization only occurs at the component level; i.e., a simulation may not deliver the optimum solution, for instance when the heuristics of two components are contradictory. Simulations with pre-defined control strategies are useful to assess existing technologies, but they do not provide insight into the best way to operate or design a system. Additionally, simulations are used to predict dynamic behavior of its components (A.E. Eiben et al., 2015) [16].

For several years, techno-economic assessments of DER's compositions aggregated in microgrids, have attracted a lot of attention. The focus of the research was on the simulation of demand-response scenarios, impact analysis of policies in different configurations and sites. Other studies covered the optimal microgrids design and optimization problems of energy balance subjected to the minimization of energy costs. Scopus, the source-neutral abstract, and citation database, returns almost 16000 documents related to these topics.

In parallel to the latter research, a great effort has been directed to the advancement of microgrid modeling and optimizations algorithms to give to system developers an increasingly effective support to MG design decisions and operational constraints. Four types of optimization can be performed in energy systems: 1) optimization of operation, 2) system design optimization, 3) optimization of location, and 4) system evolution optimization.

In the first type of optimization, the power generation equipment is fixed, but the dispatch is optimized to minimize energy consumption, rejected nonrecoverable heat or

entropy production as well as a maximization of the useful effect (M. Blaise el al., 2018) [17]. The second optimization aims at searching the optimal set of components and their optimal operation (Frangopoulos, C. A., 2003) [18]. The third type of optimization searches the best geolocation of a well-defined MG configuration. The fourth optimizes the overall design of a system (H. Aki et al. in 2005) [19] taking into account influence of the change in conditions (i.e., shift in electric, gas tariff) to manage in a prospective installation over the long-term, including the decommissioning and infrastructure. Operations are usually not in the scope of the system evolution optimization model.

In the past decades, various tools have been proposed to address the challenge of finding the optimal DG compositions in MG systems. Models incorporated specific aspects and scenarios. The models concerning electricity prevailed over heat models, because the balancing of the electric energy flows in a grid are a critical task (due to the short time responses). An early contribution in the simulation of microgrids has been delivered by M. Indrani et al. in 2010 [20]. They proposed a simulation framework for a microgrid such as small township that generates electrical power from solar energy and uses it directly when possible, and via stored battery power at other times. The problem was described as a microgrid system with many consumers and suppliers and there was no communication or coordination among the agents.

L. Montuori et al. (2014) [21] presented a work dealing with economic evaluation of the micro-power with the HOMER Energy simulator tool. This work examines how demand response can contribute to the better integration of DER. Later, B. Zhao et al. in 2015 [22] proposed a simulator based on real-time micro-controllers for validating multi-agent energy management strategies of PV-small hydro hybrid microgrids operating at high altitude.

C. Marnay et al. in 2016 [23] provided an integrated framework to forecast the adoption of distributed energy resources (DER), both by electricity customers and by the various institutions within the industry itself in California, and for evaluating the effect of this adoption in to the power system, particularly on the overall reliability and quality of electrical service to the end-user.

D. Zafirakis et al. in 2017 [24] examined different energy strategies and scenarios for the Aegean Sea Islands microgrids with a simulator that considers stand-alone operation and interconnection to a host electricity system. P. Michalitsakos et al. in 2017 [25]

published a sequel that included the minimization of costs, CO_2 emissions and a DER reliability maximization for the Greek Islands.

The DER-CAM (Distributed Energy Resources Customer Adoption Model) decision support tool was used for the multi-objective analysis, which gives a set of optimal solutions of DG technologies, the storage capacities and the optimal dispatch of the MG.

More recently, Stevanato, et al., in 2020 [26] developed a novel, long-term optimization model formulation, capable of accounting for load evolution and performing suitable investment decisions. This ensure access to energy in rural areas located far from the main grid. Multiple scenarios of load evolution are considered through the coupling of the model with a tool for stochastic load profile generation. The results show how this implementation reduces the overall costs of the project and connectivity between actual electricity demand and, microgrid sizing is improved. Morstyn T. et al., in 2020 [27] created an open-source tool for integrated modeling, optimization and simulation of MG. The tool provides a platform for developing and testing novel DER management strategies, grid power flow, energy market and storage modeling.

Bhamidi L., et al., in 2020 [28] proposed a joint optimization model for grid-tied residential MG planning and operation with the support of the demand-side management tool (DSM). In this model, the residential MG is included with various DER, such as PV, WT, micro-turbines, OG, and ESS. The proposed model is formulated as a bi-objective optimization problem. The minimization of the total annual costs and of the total annual emissions are combined objectives. The results of the simulation demonstrate the economic and environmental benefits of the DMS tool in the planning and operation of a residential community microgrid consisting of 1000 smart homes.

Only in the recent years, the optimization problem of a multi-microgrid has been deeply investigated. H. Karimi et al. in 2020 [29] discussed a multi-objective optimization method for interconnected microgrids. An independence performance index has been proposed to measure the energy exchanged with the main grid. The simulation results show that the proposed method reduces the emissions and the energy outflow to the main grid. S. E. Ahmadi et al. (2020) [30] proposed a novel energy management system (EMS) for an isolated structure of interconnected microgrids. The outer-level of the EMS is aimed to exchange the required information and power between the interconnected microgrids. The inner-level of the EMS is dedicated to the

energy scheduling to manage interconnections' fault. The optimization problem is based on MILP. The simulation results show that the proposed EMS minimizes the operational costs and increases the performance (i.e., increase of active power) of DG.

1.2.2 Performance assessments in techno-economic analysis

Type, sizing, operation management, geo-location of distributed energy sources are all key factors that affect the technical, i.e., reliability, efficiency, lifetime and economic i.e., costs, profitability, performance of the MG. The state-of-the-art demonstrates the relevance of techno-economic simulation and optimization of MG more than it is for fossil-fuel based energy systems. Centralized energy systems are straightforward: they are composed of a single energy generation unit (i.e., thermoelectric power plant) connected to the grid with a high-voltage transmission line. Thus, their location, design and operations do not need to be necessarily correlated to other energy resources.

Then, what is the best system configuration and an optimal operational strategy? In microgrids several types of energy generation systems (intermittent as RES and not as gas turbine), and types of energy storage (electrochemical, mechanical, electrical), are directly interconnected with different types of loads. A common approach to measure an optimal dispatch of energy in these complex energy systems is based on the so called: "Levelized Cost of Energy" (LCOE). This economic assessment criterion for the cost of the energy-generating system is a quick and effective method to compare several options of energy production as it measures lifetime costs divided by energy production. The LCOE consents to the comparison of different technologies (e.g., WT, PV, FC) of unequal life spans, project size, different capital cost, risk, return, and capacities involved in energy production. LCOE expresses investment costs, fuel costs, fixed, variable operation and management costs, and optionally taxes, in terms of costs per unit of energy. Many studies concern the analysis of LCOE of microgrids. E. Hittinger et al. in 2015 [31] proposed a high-resolution model allowing for the comparison of different battery energy storage technologies in a variety of realistic microgrid settings. The model is used to evaluate how the temperature effects, rate-based variable efficiency and capacity fade influence the optimal system design and the LCOE. S. V. Nielen (2016) [32] assessed the LCOE of MG embedding Solid Oxide Fuel Cells (SOFCs) and Solid oxide fuel assisted electrolysis cells (SOFECs) in future Dutch energy systems.

However, there are challenges (e.g., critical loads) where the optimum should be found not only in terms of LCOE but also the reliability and lifetime need to be included.

In several studies for example M. Y. A. El-Sharkh et al. (2005) [33], M. Gulin et al. (2013) [34] and more recently Eman Hassan Beshr (2018) [35] the optimization models are used to search for the conditions (i.e., values of power variables), that return the best economic performance.

1.2.3 State-of-art of techno-economic tools

A wide selection of commercial simulation tools is available for economic technical analysis of energy systems. For example, H. Lund of Aalborg University in Denmark has developed EnergyPLAN [36] a computer model for technical and economic assessments of different energy systems and investments. The continued interest in energy system planning has resulted in increasing number of tools. Further examples of software packages include (W.Feng et al., 2018) [37]: DER-CAM, DEEP developed by Berkeley Lab (US), HOMER developed by the National Renewable Energy Laboratory (US), Microgrid Design Toolkit developed by the Sandia National Laboratory (US), Smart Grid Computational Tool developed by the Electric Power Research Institute (US), GridLAB-D developed by the Pacific Northwest National Laboratory (US), energyPRO (Denmark).

The research study conducted by by D. Connolly in 2010 [38] has identified over 68 different tools, ranging from short-term dispatch optimization software at the level of individual houses (e.g., HOMER), to optimization tools for long-term investment and replacement planning (e.g., Balmorel, MARKAL/TIMES).

This work provides a guideline to identify and select the most suitable tool fitting the different needs of integrating a RES into various energy-systems under different objectives. All these energy tools are depicted in Appendix D / Table D.1.

The early-stage simulation/optimization tools cover the following application domains: 1) Simulation tools to analyze the operation of a given energy-system to supply a given set of energy demands. The latter, usually operates in hourly time-steps over a one-year time-period. 2) A scenario tool usually combines a series of years into a long-term scenario. A scenario tool functions in time-steps of 1 year and combine such annual results into a scenario of typically 20–30 years. 3) Equilibrium tools are used to explain the behavior of supply, demand, and prices in a whole economy or part of an

economy (general or partial) with several or many markets. It is often assumed that agents are price takers and that equilibrium can be identified. 4) Top-down tools are macroeconomic models which are used to determine growth in energy prices and demands. Top-down tools are also equilibrium tools. 5) Bottom-up tools are used to identify and analyze the specific energy technologies and thereby determine the investment options and alternatives. 6) Operation optimization tools focus on the best operational strategy for a given energy-system. 7) Investment optimization tools optimize the investments in an energy-system. Such tools are suitable to optimize investments in new energy technologies.

In more recent years, an increasing number of open-source models have been added. The wide variety is a result of the diversity in problem definitions and optimization algorithms. The repository listed in Appendix D / Table D.2 is available in the Wiki Workspace of "Openmod initiative" [39], fostering Open Source and Open Data in energy modeling. These models are not confined to the electricity sector but can also be applied to the heat, gas, end-use, and mobility sectors. Some embed market clearing while others assume single-actor cost minimization.

For over two decades the HOMER tool has been instrumental in helping stakeholders understand the complexities and tradeoffs in designing cost-effective, reliable microgrids, and hybrid-energy systems. Many researchers, consultants, and policymakers still use this simulation tool worldwide. The HOMER tool is developed to evaluate small-scale microgrids including DER options with constraints. The overall modeling methodologies for HOMER are similar to those used in DER-CAM: to minimize microgrid system investment and operation life-cycle costs. HOMER can perform both simulation and optimization for one-year performance analysis. For microgrid system control, HOMER is implemented with rule-based strategies to optimize system operation with time-steps. Sensitivity analysis is commonly used in HOMER for users to compare the techno-economic performance of the proposed microgrids (H. Omar et al., 2012 [40]). HOMER can simulate demand response in a microgrid and calculate the economics through balancing load reduction with distributed energy resource generation (Montuori et al. 2014 [41]).

1.3 Objectives of the thesis

The scope of this thesis is centered on a techno-optimization study for finding the optimal operation, design, sizing and siting of CHP-MMG.

To this aim, the following sub-objectives have been defined: 1) development of a novel stochastic techno-economic model to represent the DER of a CHP-MMG; 2) design of innovative optimization architectures 3) development of innovative machine learning approaches supporting techno-economic optimizations 4) research of innovative scenarios for the installation and operation of CHP-MMG.

The optimization of CHP-MMG is a complex non-convex and non-linear problem with multiple local minima and not unique solutions that require a stochastic optimization approach. To this aim, a novel stochastic multi-objective optimization algorithm has been developed. The algorithm makes use of evolutionary computing at the upper layer and sequential least squares programming at the lower layer to find the global optimal solution. Moreover, machine learning techniques have been combined with analytical techno-economic models to reduce the computational time.

The solution of the problem is given by computing the values of 38 variables that returns the minimum levelized cost of energy and maximum internal return rate of investment of a CHP-MMG.

The list of the 38 variables is reported in detail in Appendix A.2; 36 variables are the size of the DER while the remaining 2 variables identify the geographic location in terms of latitude and longitude (i.e., the siting).

The evolutionary algorithm produces a trial set of the 38 variables at each generation. The latter feed the techno-economic models: 1) to compute the actual financial variables (e.g., TCO, LCOE, IRR), 2) to set up the boundaries of the sequential least squares programming (SLSQP). SLSQP provides an optimal balance between the generation and consumption of energy each time-step (i.e., hour) at minimal operational costs and the highest revenues streams.

Since such an analytical model requires computing time and is not suitable for usage in the context of global optimization, in this thesis three alternative machine learning models have been also developed, evaluated and combined with the analytical model for the reduction of the computation time.

1.4 Thesis outline

In the **second chapter** a method for prediction of climate variables with Fast Fourier Transform and polynomial regression is proposed. This leads to the setup of the analytical techno-economic model of two interconnected MG. The Sequential Least Squares Programming optimization method is introduced and will be used at each time-step to minimize a cost-function while the electricity and heat dispatched are constrained. Furthermore, a business case dealing with two microgrids of household communities nearby the city of Bremen (Germany) is formulated in the last part of the chapter. The examined scenarios demonstrate how the interconnection of multiple hybrid microgrids can be optimally operated with the SLSQP optimization method. The **third chapter** proposes three alternative approaches to the analytical TE model. After the introduction of different preprocessing techniques, multiple linear regression (MLR), is unveiled. Then, a three-layer neural network (NN) is presented. A third method (DNN) that extends the layers and adds further deep features to the NN is proposed. The results from the simulations are evaluated; the applicable domain of MLTE outputs is discussed at the end of this chapter. In the **fourth chapter**, two different novel self-adaptive differential evolution algorithms named ADE and AIE, are introduced. In the first part, the adaptive approach applied to ADE aiming to improve the search radius and increases the convergence is explained. Then, the mechanism of AIE to generate the mutant vector driven by the population diversity method is described. Moreover, the benefit of the horizontal gene transfer technique to recombine individuals of previous trials with the mutant is demonstrated. The chapter is concluded by analyzing different business scenarios with the aim of examining how the cost and type of hydrogen, interconnection with the utility grid influences both the configurations and the financial performance in the different geolocations. The **fifth chapter** introduces the criterion for selecting and validating in overall scenarios the best probabilistic solution of a cluster. Moreover, the performances of the different models are discussed and a comparison between the quality of the results and computational techniques is provided. In the **sixth chapter,** the conclusions are drawn. Moreover, the perspectives for future work are outlined with the aim of: 1) assessing the impact of solar radiation, temperature changes on energy yields of renewables systems under different greenhouse gas emissions scenarios; 2) extending the optimization problem to a larger number of interconnected microgrids; 3) investigating optimal CHP-MMG suitable for manned lunar outposts.

1.5 References

[1] J. Rifkin, 2019, The Green New Deal:Why the Fossil Fuel Civilization Will Collapse by 2028, and the Bold Economic Plan to Save Life on Earth, St. Martin's Press, ISBN-13: 978-1250253200.

[2] Kirsi Kotilainen , Ulla A. Saari. Policy Influence on Consumers' Evolution into Prosumers—Empirical Findings from an Exploratory Survey in Europe. MDPI, January 2018

[3] Yue Zhou, Jianzhong Wu, Chao Long, Wenlong Ming, 2020, State-of-the-Art Analysis and Perspectives for Peer-to-Peer Energy Trading, Engineering, Volume 6, Issue 7, Pages 739-753 ISSN 2095-8099, https://doi.org/10.1016/j.eng.2020.06.002.

[4] Chris Giotitsas, Alex Pazaitis, Vasilis Kostakis, 2015, A peer-to-peer approach to energy production,Technology in Society,V olume 42, Pages 28-38, ISSN 0160-791X,https://doi.org/10.1016/j.techsoc.2015.02.002.

[5] Maarten Wolsink, 2020, Distributed energy systems as common goods: Socio-political acceptance of renewables in intelligent microgrids, Renewable and Sustainable Energy Reviews, Volume 127, 109841, ISSN 1364-0321, https://doi.org/10.1016/j.rser.2020.109841.

[6] Bullich-Massagué, E., Díaz-González, F., Aragüés-Peñalba, M., Girbau-Llistuella, F., Olivella-Rosell, P., & Sumper, A. (2018). Microgrid clustering architectures. Applied Energy, 212. https://doi.org/10.1016/j.apenergy.2017.12.048

[7] Meng, L., Shafiee, Q., Trecate, G. F., Karimi, H., Fulwani, D., Lu, X., & Guerrero, J. M. (2017). Review on Control of DC Microgrids and Multiple Microgrid Clusters. IEEE Journal of Emerging and Selected Topics in Power Electronics, 5(3). https://doi.org/10.1109/JESTPE.2017.2690219

[8] Bandeiras, F., Pinheiro, E., Gomes, M., Coelho, P., & Fernandes, J. (2020). Review of the cooperation and operation of microgrid clusters. In Renewable and Sustainable Energy Reviews (Vol. 133). https://doi.org/10.1016/j.rser.2020.110311

[9] Insights Guidehouse. Microgrid deployment tracker 1Q20. Available online: https://guidehouseinsights.com/subscription-services/microgrids.

[10] Adam Wilson, and Peter Asmus (2017). Microgrid Deployment Tracker 4Q17, Navigant Consulting, Inc.

[11] John Romankiewicz, Min Qu, Chris Marnay, Nan Zhou (2013). International Microgrid Assessment: Governance, INcentives, and Experience (IMAGINE), Lawrence Berkeley National Laboratory

[12] Taha Selim Ustun, Cagil Ozansoy, Aladin Zayegh (2011). Recent developments in microgrids and example cases around the world—A review. Renewable and Sustainable Energy Reviews. Volume 15. pp 4030-4041.

[13] Keiichi Hirose (2013). Behavior of the Sendai Microgrid during and after the 311 Great East Japan Disaster, Telecommunications Energy Conference 'Smart Power and Efficiency' (INTELEC), IEEE

[14] Energy Foundation (2012), Research on Key Technologies and Development of Distributed Smart Microgrid, Research Report

[15] Anders Hove, Qian Wenyun, Zhao Kaiming, Nicole Kim Fuerst, China Energy Transition Status Report, 2020, Sino-German Energy Transition Project commissioned by Federal Ministry for Economic Affairs and Energy (BMWi)

[16] Eiben A.E., Smith J.E., 2015, Problems to Be Solved.Introduction to Evolutionary Computing. Natural Computing Series. Springer, Berlin, Heidelberg. https://doi.org/10.1007/978-3-662-44874-8_1

[17] Blaise, M., Feidt, M., 2018, A four objectives optimization for an energy system considered in the environment. Int J Energy Environ Eng 9, 1–11.

[18] Frangopoulos, C. A. Methods of energy systems optimization. In Summer school: Optimization of energy systems and processes. Gliwice, 2003.

[19] Aki, H., Murata, A., Yamamoto, S., Kondoh, J., Maeda, T., Yamaguchi, H., & Ishii, I. (2005). Penetration of residential fuel cells and CO2 mitigation–case studies in Japan by multi-objective models. International Journal of Hydrogen Energy, 30(9), 943–953. doi: 10.1016/j.ijhydene.2004.11.009.

[20] Indrani Maity, Shrisha Rao.,2010' Simulation and Pricing Mechanism Analysis of a Solar-Powered Electrical Microgrid. IEEE Systems Journal (Volume: 4, Issue: 3).

[21] Lina Montuori , Manuel Alcázar-Ortega, Carlos Álvarez-Bel, Alex Domijan. Integration of renewable energy in MG coordinated with demand response resources: Economic evaluation of a biomass gasification plant by Homer Simulator. Applied Energy 132 (2014) 15–23.

[22] Bo Zhao, Meidong Xue, Xuesong Zhang, Caisheng Wang, Junhui Zhao. An MAS based energy management system for a stand-alone MG at high altitude. Applied Energy 143 (2015) 251–261

[23] Marnay, C.; Kawaan, C.P.; Blanco, R.; Osborn, J.G.; Hamachi, K.S.; Rubio, F.J. Integrated Assessment of Dispersed Energy Resources Deployment—LBNL No. 46083. 2000. Available online: https://escholarship. org/uc/item/22f8m8t1 (accessed on 17 March 2016).

[24] Dimitrios Zafirakis, Georgios Tzanes, John K. Kaldellis. An Advanced Microgrid Simulator for Stand-Alone and Market-Dependent Energy Strategies. 978-1-5386-3917-7/17-2017 IEEE.

[25] Panagiotis Michalitsakos, Lucian Mihet-Popa, George Xydis. A Hybrid RES Distributed Generation System for Autonomous Islands: A DER-CAM and Storage-Based Economic and Optimal Dispatch Analysis. Open access article - Creative Commons Attribution. November 2017.

[26] Stevanato, N., Lombardi, F., Guidicini, G., Rinaldi, L., Balderrama, S.L., Pavičević, M., Quoilin, S., Colombo, E., 2020, Long-term sizing of rural microgrids: Accounting for load evolution through multi-step investment plan and stochastic optimization, Energy for Sustainable Development, 58, pp. 16-29.

[27] Morstyn, T., Collett, K.A., Vijay, A., Deakin, M., Wheeler, S., Bhagavathy, S.M., Fele, F., McCulloch, M.D., 2020, OPEN: An open-source platform for developing smart local energy system applications, Applied Energy, 275, art. no. 115397

[28] Bhamidi, L., Sivasubramani, S., 2020, Optimal Planning and Operational Strategy of a Residential Microgrid with Demand Side Management, IEEE Systems Journal, 14 (2), art. no. 8730494, pp. 2624-2632.

[29] Hamid Karimi, Shahram Jadid, 2020, Optimal energy management for multi-microgrid considering demand response programs: A stochastic multi-objective framework, Energy, Volume 195, 116992, ISSN 0360-5442, https://doi.org/10.1016/j.energy.2020.116992.

[30] Seyed Ehsan Ahmadi, Navid Rezaei, 2020, A new isolated renewable based multi microgrid optimal energy management system considering uncertainty and demand response, International Journal of Electrical Power & Energy Systems, Volume 118, 105760, ISSN 0142-0615, https://doi.org/10.1016/j.ijepes.2019.105760.

[31] Eric Hittinger, Ted Wiley b, John Kluza, Jay Whitacre. Evaluating the value of batteries in MG electricity systems using an improved Energy Systems Model. Energy Conversion and Management 89 (2015) 458–473

[32] Sander van Nielen. Techno-economic Assessment of Solid Oxide Fuel Cells and Fuel-assisted Electrolysis Cells in Future Energy Systems. Thesis at University of Delft. 2016

[33] M.Y.El-SharkhA.Rahman M.S.Alam. Evolutionary programming-based methodology for economical output power from PEM fuel cell for micro-grid application. Journal of Power Sources September 2004.

[34] Marko Gulin, Mario Vasˇak, and Mato Baotic´ . Analysis of Microgrid Power Flow Optimization with Consideration of Residual Storages State. IEEE Energy Systems, vol. 43, no. 1, pp. 779–787, 2013.

[35] Eman Hassan Beshr , Hazem Abdelghany, Mahmoud Eteiba. Novel optimization technique of isolated MG with hydrogen energy storage Published: February 21,2018 https://doi.org/10.1371/journal.pone.0193224.

[36] Lund, H. (2007). EnergyPLAN–Advanced Energy Systems Analysis Computer Model. Aalborg University, Denmark. http://www.energyplan.eu

[37] Wei Feng, Ming Jin, Xu Liu, Yi Bao, Chris Marnay, Cheng Yao, Jiancheng Yu, 2018, A review of microgrid development in the United States – A decade of progress on policies, demonstrations, controls, and software tools, Applied Energy, Volume 228

[38] D. Connolly, H. Lund, B.V. Mathiesen, M. Leahy, 2010, A review of computer tools for analysing the integration of renewable energy into various energy systems, Applied Energy, Volume 87, Issue 4, Pages 1059-1082, ISSN 0306-2619, https://doi.org/10.1016/j.apenergy.2009.09.026

[39] Openmod initiative, 2021, https://openmod-initiative.org/index.html#

[40] Hafez Omar and Kankar Bhattacharya (2012). Optimal planning and design of a renewable energy based supply system for microgrids. Renewable Energy. Vol. 45. September. pp 7-15.

[41] Montuori, Lina, Manuel Alcázar-Ortega, Carlos Álvarez-Bel, and Alex Domijan (2014). Integration of renewable energy in microgrids coordinated with demand response resources: Economic evaluation of a biomass gasification plant by HOMER Simulator. Applied Energy. Vol. 132. 1 November. pp 15-22.

CHAPTER 2: Analytical techno-economic model

This chapter presents a techno-economic model of two interconnected hybrid microgrids (MG) whose electricity and thermal dispatch strategy are managed with a Sequential Least Squares Programming (SLSQP) optimization technique. MG combine multiple thermal and electric power generation, transmission, and distribution systems as a whole, to gain a tight integration of weather-dependent distributed renewable generators with multiple stochastic load profiles. Moreover, MG can achieve an improvement in the return on investment and a better cost of energy. The first part of the work deals with setting up a method to obtain an accurate prediction of climate variables. This method makes use of Fast Fourier Transforms (FFT) and polynomial regression to manipulate climate datasets issued by the European Centre for Medium-Range Weather Forecasts (ECMWF). The second part of the work deals with the optimization of interconnected MG operations through the SLSQP algorithm. The objective is to obtain the best financial performance (IRR) when clean distributed energy resources (DER) are exchanging both thermal and electric energy. SLSQP optimizes the energy flows by balancing their contribution with their nominal Levelized Cost of Energy (LCOE). The proposed algorithm is used to simulate innovative business scenarios where revenue streams are generated via sales of energy to end-users, sell backs and deliveries of demand response services to the other grids. A business case dealing with two MG providing clean thermal and electric energies to household communities nearby the city of Bremen (Germany) is examined in the last part of the chapter. This business case with a payback in two years, an internal rate of return (IRR) of 65% and a LCOE of 0,14 €/kWh, demonstrates how the interconnection of multiple hybrid MG with SLSQP optimization techniques, makes renewables and DER superior and could strand investments in fossil fuel generation, shaping the future of clean energy markets.

Based on: Fracas P., Edwin Zondervan, 2019, Fast Fourier Transforms for Microgrid Climate Computing, Computer Aided Chemical Engineering, Elsevier, Volume 46, Pages 1657-1662, ISSN 1570-7946, ISBN 9780128186343, https://doi.org/10.1016/B978-0-12-818634-3.50277-0

Fracas, Paolo, Camarda, Kyle V. and Zondervan, Edwin. "Shaping the future energy markets with hybrid multimicrogrids by sequential least squares programming", Physical Sciences Reviews, 2021, pp. 20200050. https://doi.org/10.1515/psr-2020-0050

2.1 Introduction

The MG is a controllable, independent small energy systems comprising DG, loads, ES, and control devices. It is a promising concept to overcome energy balance issues and thus to secure the energy supply and to reduce the overall cost of energy generated from RES. University campus microgrids, residential, commercial, industrial districts, off-grid users in a remote area, not connected to any utility grid, datacenter, telecom-towers are examples of MG applications. This study explores the route of interconnection of optimized MG that embed a mix of clean thermal and electric DER. The main scope of this work is to analyze their economic throughputs when swarmed thermal and electric energy flows are optimized thru an SLSQP algorithm.

In the first part of this work, different methods to obtain an accurate prediction of climate variables are described. Fast Fourier Transform and polynomial regression to manipulate climate datasets issued by the European Centre for Medium-Range Weather Forecasts (ECMWF) are outlined.

The second part of the work is focused on detailing the analytical techno-economic models (ATE) of the DER which are embedded in two interconnected microgrids

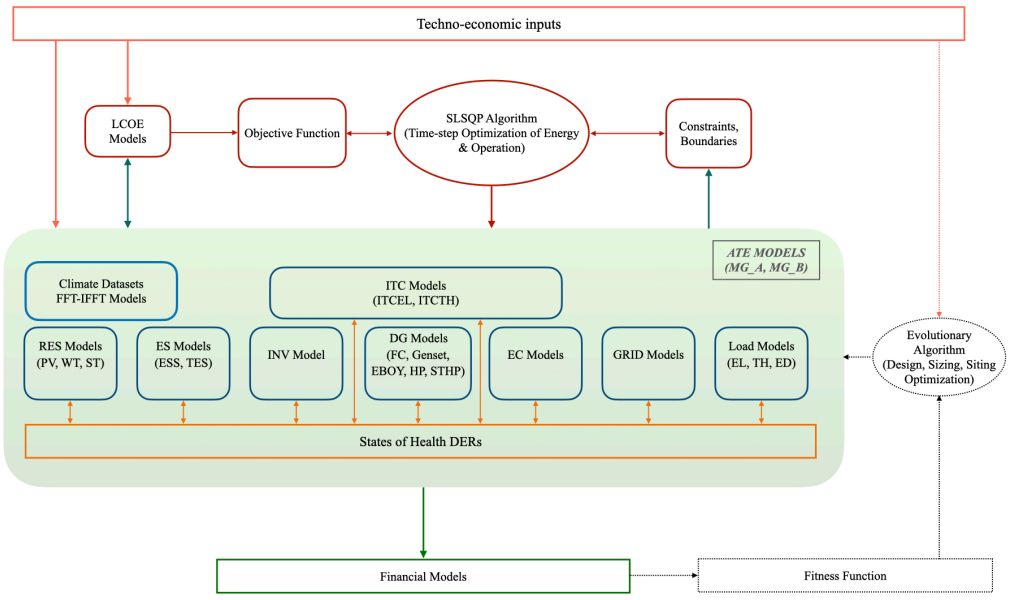

Figure 2.1 *Structure of techno-economic models (ATE) and their interrelation with SLSQP*

(MG_A, MG_B). In the third part, the cost-revenues objective function, the constraints to balance the thermal and electric energy flows and related boundaries associated with the SLSQP algorithm are outlined. The overall framework of the models and their interrelations are depicted in Figure 2.1. In the final part of this work, the result of the simulation of two microgrids giving thermal and electric energies to neighboring communities nearby the city of Bremen (Germany) are introduced. The business cases treat revenue streams which are achieved thru the sale of energy to end-users, the sell-backs to the nearby microgrid and the deliveries of demand response services to utility grids.

2.1.1 Prediction of climate variables

Within the techno-economic model (ATE) of MG, the accuracy of climate datasets plays an important role in the prediction of power generated by DER. Thus, at the beginning of this work, we investigated the use of recent monthly daily means datasets covering Earth's areas by latitude and longitude coordinates, which are available from the historical archive of ECMWF. The periodic components of solar radiation, wind speed, temperature, and cloudiness are generated with FFTs and then filtered. These climate datasets are subsequently extrapolated over the timeframe of the project with inverse FFT (IFFT). Polynomial and forest tree regression methods are also used to correlate coupled of best-fitting variables. The spectral transform method has been successfully applied in climate datasets for more than 30 years, with the first spectral model introduced into reanalysis at ECMWF in April 1983 and it performs well. Fourier Transform method was introduced to numerical weather prediction starting from the work of Eliasen et al. [1] and Orszag [2] who achieved high efficiency by alternating the computations between a grid-point and a spectral representation at every time-step. Joly and Voldoire [3] have developed a method to manipulate gridded datasets with FFT to better understand the coupled ocean–atmosphere processes. Inter-annual variability has been studied by filtering long-term change data in both the observed and simulated time-series. Kent et al. [4] reanalyzed in situ measurements and satellite retrievals of monthly mean marine wind speeds. The results have been used to validate the accuracy required in the calculation of air–sea heat fluxes. Wang and Zeng [5] have used observed data to quantify the land surface air temperature, which is one of the fundamental parameters to represent heat transfer and to modulate the moisture cycle between land and atmosphere.

Amendola et al. [6] used FFT to recombine Gaussian distributions of monthly datasets obtained via a neural network for seasonal weather forecasts.

Different approaches have been adopted to convert the monthly mean of solar radiation and wind speed variables into the hourly mean time-step of the ATE. For solar radiation, an empirical model deriving from the literature and validated with experimental results has been used in this work. The model is based on the work of Liu and Jordan [7] in 1960 and several other researchers, i.e., H. P. Garg et al. [8] and Jain [9] who improved the hourly horizontal global radiation with a Gaussian function. The cloudiness effect is then added to the solar radiation with a normal probability density function. The hourly mean average for wind speed is obtained via a normal distribution of the wind speed values at 50 m above the surface of the earth. A global wind speed distribution is obtained from the NASA surface meteorology and solar energy database.

2.1.2 Electric system operations

The hourly mean climate datasets are utilized to calculate the renewable thermal and electric energy generated by wind turbines (WT), photovoltaic panels (PV), and solar thermal collectors (ST) net of losses and actual efficiencies, deriving from the remaining useful life (RUL) under the steady-state conditions.

Combined Heat and Power Proton Exchange Fuel Cell (PEMFC-CHP), diesel gensets (OG), electrolyzers (EC), electric boilers (EBOY), stand-alone heat pumps (HP), heat pumps combined with ST (STHP) inverters (INV) thermal (TES), and electric energy storage systems (ESS) are additional distributed energy resources (DER) contemplated in the MG configurations of this work. The techno-economic model keeps updated the states of health (SoH) of each DG every time-step, in relation to their actual calendar lifetime and lifecycles (number of start-stops, charge/discharge).

Lifecycle and calendar lifetime of lithium-ion batteries are modelled with a function having an “Arrhenius-like” form that takes into account the time, temperature, SOC, and Delta % SOC of the batteries. These models were developed according to the results of test conducted on 18650-size, lithium-ion battery cells by the US Department of Energy in 2001.

The model of thermal and electric load demands is based on the result of statistical analysis carried on by K. Konstantinos in 2017 [10] with loads of more than 100 households. Additional stochastic virtual load profiles such as load shedding and load

shifting are introduced in the techno-economic model. This contribution simulates additional energy services that the MG can provide as controlled options to respond to unplanned energy flows that occur in the main electric power grid.

A sub-model to simulate the purchase and the sell-back of electric energy to the main grid is also considered in conjunction with stochastic grid outage events.

2.1.3 Outline of the proposed optimization strategy

Based on the thermal- and electric-distributed energies resources which have been discussed in the previous paragraph, the objective of this work is to analyze how two interconnected MG whose energy flows are governed by the sequential least squares programming algorithm, improve the resilience of energy systems embedding RES, reduce the cost of energy, increment IRR while providing electric, thermal energy, and water to users and demand response services to the main grid. It is worth noting that enhancement of the energy system resilience is one of the main scopes of the SLSQP application, and it is obtained with the successful balancing of the constrained energy flows.

At each time-step, the proposed optimization algorithm minimizes a non-linear objective function composed by the difference of two terms: to the first term that groups the costs inherent the generation of energy, the revenues stream (deriving from the use of energy) is subtracted. Costs and revenues are obtained as the product of the average energy flow in the time-step and, respectively, the nominal LCOE and the levelized sale of energy (LSOE). The estimation of LCOE is based on a simplified model of Department of US Energy [37].

The revenue streams are generated from the contemporary sale of energy to the end-users and sale of ED response services. Nominal LCOE, LSOE (i.e, sell-back prices and remunerations prices for demand response services) act as weights in the objective function to balance the thermal and electric energy flows. The SLSQP algorithm searches the best contribution of energy flow for each DER that maximizes the whole economic performance. The calculation is executed, respecting the set of constraints related to thermal and electric power flow under the steady-state conditions. The range of the boundaries of each DER is dynamically shaped in relation to the available energy they can provide each time-step.

The results given by SLSQP feed a financial model. Maintenance and operational costs (OPEX) are added to the initial investment costs (CAPEX) to obtain the total cost of ownership (TCO). Total revenues, contribution margin, total energy generated, actual LCOE, and the following key financial performance indicators are finally calculated.

Optimizations of electric system operations have been the subject of several recent works. S. Wang et al. [11] propose an optimization method based on differential evolution (DE) for dynamic economic dispatch of MG, considering various distributed generations, ES, the transaction between the MG and power grid, as well as multiple kinds of loads. J. Radosavljević et al. [12]; propose an efficient algorithm based on particle swarm optimization (PSO) for energy and operation management (EOM) of MG including different distributed generation units and energy storage devices. PSO minimizes the total energy and operating cost of the MG via optimal adjustment of the control variables of the EOM, while satisfying various operating constraints. Owing to the stochastic nature of energy produced from renewable sources: WT, PV, load uncertainties, and market prices, a probabilistic approach in the EOM is proposed.

Soares et al. [13] have proposed an evolutionary algorithm to offer residential end-users an integrated management of energy resources minimizing the electricity bill while keeping the best possible quality of energy service. Simulation results show that a minimum savings of 10% might be achieved by optimizing load scheduling, local micro generation, and storage systems including electric vehicles (EVs) in both grid-to-vehicle (G2V) and vehicle-to-grid (V2G) modes. Jamaledini et al. [14] introduced an evolutionary algorithm based on the multicellular organism mechanism applied to MG operations. For optimization, both DE and PSO algorithms is used for the comparison of results.

More recently (2019), Nagapurkar P. et al. [15] presented a methodology that assessed the techno-economic and environmental performance of MG-conventional grid integration scenarios for homes located in US cities. A genetic algorithm optimization technique is implemented to determine the lowest LCOE for different MG-conventional grid integration and carbon taxes scenarios.

Based on the state-of-art that has been discussed earlier, this work aims to extend the analysis at the optimization of interconnected heat and power (hybrid) MG through the SLSQP algorithm.

2.2 Methods of climate data processing

In the following paragraph, a model to project climate daily means datasets issued by ECMWF with the Fast Fourier Transform is described. This method reveals very useful and effective to predict periodic datasets. The results discussed in the following section have been also published by P. Fracas et al. [30] and presented at the 29th European Symposium on Computer Aided Chemical Engineering (Eindhoven, The Netherlands, 2019).

2.2.1 Prediction model by inverse fast Fourier transform

Fourier analysis is a method for expressing a function as a sum of periodic components and for recovering the function from those components. Cooley and Tukey [16] and more recently Press et al. [17] provided a computing approach to Fourier analysis for discretized counterparts: the FFT. The following reanalyzed monthly mean type of daily means datasets issued by ECMWF have been considered: 1) ssr[n] (solar net surface radiation, kW/m2), 2) 10si[n] (10 meter wind speed, m/s), 3) t2m[n] (Temperature at 2 meters from soil, K), 4) tcc[n] (total cloud cover, %). Here the number of months is named: n. A continuous sequence of n = 84 months is considered.

With these datasets, two predictive discrete curves of N_i-dimension: $X_d(n)$ and $X_f(n)$ have been generated. The first set of data has a dimension N_1=72 and it is used to train the IFFT model (January 2010 to December 2015). The second dataset with dimension N_2=12 is used to test the model (June 2017 to June 2018). A one-year timeframe is chosen as it is the typical test period for simulations of microgrids and it is suitable for conversion in hourly solar radiation data (T. Khatib, et al., 2015) [18] as described later in this paper.

The following relation:

$$Y_d(k) = \sum_{n=0}^{N-1} e^{-2\pi j \frac{kn}{N}} x_d(n), \qquad [2.1]$$

transforms the climate datasets array $x_d(n)$ from the time domain to different complex arrays $Y_d(k)$ of dimension K_1 where k is the index of the complex element.

A first complex array of K_1-dimension is generated in the frequency domain from the original N_1 dataset. The monthly averages of the original N_1 over a five years period have been used to generate a second complex array of K_2-dimension.

A third complex array is generated from an optimized subset of the original K_1 -complex array thru a low-pass filter (LPF) that iterates until the cut-off frequency. This third optimized complex array has a K_3-dimension. The LPF algorithm minimizes the mean squared error (MSE). As described in the following Eq. [2.2] the array in the time domain, $X_p(n)$ obtained with an optimized subset (K_3) of K_1 is compared with the original until MSE is minimized.

$$\min f(K) = \frac{1}{N_1}\sum_{n=1}^{N}\left(x_d(n) - \frac{1}{K}\sum_{k=0}^{K-1} e^{2\pi j\frac{kn}{P}} y_p(k)\right)^2. \qquad [2.2]$$

Here $f(K)$ is the objective function MSE to minimize and N_1 is the dimension of training (original) dataset, $x_d(n)$ is the n-element of the training climate dataset $X_d(n)$, k is the index of the k-element of the complex array, P is the dimension of complex array, $y_p(k)$ is the k-complex element.

The three complex arrays return then, into the time domain by the inverse discrete transform as follows:

$$X_f(n) = \frac{1}{F}\sum_{k=0}^{F-1} e^{2\pi j\frac{kn}{F}} y_f(k) \quad . \qquad [2.3]$$

Here $X_f(n)$ represents the predicted dataset in the time domain of n elements $x_f(n)$. F is the dimension of the best subset of complex arrays, $y_f(k)$ is the k-complex element of the best complex array. And finally the coefficient of determination named R^2 which estimates the ratio between the square error and the variance is used to compare the performances against the test datasets.

$$R^2 = 1 - \frac{\sum_{n=1}^{N}\left(x_d(n) - x_f(n)\right)^2}{\sum_{n=1}^{N}\left(x_d(n) - \mu_x\right)^2} \quad , \qquad [2.4]$$

where μ_x denotes the sample mean of the corresponding feature.

2.2.2 Prediction of datasets by regression models

In the following part of the work, we analyzed different regression models to identify interrelations among the four climate variables. The scope is to setup an indirect method to build quickly accurate predicting curves, among best-fitting coupled variables. We utilized exploratory data analysis to identify the presence of outliers, the distribution of the data, and the relationships between the variables, then a scatterplot matrix to visualize the pair-wise correlations has been created. To quantify the linear relationship between the variable, we proceed to build a correlation matrix embedding the Pearson product-moment covariance coefficients as follows:

$$P_{x,y} = \frac{\sum_{n=1}^{N}\left[\left(x_d(n)-\mu_x\right)\left(y_d(n)-\mu_y\right)\right]}{\left[\sum_{n=1}^{N}\left(x_d(n)-\mu_x\right)^2\right]^{-2}\left[\sum_{n=1}^{N}\left(y_d(n)-\mu_y\right)^2\right]^{-2}}. \qquad [2.5a]$$

Here μ denotes the sample mean of the corresponding variable, $x_d(n)$ and $y_d(n)$ are correlated training datasets.

As introduced by S. Raschka [19] the linear dependence between pairs of variables is strictly related to the value of Pearson coefficient within the range -1 and 1. A perfect positive linear correlation is expressed by $P_{x,y}$ =+1 / -1, while no correlation if $P_{x,y}$ = 0. The relationship among monthly climate variables with the Pearson's coefficient higher than 0,7 has been modeled by using: linear, quadratic and cubic polynomials. For variables with the weakest Pearson's coefficient, as proposed by A. Liaw et al. [20] the random forest method has been used.

This further method allows dividing the continuous regression curve into a sum of linear functions. The decision tree is generated by splitting its nodes until the Information Gain (IG) is maximized as follows:

$$IG\left(D_p, x\right) = I\left(D_p\right) - \left(\frac{N_l}{Np}I(D_l) + \frac{N_r}{Np}I(D_r)\right), \qquad [2.5b]$$

where x is the feature to perform the split, Np is the number of samples in the parent node, I is the impurity function (i.e., MSE), Dp is the subset of training samples in the parent node. Moreover, D_l, D_r are the subsets of training samples in the left and right

child node after the split and N_l, N_r are the number of samples in the child nodes. The performance of the forest regression is again evaluated with R^2 estimator.

2.3 Techno-economic models of the distributed energy resource

The following paragraphs are dedicated to describe all the techno-economic models that are used in the objective function, the associated boundaries and constraints.

2.3.1 Photovoltaic panels

The calculation of the hourly mean power generated by PV starts with an expression to convert the daily mean solar radiation into hourly solar radiation. The Cooper [31] relation defined in Eq. 2.6 is commonly used to detect the angle between the equatorial plane and a straight line drawn between the centre of the Earth and the centre of the sun for every day of the year. This angle is known as the solar declination, δ (degree). For the present purposes, it may be considered as approximately constant over the course of any one day. If angles north of the equator are considered as positive and south of the equator are considered negative, the solar declination $\delta(n)$, can be described as:

$$\delta(n) = 23.45^{o} \sin\left[360^{0} \cdot \left(\frac{284+n}{365}\right)\right], \qquad [2.6]$$

where n is the number of day. The standard deviation is then calculated:

$$\sigma_g(n,\theta) = 1.983 - 0.022 \cdot \arccos\left[-\tan\theta \cdot \tan\delta(n)\right], \qquad [2.7]$$

where θ is the latitude (degree).

Finally the normal distribution is calculated as follows:

$$g(t_s,n,\theta) = \frac{1}{k_a \cdot \sigma_g(n,\theta)} e^{-\frac{(t_s - 12)^2}{k_C \cdot \sigma_g(n,\theta)^2}} \quad . \qquad [2.8]$$

In relation [8] t_s represents the time unit for the calculation of mean values expressed in hourly value and k_a and k_c are constants. The choice of a time unit t_s with a step of one hour (referred later in the paper as time-step), permits to express the terms of energy equal to the hourly power average.

The conversion between the mean monthly value and the mean hourly value is computed via the following Eq. 2.9:

$$G(t_s, \theta, \phi) = g(t_s, \theta, n) \cdot H(\theta, \phi, n), \quad [2.9]$$

where $H(\theta, \phi, n)$ is the daily radiation monthly means returned by equation [2.3] and ϕ is longitude (degree). These values are delivered for the tilted angle $\beta_o = 0$. Then, the probability density function of the normal distribution, (defined here as $N(\mu, \sigma)$) is used to adjust the hourly radiation with the monthly mean cloudy cover datasets; therefore the final expression of the hourly radiation mean with the cloudy effect can be calculated as follows:

$$G_c(t_s, \theta, \phi) = G(t_s, \theta, \phi) \cdot \left(1 - N\left(\mu\left(t_s, \theta, \phi\right), \sigma\right)\right), \quad [2.10]$$

The random number generator [32], $N\left(\mu\left(t_s, \theta, \phi\right), \sigma\right)$ returns a uniformly distributed random number within the range $0 \leq G_c(t_s, \theta, \phi) \leq G(t_s, \theta, \phi)$. Here $\mu\left(t_s, \theta, \phi\right)$ denotes the daily monthly mean cloudiness dataset and σ is standard deviation defined as a constant (e.g., 0,25). The mean hourly radiation with clouds is finally modified with the vegetation by multiplying $v\left(\theta, \phi\right)$ with Eq. 2.11:

$$G_{vc}(t_s, \theta, \phi) = G_c(t_s, \theta, \phi) \cdot \left(1 - v\left(\theta, \phi\right)\right), \quad [2.11]$$

where $v(\theta, \phi)$ assumes only the value '0', if the vegetation is not present or '1' if the ground is vegetated. The function $G_{vc}(t_s, n, \theta, \phi)$ is then adjusted taking into account the angle between the horizontal plane and the solar panel which is called the tilt angle. As proposed by A. Luque and S. Hegedus in 2011 [21] the optimal inclination angle can be obtained with the following linear equation [2.12]:

$$\beta_{\text{opt}} = 3.7 + 0.69\,|\phi|, \quad [2.12]$$

where β and ϕ are given in degree.

Thus, with a second-order polynomial equation the ratio between radiation and a different tilt can be described with accuracy as follow:

$$g\left(\beta, \beta_{opt}\right) = 1 + p_1\left(\beta - \beta_{opt}\right) + p_2\left(\beta - \beta_{opt}\right)^2, \quad [2.13]$$

where the function $g\left(\beta,\beta_{opt}\right)$ is expressed as follow:

$$\frac{G_c(\beta)}{G_c\left(\beta_{opt}\right)} = g\left(\beta,\beta_{opt}\right). \quad [2.14]$$

Hence, the maximum radiation can be calculated, combining the hourly mean radiation with clouds described in Eq. 2.11 which is related to $\beta_o = 0$, to the polynomial Eq 2.14:

$$G_{vc}(t_s,\theta,\phi,\beta_{opt}) = \frac{G_{vc}(t_s,\theta,\phi)}{g\left(\beta_o,\beta_{opt}\right)}. \quad [2.15]$$

Eq. 2.14 can be used again to adjust the title angle in the radiation as follows:

$$G_{vc}(t_s,\theta,\phi,\beta) = G_{vc}(t_s,\theta,\phi,\beta_{opt}) \cdot g\left(\beta,\beta_{opt}\right) \quad . \quad [2.16]$$

The further step is the definition of a model for the temperature which is used in the ATE model of DG. The Pearson's coefficient indicates that this variable can be derived from the hourly mean solar radiation via a linear regression model as follows:

$$T_{amb} = w_o + w_1 \cdot G_{vc}(t_s,\theta,\phi). \quad [2.17]$$

Here, the weight w_o represents the y-axis intercept and w_1 is the coefficient of the explanatory variable G_{vc} . T_{amb} is the environmental temperature (K).

Finally, the total available power generated by the photovoltaic panels can be derived from the adjusted hourly radiation, the solar panel yield and the power losses due to temperature, power conditioning (e.g., MPPT), AC/DC cables, shading, snow, dust is described as follows:

$$P_{pv\_available}\left(t_s,\theta,\phi,\beta\right) = \lambda_{st} \cdot G_{vc}(t_s,\theta,\phi,\beta) \cdot \prod_{i}^{N}\left(1-\eta_i\right) \cdot A_{pv}\,, \quad [2.18]$$

where: λ_s is the PV solar yield (kWh/kW$_{peak}$), N is the dimension of the power losses η_i are and A_{pv} (m^2) is the surface of the PV panel.

Similarly, the Eq. 2.19 describes the total available power generated by the thermal solar collector. The latter derives from the hourly net radiation, the solar panel yield and the power losses due to temperature, shading, snow, dust and tilt as follow:

$$P_{st\_available}\left(t_s,\theta,\phi,\beta\right)=\eta_{st}\left(\Delta T_{st}\left(t_s,\theta,\phi\right)\right)\cdot G_{vc}(t_s,\theta,\phi,\beta)\cdot\prod_{i}^{N}\left(1-\upsilon_i\right)\cdot A_{st} \quad [2.19]$$

$$\eta_{st}\left(\Delta T_{st}\left(t_s,\theta,\phi\right)\right)=\eta_o+k_o\left(T_{in}-T_{amb}\left(t_s,\theta,\phi\right)\right). \quad [2.20]$$

Eq. 2.20 is the relation for the thermal solar collector efficiency. The latter is obtained as a linear correlation between the input collector mean temperature (T_{in}, K), and the environmental temperature (Eq.2.17). The terms υ_i represent the power losses and A_{st} (m^2) is the area of the thermal solar collector.

2.3.2 Wind turbines

For the wind turbines, the definition of the techno-economic model starts with the wind speed daily mean of each month, here defined as $w\left(t_s,\theta,\phi\right)$.

In this thesis, two alternative approaches have been proposed to convert the wind speed daily mean into an hourly mean dataset. The first is based on the Weibull distribution, which is widely used as an approximation for the wind speed simulation (E.1 References [1,2].

$$W_s(t_s,\theta,\phi)=\begin{cases} Weibull\left[\alpha_s\left(\theta,\phi\right), \quad 8760\right]\cdot w\left(t_s,\theta,\phi\right) \\ W_s(t_s,\theta,\phi) \quad \geq \quad 0 \end{cases}. \quad [2.21]$$

The second uses the probability density function of the normal distribution (Appendix E).

The optimal values of the given shape parameter $\alpha_s\left(\theta,\phi\right)$ for the Weibull distribution in Eq. 2.21 has been computed by minimizing the MSE error between the result of Eq. 2.21 and the profile that for each geographic location, can be derived from the NASA Surface meteorology and Solar Energy (SSE) database [35]. It has been observed that the Weibull distribution replicates the original profile issued by NASA with a MSE error lower than 0,01% .

The available power generated by a WT is a function of the hourly mean wind speed and the characteristic curve of WT delivered by the manufacturer that correlates power of the WT to the wind speed.

The sum of the losses, η_i caused by the cables, MPPT will be deducted to obtain the available wind power as:

$$P_{wt\_available}\left(t_s,\theta,\phi\right) = P_{wt}\left(W_s(t_s,\theta,\phi)\right)\cdot\prod_{i}^{N}\left(1-\eta_i\right). \quad [2.22]$$

2.3.3 Thermal and electric load profiles

In this work, both thermal and electrical loads have been considered. These loads represent a sum of multiple consumptions of energy that are powered by the MG. The monthly profiles of the thermal loads (P_{th_load}) and electric loads (P_{el_load}) are obtained from the input of minimum and maximum daily mean power (respectively, P_{max}, P_{min}) as follows:

$$P_{a\_load}(n) = \cos\left(\frac{4\pi}{12}n\right)0.5\left(P_{max}-P_{min}\right)+0.5\left(P_{max}+P_{min}\right), \quad [2.23]$$

$$P_{b\_load}(n) = \sin\left(\frac{4\pi}{12}n\right)0.5\left(P_{max}-P_{min}\right)+0.5\left(P_{max}+P_{min}\right), \quad [2.24]$$

$$P_{el\_load}(n) = \begin{cases} P_{load\_a}(n) & peak\ \ in\ \ first\ \ semester \\ P_{load\_b}(n) & peak\ \ in\ \ second\ \ semester \end{cases}, \quad [2.25]$$

$$P_{th\_load}(n) = P_{a\_load}(n) + P_{b\_load}(n), \quad [2.26]$$

where n denotes the number of the month.

Based on the work done by A.M. Breipohl et al. [22] the Gauss Markov function, defined in Eq.2.27 is used to convert the monthly load profile into the stochastic daily electric load. The mean and standard deviations (i.e., μ_l σ_l) inside the function f_{gm} are derived from a statistical analysis of electric loads profiles of more than 100 households.

This work has been conducted by K. Konstantinos [10] and converted into a library of python programming language in 2017.

$$P_{elst\_load}(t_s) = f_{gm}\left(\left(P_{el\_load}(n), \quad N(\mu_l \quad \sigma_l\right), \quad t_s\right). \qquad [2.27]$$

Finally, a stochastic electrical load profile is drawn from the following normal distribution in Eq.2.28. The mean is derived from the previous Eq.2.27; while the standard deviation (σ_{noise}) is given as input.

$$P_{el\_load}(t_s) = N(P_{elst\_load}(t_s), \quad \sigma_{noise}). \qquad [2.28]$$

The thermal load $P_{th}(t_s)$ is defined with the following relation with a similar approach such as Eq. 2.27 but with two periodic peaks (to simulate heating in winter and cooling in summer) :

$$P_{th\_load}(t_s) = f_{gm}\left(\left(P_{th\_load}(n), \quad N(\mu_l \quad \sigma_l\right), \quad t_s\right). \qquad [2.29]$$

Load shedding and load shifting (peak-shaving) are then applied as a controlled option to respond to unplanned electric power underflow.

Simulation of a demand response mechanism that makes the load profile less peaky has been introduced to explore in a micro-grid paradigm, the economic benefit of providing energy services.

The electric load profile is analyzed per monthly period and the peak hours have their load shifted to low load hours or are shaved. When not shaved, the total load is the same as that one from the original, otherwise it is smaller due to the shaved peaks. The peak load is reduced by a predefined percentage.

The electric load profile corresponding to the desired demand response profile is obtained by:

$$P_{eldr\_load}(t_s) = f\left(P_{elst\_load}(t_s), \quad k_{hm} \quad , \quad k_{shifted}\right) \cdot \left(1 - k_{shedding}\right). \qquad [2.30]$$

The parameters: $k_{shedding}, k_{hm}, k_{shifted}$ express the whole fraction of load to cut, fraction of hours to shift, fraction of energy to shift respectively.

2.3.4 Energies exchanged among interconnected microgrids

Outflow and inflow energies exchanged among microgrids and the main grid are respectively represented by the following relationship :

$$P_{grid\_sellback,grid\_buy}\left(t_s\right) = N(\left[0,1\right], p) \cdot P_{grid\_sb,grid\_by}\left(t_s\right) \quad . \qquad [2.31]$$

Where the index “grid_sellback” and “grid_buy” represents respectively the outflow energy and inflow energy for each MG to the main grid.

$N([0,1],p)$ is a random number generator that returns a sample from the given 1-D array [0,1] to consider grid outage events spread with the probability ‘p’.

2.3.5 Thermal and electric distributed generators

Two types of Electric DG ($P_{der,j}$) are considered: PEMFC-CHP and OG. The mean power they deliver in each time-step (t_s) is defined respectively as: $P_{fc}(t_s)$ and $P_{genset}(t_s)$. On the contrary the mean power absorbed by an electrolyzer to convert electric energy into chemical energy (H_2) is denoted as: $P_{ec}(t_s)$. The efficiency of the conversion from electricity into hydrogen is equal to the energy content (based on the higher heating value) of the hydrogen produced divided by the amount of electricity consumed.

For the thermal generators, the following relations correlate the hourly mean energy produced respectively by electric boilers, stand alone heat pumps and combined to solar panels as follows:

$$P_{eboy}(t_s) = \eta_{eboy} \cdot P_{el\_eboy}(t_s) \quad [2.32]$$

$$P_{hp}(t_s) = \eta_{hp} \cdot P_{el\_hp}(t_s) \quad [2.33]$$

$$P_{sthp}(t_s) = \eta_{sthp} \cdot P_{el\_sthp}(t_s). \quad [2.34]$$

Where η represents for each DG the efficiency of the conversion from electric to thermal energy.

A DG is converting the chemical energy of a fuel into electric energy. The fuel has a purchase cost per liter and a transportation cost of C_{fuel}, C_{trp} (€/l), respectively. The conversion of energy occurs with a certain efficiency ($\eta_{dg,g}$) depending upon the type of DG. For example, in the fuel cell, the efficiency is defined as a ratio between the electricity produced and the hydrogen consumed.

The efficiency is related to the performance of the fuel cell stack, the balance of plant and the reformer unit, if installed. The overall costs are then related to the volumetric energy density of the fuel (V_{ed_fuel}, kWh/l).

For HP, the efficiency is denoted by the coefficient of performance (COP). This term is determined by the ratio between the energy usage of the compressor and the amount of useful cooling at the evaporator. For a heat pump a COP value of 4, means that the addition of 1 kW of electric energy is needed to have a release of 4 kW of heat at the condenser.

2.3.6 Thermal and electric energy storage systems

The techno-economic model of the electric energy storage systems (ESS) and the thermal energy storage system (TES) are defined with a set of equations that describe charging and discharging hourly mean power (energy charged and discharged in the time-step of 1 hour) in relation to *SoC* (State of Charge), *SoH* (State of Health), $P_{ess\_rated\_capacity}$, $P_{ess\_aged\_capacity}$ (rated and aged energy capacity, kWh).

The C-rate function, i.e., $C_{ess\_charge\_rate}(t_s)$ is a function of the rate at which the battery is discharged/charged and the maximum capacity. We assume the convention that the energy flows coming out the ES, are negatives (charging storages, absorptions of loads, sell-back to main grid).

$$P_{ess\_aged\_capacity}(t_s) = f\left(P_{ess\_rated\_capacity}, SoH_{ess}(t_s), T_{amb}(t_s)\right) \quad , \qquad [2.35]$$

$$P_{max\_aged\_capacity}(t_s) = P_{ess\_aged\_capacity}(t_s) \cdot SoC_{ess\_max} \quad , \qquad [2.36]$$

$$P_{ess\_aged\_charge\_min}(t_s) = \begin{cases} P_{ess\_storage}(t_s) - P_{max\_aged\_capacity}(t_s) \\ P_{ess\_aged\_charge\_min}(t_s) < 0 \end{cases} \quad , \qquad [2.37]$$

$$P_{ess\_aged\_charge}(t_s) = \begin{cases} -P_{ess\_aged\_capacity} \cdot C_{ess\_charge\_rate}(t_s) \\ P_{ess\_aged\_charge\_min}(t_s) \le P_{ess\_aged\_charge}(t_s) \le 0 \end{cases} , \qquad [2.38]$$

$$P_{min\_aged\_capacity}(t_s) = P_{ess\_aged\_capacity}(t_s) \cdot SoC_{ess\_min} , \qquad [2.39]$$

$$P_{ess\_aged\_discharge\_max}(t_s) = \begin{cases} P_{ess\_storage}(t_s) - P_{min\_aged\_capacity}(t_s) \\ P_{ess\_aged\_discharge\_max}(t_s) > 0 \end{cases} , \qquad [2.40]$$

$$P_{ess\_aged\_discharge}(t_s) = \begin{cases} P_{ess\_aged\_capacity} \cdot C_{ess\_discharge\_rate}(t_s) \\ 0 \le P_{ess\_aged\_discharge}(t_s) \le P_{ess\_aged\_discharge\_max}(t_s) \end{cases} . \qquad [2.41]$$

Each thermal generator is coupled with thermal storage (TES); the hourly mean power discharge is defined in Eq. 2.43 as the minimum among the discharge rate of the thermal power capacity and the thermal energy storage in the "*i*" tank.

Similarly, the hourly mean power charge can be defined as the minimum among the charge rate of the thermal power capacity, the remaining thermal energy storage to fill the *i*-tank as reported in Eq. 2.45.

$$P_{esth\_aged\_capacity,i}(t_s) = f\left(P_{esth\_rated\_capacity,i}(t_s), SoH_{esth,i}(t_s), \eta_{esth,i}\right), \quad [2.42]$$

$$P_{esth\_discharge,i}(t_s) = \begin{cases} P_{esth\_aged\_capacity,i}(t_s) \cdot C_{esth\_discharge\_rate,i}(t_s) \\ 0 \le P_{esth\_discharge,i}(t_s) \le P_{esth\_storage,i}(t_s) \end{cases}, \quad [2.43]$$

$$P_{esth\_aged\_charge\_min,i}(t_s) = \begin{cases} P_{esth\_storage,i}(t_s) - P_{esth\_aged\_capacity,i}(t_s) \\ P_{esth\_aged\_charge\_min,i}(t_s) < 0 \end{cases}, \quad [2.44]$$

$$P_{esth\_aged\_charge,i}(t_s) = \begin{cases} -P_{esth\_aged\_capacity,i}(t_s) \cdot C_{esth\_charge\_rate,i}(t_s) \\ P_{esth\_aged\_charge\_min,i}(t_s) \le P_{esth\_aged\_charge,i}(t_s) \le 0 \end{cases}. \quad [2.45]$$

2.4 Cost models and optimization of microgrid's operations

SLSQP is a sequential least squares programming algorithm that evolved from the least squares solver proposed by Lawson and Hanson in 1974 [23]. The optimizer uses the Han–Powell method and the Broyden–Fletcher–Goldfarb–Shanno (BFGS) update of the quasi-Newton Hessian approximation for non-linear programming (NLP) in the line search algorithm. Dieter Kraft [24] has originally applied in 1988 this algorithm to aerodynamic and robotic trajectory optimization.

The SLSQP method minimizes a function of several variables with any combination of bounds, equality- and/or inequality constraints. It can be used to solve linear and non-linear programming problems to minimize scalar functions. In this work, the off-the-shelf SLSQP optimizer available in SciPy has been used. SciPy [34] is a Python-based ecosystem of open-source software for science, and engineering.

In each time-step, SLSQP minimizes a non-linear objective function that contains costs and revenues, while the thermal and electric power and the interconnected energy

flows are balanced. The objective function is the difference between the sum of costs and revenues. The firsts are related to the energy inflows from DG to the MG, the energy to generate hydrogen, the purchase of energy from others MG and the main grid and the discharge of energy storage systems.

The revenues are inherent to the electric and thermal load consumptions, the sell-back of electricity and heat to other MG, the generation of water and carbon black by PEMFC-CHP, the delivery of energy services (load shedding, peak shaving, load shifting), the sell-back electricity to the main grid.

Costs and revenues are calculated as product between the LCOE (€/kWh), LSOE (€/kWh), and the related energy generated and consumed in each time-step.

LCOE is the ratio between the initial costs, the nominal operational and maintenance costs along the lifetime of the DER and the whole energy generated during the lifetime. The general expression of the objective function can be summarized as follows:

$$f(X) = \sum_{c=1}^{C} LCOE_c \cdot x_c - \sum_{r=1}^{R} LSOE_r \cdot x_r \,. \qquad [2.46a]$$

Where x_c, x_r (kWh) are the fractions of energy flows of the DER to optimize every time-step. The indexes *C, c* indicate the number of DER that generate costs; *R, r* the number of DER that generate revenues. The $X-array$ embeds the elements x_c, x_r as depicted in the following term:

$$X = \left[x_c(t_s)_1, \ldots, x_c(t_s)_C, \quad x_r(t_s)_1, \ldots, x_r(t_s)_R \right]. \qquad [2.46b]$$

The final profitability depends on the assumed values of the $X-array$. The elements of the $X-array$ are optimized for obtaining the highest profitability. The contribution to the profitability of each single element is detailed in the Paragraph 2.4.1.

The weights (i.e., LCOE, LSOE) direct the SLSQP algorithm to choose the optimal bounded value for every element of the $X-array$ to maximize the right terms ($LSOE_r \cdot x_r$) while minimizing the left terms ($LCOE_c \cdot x_c$).

In other words, SLSQP acts to better counterbalance the energy flows with the weight mechanism. The highest costs of generation are penalized while on the contrary, the highest revenue streams are prioritized.

The LCOE for each inlet thermal and electric *i*-DER can be obtained from the definition of LCOE:

$$LCOE_c = \frac{\sum_{j=1}^{n} \frac{C_j + O_j + F_j}{(1+r)^j}}{\sum_{j=1}^{n} \frac{P_j}{(1+r)^j}}, \quad [2.47]$$

where: C_j is the investment expenditures in year j (including financing), O_j is the operations and maintenance expenditures in year j, F_j is the fuel expenditures in year j (only for DG), P_j energy generation in year *j*; *r* is the discount rate and *n* is life of the system expressed in years.

It is relevant to note that the terms *LCOE* and *LSOE* embedded in the objective function (i.e., Eq. 2.46a) are computed with the nominal values of expenditures and energy generation thus, they are constants. At the exit of the loop of the time-steps optimizations, the financial models - that are discussed in the following Paragraph 2.4.4 - computes both terms again but with the actual costs and revenues deriving from the time-steps optimizations.

2.4.1 Cost models of distributed energy resources

This section details the cost and revenue terms incorporated in Eq. 2.46a.

The mean hourly costs of energy generated by the renewable energy sources (RES) is obtained as follow:

$$C_{res}(t_s) = \sum_{i=1}^{M} \frac{\sum_{j=1}^{n} \frac{C_{res,j,i} + O_{res,j,i}}{(1+r)^j}}{\sum_{j=1}^{n} \frac{P_{available,j,i}(t_s, \theta, \phi, \beta)}{(1+r)^j}} \cdot x_{res,i}(t_s), \quad [2.48]$$

where *i* is the type of electric RES (i.e., PV, WT) and ST.

The general expression of the costs and revenues for the thermal (TES) and electric (ESS) energy storages is denoted in the following Eq.2.49:

$$V_{es}(t_s) = \begin{cases} \sum_{t=1}^{T} \dfrac{\sum_{j=1}^{n} \dfrac{(C_{es,j,t} + O_{es,j,t})}{(1+r)^j}}{\sum_{j=1}^{n} \dfrac{P_{es\_rated\_discharge,j,t} \cdot \eta_t}{(1+r)^j}} \cdot x_{es,t}(t_s) & if \quad x_{es,t} \geq 0 \quad (discharge) \\ \sum_{t=1}^{T} \left[S_t(t_s) - \dfrac{\sum_{j=1}^{n} \dfrac{(C_{es,j,t} + O_{es,j,t})}{(1+r)^j}}{\sum_{j=1}^{n} \dfrac{P_{es\_rated\_discharge,j,t} \cdot \eta_t}{(1+r)^j}} \right] \cdot x_{es,t}(t_s) & if \quad x_{es,t} \leq 0 \quad (charge) \end{cases} .$$

The cost contribution of the thermal (i.e., EBOY, HP, STHP) and electric DG (i.e., PEMFC-CHP, OG) can be described as the following Eq.2.50a:

$$C_{dg}(t_s) = \sum_{g=1}^{G} \frac{\sum_{j=1}^{n} \dfrac{C_{dg,j,g} + O_{dg,j,g} + \dfrac{(C_{fuel,j,g} + C_{trp,j,g})}{V_{ed\_fuel,g} \cdot \eta_{dg,g}} \cdot P_{dg,j,g}}{(1+r)^k}}{\sum_{j=1}^{n} \dfrac{P_{dg,j,g} \cdot G_t}{(1+r)^j}} \cdot x_{dg,g}(t_s) \quad .$$

Here, g is the type of DG.

The parameter G_t is correlated to the "products" that are generated and it assumes a different value as follows:

$$G_t = \begin{cases} 1 & others \\ 2{,}5 & fuel \quad cell \quad system \quad (electric, \quad heat, \quad water) \end{cases} . \qquad [2.50b]$$

According to the research of K. D. Hristovski et al. in 2009 [25], the harvesting water from fuel cells should be considered as a by-product of operation.

The overall results of this study indicate that water generated from fuel cells is very pure, with contaminant levels lower than the MCL (Maximum Contaminant Level) values.

Typically, a fuel cell is operated at its peak power output, which corresponds to a current density of 1 A/cm^2, which results in a ratio of 0,5 l/kWh.

The costs and revenues associated to the exchange of electric and thermal energy among microgrids and main grid is represented in the following Eq. 2.51:

$$V_{grid}(t_s) = \begin{cases} \left[LCOE_{grid} + \dfrac{\sum_{j=1}^{n} \frac{C_{grid,j} + O_{grid,j}}{(1+r)^j}}{\sum_{j=1}^{n} \frac{P_{grid,j}}{(1+r)^j}} \right] \cdot x_{grid}(t_s) & if\ x_{grid} > 0 \\ \left[LSOE_{grid} - \dfrac{\sum_{j=1}^{n} \frac{C_{grid,j} + O_{grid,j}}{(1+r)^j}}{\sum_{j=1}^{n} \frac{P_{grid,j}}{(1+r)^j}} \right] \cdot x_{grid}(t_s) & if\ x_{grid} < 0 \end{cases} .$$

A variety of thermal and electrical loads are embedded in the CHP-MMG. These are the primary sources of the revenue stream. The expression to describe their economic contribution is denoted as follows:

$$R_{load}(t_s) = S_{th}(t_s) \cdot x_{th\_load}(t_s) + S_{el}(t_s) \cdot x_{el\_load}(t_s) \quad . \qquad [2.52]$$

Where $S_{th}(t_s)$ and $S_{el}(t_s)$ are the unit prices of the thermal and electric energy supplied to the end-user. The terms x_{th_load}, x_{el_load} are respectively the thermal and electric loads.

An additional source of revenues are the services to the main grid. Electric loads of MG can contribute to balance the main grid by taking part at demand response or frequency response markets. The framework of these programs foresees incentives and penalties to users when they provide additional power or they shape their consumption from the grid at peak periods.

The following Eq. 2.53 - 2.55 propose a scheme to calculate a revenues streams issued by grid services (DR):

$$R_{dra}(t_s) = P_{eldr\_load}(t_s) \cdot S_{eldr}(t_s) - (x_{el\_load}(t_s) - P_{eldr\_load}(t_s)) \cdot C_{dr}(t_s), \qquad [2.53]$$

$$R_{drb}(t_s) = x_{el\_load}(t_s) \cdot S_{eldr}(t_s) - (P_{eldr\_load}(t_s) - x_{el\_load}(t_s)) \cdot C_{dr}(t_s), \qquad [2.54]$$

$$R_{dr}(t_s) = \begin{cases} R_{dra}(t_s) & if \quad x_{el\_load}(t_i) > P_{eldr\_load}(t_i) \\ R_{drb}(t_s) & if \quad x_{el\_load}(t_i) < P_{eldr\_load}(t_i) \end{cases} , \qquad [2.55]$$

where P_{eldr_load} is the energy demanded by the main grid, S_{eldr} is the remuneration per kWh for the demand response service while C_{dr} is the penalty for exceeding energy absorbed by the electric loads.

These relations describe possible business scenarios to foster the diffusion of prosumers communities (those who consume and produce energy).

EC is a special internal load that absorbs electric energy to convert it into hydrogen, an energy carrier that can be converted later in electric energy. The term η_{he}represents the efficiency in the conversion of electric energy to hydrogen back and forward.

The contribution in term of revenue streams of the EC is expressed with the following Eq. 2.56:

$$R_{ec}(t_s) = \left[S_{el}\left(t_s\right) \cdot \eta_{he} - \frac{\sum_{j=1}^{n} \frac{(C_{ec,j} + O_{ec,j})}{(1+r)^j}}{\sum_{j=1}^{n} \frac{P_{ec,j}}{(1+r)^j}} \right] \cdot x_{ec}\left(t_s\right) . \qquad [2.56]$$

2.4.2 Objective function and constraints

In this section the terms of the non-linear objective function indicated in Eq. 2.46a are decomposed and thus the contribution to costs and revenues of each DER is indicated. The overall revenue streams $R(t_s)$ (€) generated by the thermal, electric loads, DR and EC every time-step are indicated as follow:

$$R\left(t_s\right) = R_{load}(t_s) + R_{ec}(t_s) + R_{dr}(t_s) . \qquad [2.57]$$

In addition to Eq. 2.57, grids sell-back and ES charging functions are further additional contributions to the revenues embedded in the "V" terms of the following Eq. 2.58. Therefore the objective function indicated in Eq. 2.46a can be expressed as follows:

$$f\,(x) = \left[C_{res}\left(t_s\right) + C_{dg}\left(t_s\right) \pm V_{es}\left(t_s\right) \pm V_{grid}\left(t_s\right) \right] \cdot k_c - R\left(t_s\right) \cdot k_r , \qquad [2.58]$$

where k_c, k_r are parameters to calibrate the weights of the two terms. The objective function in Eq. 2.58 is solved by keeping balanced the energy flows of the components

embedded in the *X-array* indicated in Eq. 2.46b. Here, is assumed the convention that the outer energy flows of each DER and MG are negative.

The unequal constraints Eq.2.59 are non-linear and respectively express the thermal and electric balances:

$$\begin{cases} \left[g_{el\_der}\left(t_s\right)\right] \cdot k_{der} - \left[g_{el\_load}\left(t_s\right)\right] k_l \geq 0 \\ \left[g_{th\_der}\left(t_s\right)\right] \cdot k_{der} - \left[g_{th\_load}\left(t_s\right)\right] k_l \geq 0 \end{cases}, \qquad [2.59]$$

where k_{der}, k_l are parameters to calibrate the two terms. The latter are detailed in the following Eq. 2.60 - 2.63:

$$g_{el\_der}\left(t_s\right) = \sum_{i=1}^{Me} x_{el\_res,i}\left(t_s\right) + \sum_{i=1}^{Te} x_{ess\_disch,i}\left(t_s\right) + \sum_{i=1}^{Ge} x_{el\_dg,i}\left(t_s\right) + x_{grid\_buy}\left(t_s\right)$$

$$g_{el\_load}\left(t_s\right) = \frac{\sum_{i=1}^{Ge} x_{th\_dg,i}\left(t_s\right)}{\eta_{dg\_thermal,i}} + x_{el\_load}\left(t_s\right) + x_{grid\_sellback}\left(t_s\right) + \sum_{i=1}^{Te} x_{ess\_ch,i}\left(t_s\right) + x_{ec}\left(t_s\right)$$

$$g_{th\_der}\left(t_s\right) = \sum_{i=1}^{Mh} x_{th\_res,i}\left(t_s\right) + \sum_{i=1}^{Th} x_{esth\_disch,i}\left(t_s\right) + \sum_{i=1}^{Gh} x_{th\_dg,i}\left(t_s\right) + k_{chp} \cdot x_{_{fc}}\left(t_s\right)$$

$$g_{th\_load}\left(t_s\right) = x_{th\_load,i}\left(t_s\right) + \sum_{i=1}^{R} x_{esth\_ch,i}\left(t_s\right) .$$

Where *Me, Te, Ge* are respectively subsets of electric RES, ES, DG, while *Mh, Th, Gh* are respectively subsets of thermal RES, ES, DG.

The following additional equality constraint is added for both thermal and electric energies, that is exchanged among the interconnected MG:

$$x_{itc\_i}(t_s) \cdot \left(1 - \eta_{itc}\right) + x_{itc\_j}(t_s) = 0 , \qquad [2.64]$$

where η_{itc} are the losses in the MG interconnections.

The elements of the *X-array* in Eq. 2.46b vary within the boundaries indicated in the following Eq. 2.65-2.69.

Their limits are dynamically shaped based on the available mean power that can be calculated with the model defined in Paragraph 2.3.

$$0 \leq x_{res,i}(t_s) \leq P_{res\_available,i}(t_s) \quad [2.65]$$

$$0 \leq x_{dg,i}(t_s) \leq P_{dg,i}(t_s) \quad [2.66]$$

$$P_{es\_aged\_charge,i}(t_s) \leq x_{es,i}(t_s) \leq P_{es\_aged\_discharge,i}(t_s) \quad [2.67]$$

$$P_{grid\_sellback}(t_s) \leq x_{grid}(t_s) \leq P_{grid\_buy}(t_s) \quad [2.68]$$

$$min(P_{el\_load}(t_s), \quad P_{eldr\_load}(t_s)) \leq x_{el\_load,i}(t_s) \leq max\left(P_{el\_load}(t_s), \quad P_{eldr\_load}(t_s)\right). \quad [2.69]$$

Where the subscript "*i*" indicates the *i*-DER.

In conclusion, both constraints and the objective function are non-linear. These functions are the sum of piecewise-linear functions. Moreover, it can be observed that all computed eigenvalues of the Hessian matrix of the objective function are null; thus, the convex property is proved. It is noteworthy to point out that, the SLSQP optimizer, specifically designed for NLP, enables to iteratively achieve the global minimum of a constrained non-linear convex optimization problem in a computationally efficient manner.

2.4.3 State of health of distributed energy resources

The optimal configurations of the X-array calculated each time-step by SLSQP, is used to update the States of Healths (SoH, %). SoH has a relevant role in the calculation of operational costs (OPEX). It is obtained as the ratio among the energy generated until the time-step and the potential energy that can be generated by the DER until the End of Life (EOL). The following Eq. 2.70-2.77 propose how to estimate SoH of RES, DG, and ES in a simplified manner:

$$SoH_{res,i}(t_s) = min\left(\sum_{h=1}^{s-1} \frac{x_{res,i}(t_h)}{E_{res\_available\_EOL,i}(\theta,\phi)}, \sum_{h=1}^{s-1} \frac{h_i(t_h)}{L_i}\right), \quad [2.70]$$

$$SoH_{dg,i}(t_s) = min\left(\sum_{h=1}^{s-1} \frac{x_{dg,i}(t_h)}{P_{dg,i} \cdot L_i}, \sum_{i=1}^{s-1} \frac{n_i(t_h)}{N_{cycles,i}}\right), \quad [2.71]$$

$$SoH_{esth,i}(t_s) = min\left(\sum_{h=1}^{s-1} \frac{x_{esth,i}(t_h)}{P_{esth,i} \cdot L_i}, \sum_{h=1}^{s-1} \frac{h_i(t_h)}{L_i}\right). \quad [2.72]$$

Where the subscript h is the time-step (one hour), L_i is the lifetime in hours of each DER, the term N_{cycles} represents the lifecycles, $n_i(t_h)$ is the n-cycle at the time-step t_i , while $h_i(t_h)$ is cumulative run-hour and $P_{dg,i}$ and $P_{esth,i}$ are the power size of the DER. $E_{res\_available\_EOL,i}$ (kWh) is the cumulative energy at end of life generable by the RES geo-localized at latitude θ, and longitude ϕ.

The State of Health (SoH) of the lithium battery is composed of two terms: the calendar lifetime and lifecycles. These empirical models proposed by R. B. Wright and C. G. Motloch of DOE in 2001[26][33] have been validated with test on commercial 18650 cylindrical cells type with cathodes of LiNiCo, carbon anodes and as electrolyte LiPF6.

The results of testing indicate that both the discharge and R-resistances increased with time at each percentage change (delta%) of the State of Charge (SOC). The magnitude of the discharge and resistance and the rate at which they changed depended on the temperature and delta% of SOC. The square root of time dependence can be accounted for by either a one-dimensional diffusion type of mechanism, presumably of the lithium ions, or by a parabolic growth mechanism for the growth of a thin film solid electrolyte interface (SEI) layer on the anode and/or cathode.

The functional form of the model of the R-resistances are given by the following Eq. 2.73 - 2.74:

$$R(t_s, T_{amb}, SOC_{ess})_{calendar} = \sum_{h=0}^{s-1} \left[a\left(SOC_{ess,h}\right) \cdot e^{\frac{E_{act\_acal}}{RT_{amb}(t_h)}} \cdot \sqrt[2]{t_h} + c\left(SOC_{ess,h}\right) \cdot e^{\frac{E_{act\_ccal}}{RT(t_h)}} \right]$$

$$R(t_s, T_{amb}, SOC_{ess}, \Delta SOC_{ess})_{lifecycle} = \sum_{h=0}^{s-1} \left[a\left(SOC_h, \Delta SOC_{ess,h}\right) \cdot e^{\frac{E_{act\_acy}}{RT_{amb}(t_h)}} \cdot \sqrt[2]{t_h} + c\left(SOC_h, \Delta SOC_{ess,h}\right) \cdot e^{\frac{E_{act\_ccy}}{RT(t_h)}} \right] ,$$

where *a, c* are constants; E_{act_acal}, E_{act_ccal}, E_{act_acy}, E_{act_ccy} are further constants related to the activation energy. These parameters can be obtained thru characterization tests. T_{amb} is the environment temperature dataset while R is the gas constant and $\Delta SOC_{ess,h}$ is the state-of-charge swing during the cycling.

Based on the R-resistances terms, the contribution of calendar lifetime and lifecycles to SoH can be computed as follows:

$$SoH_{ess}\left(t_s\right)_{calendar} = 1 - \frac{R(t_s, T_{amb}, SOC_{ess})_{calendar}}{R_{calendar\_max}}, \quad [2.75]$$

$$SoH_{ess}\left(t_s\right)_{lifecycle} = 1 - \frac{R(t_s, T_{amb}, SOC_{ess}, \Delta SOC_{ess})_{lifecycle}}{R_{lifecycle\_max}}. \quad [2.76]$$

After the calculation of the above terms, the State of Heath of the lithium battery is defined as follows:

$$SoH_{ess}\left(t_s\right) = min\left(SoH_{ess}\left(t_s\right)_{calendar}, SoH_{ess}\left(t_s\right)_{lifecycle}\right). \quad [2.77]$$

2.4.4 The financial models

The SoH is used to calculate the replacement costs (REPEX), added to OPEX, and initial costs (CAPEX) to obtain the *TCO* (€). At the end of the calculation of all time-step, the yearly TCO is obtained by the following Eq. 2.78:

$$TCO_t = \sum_{j=1}^{J}\sum_{h=1}^{8760}\left[\left(N_{der,j}\left(t_h\right) + 1 - SoH_j\left(t_h\right)\right)\cdot C_{der,j} + O_{der,j}\left(t_h\right) + \frac{\left(C_{fuel,j}\left(t_h\right) + C_{trp,j}\left(t_h\right)\right)}{V_{ed\_fuel,j}\cdot\eta_{dg,j}}\cdot P_{dg,j}\left(t_h\right)\right].$$

The yearly energy generated (E_t), consumed by thermal and electrical loads, and sell-back is given by Eq. 2.79:

$$E_t = \sum_{j=1}^{J}\sum_{h=1}^{8760}\left[x_{th\_load,j}\left(t_h\right) + x_{el\_load,j}\left(t_h\right) + x_{th\_sellback,j}\left(t_h\right) + x_{el\_sellback,j}\left(t_h\right)\right].$$

The expression of the yearly revenue stream is obtained as contributions of each DER in the following Eq. 2.80:

$$R_t = \sum_{j=1}^{J}\sum_{h=1}^{8760}\left(R_{th\_load,j}\left(t_h\right) + R_{el\_load,j}\left(t_h\right) + R_{th\_sellback,j}\left(t_h\right) + R_{el\_sellback,j}\left(t_h\right) + R_{dr}\left(t_h\right) + R_{water}\left(t_h\right)\right),$$

where *j* and *J* identify the type of DER, *h* is the index of time-step, N_{der}, C_{der}, O_{der} are respectively the replaced number, the capital expenditures, operating expenditures of DG,RES, ES, EC and INV. After the first year, the time of calculation can be reduced

with a one-dimensional polynomial regression to extrapolate *TCO*, *E* and *R* over the timeframe of the project.

The Internal Rate of Return (*IRR, %*) is then computed by solving:

$$\sum_{t=0}^{M} \frac{-\sum_{j=1}^{J} C_{der,j} + R_t}{(1+irr)^t} = 0 \,. \qquad [2.81]$$

NPV (€) of the cash flow generated during the project is returned by:

$$NPV = \sum_{t=0}^{M-1} \frac{-\sum_{j=1}^{J} C_{der,j} + R_t}{(1+r)^t} \qquad . \qquad [2.82]$$

Where *t* identifies the year of the project, *M* are the total years of the project.

2.5 A general architecture of CHP-MMG microgrids

Figure 2.2 depicts the overall scheme of the CHP-MMG. The labeled boxes represent the techno-economic models of the DER. The red lines indicate the thermal network while the blue lines represent the electric network.

The two CHP-MMG exchange electrical energy thru the ITCEL device and the thermal energy thru the ITCH device. Each MG independently exchanges electrical energy to the main grid (GRID).

The generation of energy from renewables is represented with the labels: PV (photovoltaic panels), WT (Wind turbines) and ST (Solar thermal collectors). Fuel cells (FC) and OG (traditional gensets) are the further options for distributed generations.

The electrical energy storage of energy is represented with the label ESS. Moreover, several thermal storages are indicated here with the initials ‘TK’ (i.e., tanks) followed by the name of the correspondent thermal generator. For example, the storage of hydrogen is indicated with the label ‘TKFC’.

The conversion from electrical to thermal energy occurs with two different type of thermal distributed generators: the electric boilers (EBOY) and the heat pumps (HP, STHP). The conversion for electricity to hydrogen occurs with the electrolyzers that are labeled: ‘EC’ while the DG labeled 'FC' are the fuel cells, converting the hydrogen into electricity and heat.

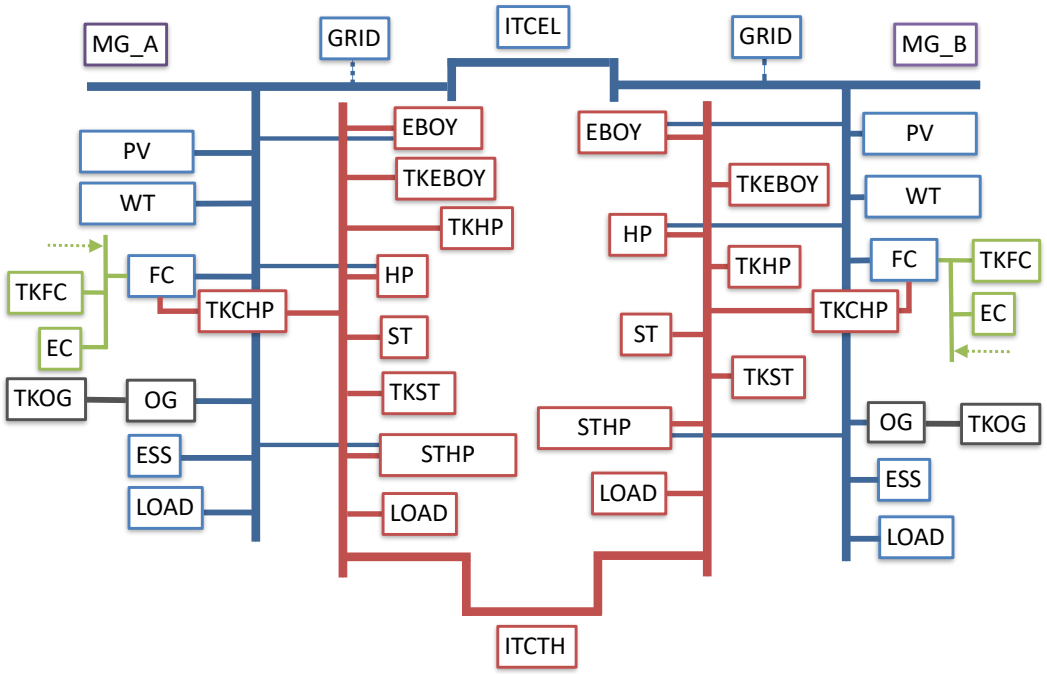

Figure 2.2 *The overall architecture of two CHP-MMG comprising 36 DER, 2 electrical, thermal loads*

The overall techno-economic model consists of 38 variables that need to be optimized to return the minimum levelized cost of energy (LCOE) and maximum internal return rate of investment (IRR). The 38 variables are listed in Appendix A.2 and they are grouped into two different categories: the fist group of 36 variables are the size of the Distributed Resources (DR) while the remaining 2 variables identify the geographic location in terms of latitude and longitude (i.e., the siting). The techno-economic models described in Paragraph 2.3 are also used to compute the generation, storage, conversions of thermal and electric energy delivered by each DR labeled in Figure 2.2.

Moreover, the techno-economic models are used to calculate the exchange of thermal, electrical, chemical energies between the two CHP-MMG under the minimum and maximum boundaries imposed by the size, the age of each DER or the available energy from renewables each time-step.

The equations in the Paragraph 2.4.1 and Paragraph 2.4.2 are used to compute every time-step the economic contribution of each DER labeled in Figure 2.2 to the energy

balances, while the SLSQP algorithm minimizes the cost-profit objective function. The equations in the Paragraph 2.4.3 are used to compute the state of health of each DER labeled in Figure 2.2 and the equations of the Paragraph 2.4.4 are used for the final computation of the financial terms (NPV, IRR).

As highlighted in Paragraph 1.3, the optimal setting for the 38 variables is obtained as a solution of a highly non linear and non-convex problem requiring stochastic optimization techniques. A novel evolutionary optimization algorithm based on the innovative ADE/AIE genetic algorithms has been proposed and validated. A detailed description is given in the following Chapter 4.

The following Paragraph 2.6, provides the results of the study carried on to investigate how the scheme of collaboration between the two microgrids (i.e.,'swarm effect') based on an optimal combination between conversions and exchanges of thermal, electrical, and chemical energies to obtain the best financial performances. In Chapter 6 a scheme of swarm effect is discussed.

The overall results demonstrate the benefit of interconnecting MG. Crossflows of thermal and electrical energies allow to convert and share fraction of the exceeding energy between the two MG and thus DR may be downsized. For example, abundant electricity not used to power loads or charge batteries in a certain time interval is transferred to the other MG to be converted into heat energy. Then, some of the heat returns to the other microgrid.

2.6 Results and discussion

2.6.1 Manipulation of climate datasets

The techno-economic model and optimization algorithm have been implemented into a Python® script. The FFT-IFFT method, utilized to manipulate original ECMWF datasets of the period from June 2017 to June 2018 has been implemented with the NumPy's, SciPy, Sklearn, and Matplotlib libraries.

The reference location for this work is nearby the city of Bremen, with latitude: 53.0758196 and longitude: 8.8071646. Firstly, FFT-IFFT was used to extrapolate a first training dataset based on the original series, a second one based on monthly averages and a third generated with the low pass filter (LPF) cutting off frequencies respectively: 1,16 [2.Hz] for radiance, cloud cover; 2,83 [2.Hz] for temperature. The performances of the three training curves, were measured with R^2 index. The low pass filter results the best method to predict the radiance; cloud cover, temperature and wind speed, are best predicted with monthly average datasets.

To use the regression method in alternative to FFT-IFFT, the pairwise correlations among variables (i.e., Figure 2.3) has been computed with the Pearson coefficient method.

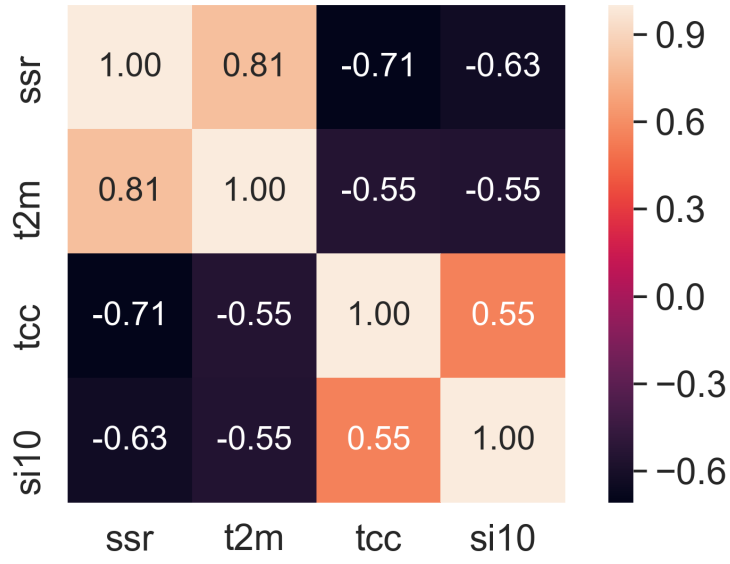

Figure 2.3 *Pearson product-moment correlation coefficients*

The best-fitting linear correlation is among the radiation and the other climate variables that are characterized by values higher than 0,6. From Pearson's relation it is obvious to implement a linear regression model for those variables to reduce the script runtime. The results delivered with linear, quadratic and cubic polynomial regressions as in Figure 2.4 were evaluated. The R^2 (0,65) equal for all degree of regressions, confirm the strong linear correlation between these coupled variables. A good level of accuracy obtained with the climate datasets has allowed to obtain an equally sound estimation of the energy generated by RES.

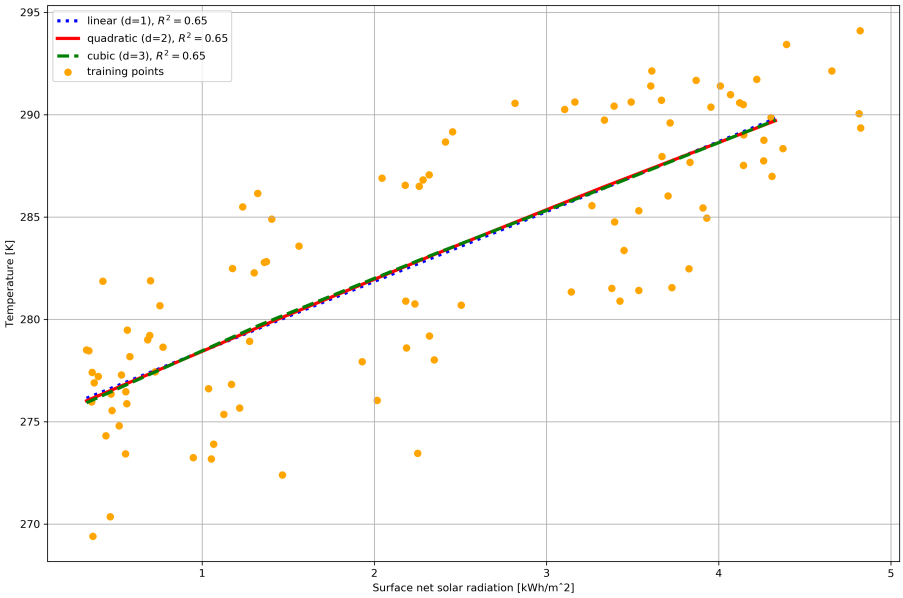

Figure 2.4 *Polynomial regressions and performance of two variables with a strong linear interrelation*

2.6.2 Inputs of the interconnected microgrids

This further part of the work concerns two interconnected community MG (MG_A, MG_B) located in the reference location of Paragraph 2.6.1. In the following example, these MG offer a way for two neighborhoods, to meet their thermal and electric energy needs. The following scenarios are discussed with investment (i.e, CAPEX) and operation and maintenance (i.e, OPEX) unit cost (i.e., €/kWh) in accordance with the technology cost database of the EnergyPLAN model [36].

DER	Interconnected		Not Interconnected		Only Main grid		Lifetime
	MG_A	MG_B	MG_A	MG_B	MG_A	MG_B	
PV	9 kW	5 kW	15 kW	5 kW	-	-	20 years
WT	9 kW	5 kW	100 kW	5 kW	-	-	20 years
ESS	3 kWh	3 kWh	6 kWh	4 kWh	-	-	8 yeas / 6.000 cycles
FC	100 kW	3 kW	81 kW	3 kW	-	-	15.000 hours / 10.000 start-stops
EC	1 kW	1 kW	1 kW	1 kW	-	-	13.000 hours / 9.000 start-stops
GRID	23 kW	69 kW	150 kW	150 kW	300 kW	300 kW	
ITCEL	78 kW	78 kW	-	-	-	-	25 years
ST	4 kW	-	170 kW	36 kW	-	-	20 years
EBOY	-	1 kW	200 kW	200 kW	300 kW	300 kW	45.000 hours
STHP	157 kW	-	1 kW	43 kW	-	-	80.000 hours
ITCTH	276 kW	276 kW	-	-	-	-	25 years
Tank EBOY	-	16.581 lt	30.000 lt	30.000 lt	30.000 lt	30.000 lt	90.000 hours
Tank ST	200 lt	-	15.000 lt	28.000 lt	-	-	90.000 hours
Tank CHP	30.000 lt	-	-	-	-	-	90.000 hours

Table 2.1 *Rounded size of DER in the three simulated different scenarios*

Power sizes of the clean DER populating the two MG are described in Table 2.1. Three different scenarios have been investigated. In the first scenario (Interconnected), an optimized combination of DER is distributed in two interconnected MG: in MG_A, RES and PEMFC-CHP have a more pronounced role in the generation than the other MG; in MG_B, the main grid (GRID) is the main external source of electric energy.

The backbone of the thermal (ITCTH) and electric (ITCEL) interconnections releases significant energy flows between the two MG. The DER configurations of this scenario have been selected among 7.000 trials giving the best combination of IRR and LCOE when the operations are managed by the SLSQP algorithm.

In the second scenario (Not_Interconnected), the absence of interconnections is compensated with a larger power size delivered through the grid utility (GRID) and RES. Also, thermal DER such as ST, EBOY have thermal storages (Tank ST, Tank EBOY) have a markedly higher size than the previous scenario.

In the third scenario (i.e.,“Only main grid”), the loads profiles are powered primarily by the grid utility; EBOY convert electric energy into thermal energy combined with thermal storage. This scenario simulates a typical residential power system of today.

In all these three scenarios, each MG is feeding the same thermal, electric load profiles which are resulting from the aggregation of 10–12 households. Figure 2.5a-2.5b

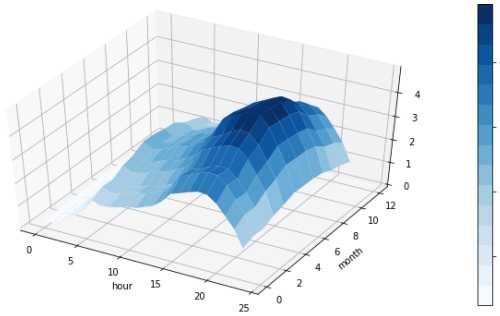

Figure 2.5a *Aggregate yearly electric load profile*

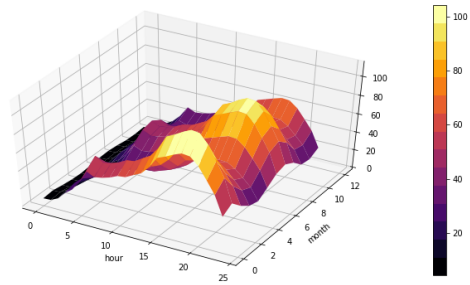

Figure 2.5b *Aggregate yearly thermal load profile*

shows the two hourly mean power profiles in each month. The mean daily monthly electric loads is ranging between 43 and 70 kWh while the mean daily monthly thermal loads is ranging between 350 and 800 kWh. Working days and weekends are built from different profiles having a different weighting (the energy is split 70% in working day 30% non-working day, respectively). The periodic peak daily electric load demand is in the second quarter, while the periodic peak daily thermal load demand is in the first (heat) and second (cool) quarter. Stochastic thermal and electric profiles have been generated with the "Gauss Markov" algorithm.

The simulations of the revenue streams consider except for the loads the delivery of demand response services and energy sell-back to a local electric utility. The demand

Service	**Price**	
	MG_A	**MG_B**
Electric energy to user	38 c€/kWh	
Thermal energy to user	22 c€/kWh	
Sellback of electric energy to grid utility	11 to 18 c€/kWh	
Demand response to grid utility	- 5 to 28 c€/kWh	
Sellback of electric energy among MG	28 c€/kWh	5 c€/kWh
Sellback of thermal energy among MG	18 c€/kWh	5 c€/kWh
Water	15c€/lt	

Table 2.2 *Price structure of the energy demand services*

response profiles have been simulated with 5% maximum value for load shedding, 25% for peak reduction, and 15% for peak hours per month.

The price structure of the services offered to the users, the electric utility and exchanges between the two MG are shown in Table 2.2. The calculation of the hourly mean available energy from solar radiation and wind, has been executed with the power losses inputs described in Table 2.3.

	PV	**ST**	**WT**
Solar Panel Yield	16%	90% @10 dT	
Temp Losses	5%		
DC Cables Losses	1%		
MPPT Losses	6%		6,0%
AC/DC Cables Losses	1%		1,0%
Shading Losses	1%	5%	
Dust Losses	0%	0%	
Other Losses	0%	1%	1,0%
BoP Losses		6%	
TILT Optimal	40,32°		

Table 2.3 *Main power losses and yields of RES*

The hourly data-frame of the environmental temperature is extrapolated with Eq. 2.17. The ESS is characterized by a charge/discharge profile (0.25C for charge and 0.5C for discharge), a round trip efficiency (98%), deep of discharge (3–98%). The performance curve of the battery in relation to the temperature is utilized to obtain the hourly aged capacity of the ESS with Eq. 2.36 - 2.39.

In these simulations, RES are coupled with PEMFC-CHP. The latter DG converts the whole chemical energy of hydrogen into electricity and heat and so the efficiency goes up to 95%. Hydrogen tanks at 200 bars are chosen to feed the FC. The fuel is transported once a day. The cost for hydrogen, including the transportation, considered in the simulation is: 3,00 €/kg_{H2}. This value is coherent to the report published in January 2020 by the Hydrogen Council [27]. The cost of renewable hydrogen produced from offshore wind in Europe starts at about 6,00 €/kg_{H2} in 2020. This rate is expected to decline by about 60% by 2030 to approximately 2,50 €/kg_{H2}.

In the simulated scenarios where FC is installed, the hydrogen is partially generated on-site by a PEM electrolyzer (PEMEC), integrated to a 200 Bar pressurized hydrogen tank. Typical commercial electrolyzer system efficiencies are 56–73% and this corresponds to 70–53 kWh/kg_{H2} [28]. An additional thermal tank is part of the configuration to storage the heat. The EC incorporates a solid proton-conducting membrane rather than the aqueous solution. This type of EC generates pressurized hydrogen and consequently reduces compression losses. The electrolyzer system efficiency considered in the simulations is 53 kWh/kg_{H2} at nominal power.

The thermal energy is also generated by ST integrated with further thermal storage tanks and auxiliary HT which are powered by electric energy, with efficiency at 400%. At each time-step, the SLSQP optimization algorithm secures the minimum of the non-linear objective function (Eq. 2.58) by choosing the highest energy contribution of RES, DG, and ES with the lowest nominal LCOE and maximizing the contribution of those DER that in opposite, provide the highest revenues streams.

2.6.3 Discussion of the results

Table 2.4 reports the cumulative energy flows among DER of three alternative scenarios. Among the loads, the thermal loads account for 95%. The demand of energy of the loads is the main decision driver of SLSQP in the use of the available distributed power sources in all scenarios. It can be argued that the remuneration attributed to the thermal and electric loads, influences the optimization strategy of SLSQP.

In the first scenario, where the two hybrid MG are interconnected, PEMFC-CHP is the main thermal and electric generation unit in conjunction with WT.

The actual LCOE (resulting after the optimization of the operations) in Table 2.5, reflect the strategy deployed by SLSQP at each time-step. Based on today manufacturing costs [29], PEMFC-CHP returns a cost of energy lower than utility grid (GRID). Whether all the available power generated by RES is provided, then it becomes more convenient produce the additional required energy with the hybrid fuel cell.

The PEMFC-CHP is able to generate electric energy at the most economical way but also is capable to produce thermal energy and water without any additional cost. The PEMFC-CHP and RES in MG_A are fulfilling not only the internal ED of thermal and electric loads and water, but their power sources are also able to deliver energy services (through both MG) and electric energy sell-back to the grid utility. This happens, by

transferring large amounts of thermal and electric energy from MG_A to MG_B (ITCEL_sellback, ITCTH_sellback of MG_A in Table 2.4). The flows of energy among the interconnections are fostered by the price policies described in Table 2.2. In this example, the prices for energy interflows are in favor of MG_A. In other words, the backbones of electric and thermal energy among MG are substituting the role of large energy storages transferring energy instead of deferring it, at most economic conditions.

The second scenario (Not_Interconnected) shows a different configuration and approaches to satisfy the ED. In MG_A, the energy is mainly dispatched with PEMFC-CHP in combination with WT.

Distributed energy sources	**Interconnected**		**Not Interconnected**		**Only Main grid**	
	MG_A (kWh)	**MG_B (kWh)**	**MG_A (kWh)**	**MG_B (kWh)**	**MG_A (kWh)**	**MG_B (kWh)**
PV	984	1.446	4.257	1.555	-	-
WT	30.432	16.825	352.851	17.643	-	-
ESS discharge	1.898	2.624	6.063	1.108	-	-
FC electric energy	792.185	5.921	545.966	9.882	-	-
Grid buy	8.456	11.782	45	451.257	514.225	513.605
ITCEL buy	10.943	469.857	-	-	-	-
ST	1.954	-	71.434	16.263	-	-
EBOY	-	2.055	4	140.514	456.373	456.334
STHP	140.233	-	9	287.752	-	-
FC thermal energy	831.794	6.217	573.264	10.376	-	-
ITCTH buy	236	449.502	-	-	-	-
Tank EBOY discharge	-	1.284	431.633	3.087	1.701	1.701
Tank ST discharge	26.591	-	88.488	3.132	-	-
Tank thermal energy FC discharg	291.609	-	-	-	-	-
Electric loads	19.796	19.065	26.660	19.145	19.600	19.060
EC	5.993	4.466	1.457	-	-	-
ESS charge	1.898	2.623	6.059	1.105	-	-
Grid sell	181.278	467.003	873.014	91	-	-
ITCEL sell-back	484.380	11.274	-	-	-	-
Tank EBOY charge	-	340	562.171	1.389	2	1
Tank STHP charge	27.124	-	87.531	1.376	-	-
Tank Thermal FC charge	289.924	-	-	-	-	-
Thermal loads	431.839	428.407	432.386	428.099	428.107	428.071
ITCTH sell-back	483.223	253	-	-	-	-

Table 2.4 *Cumulative energy exchanged among DER in the three scenarios*

DER	MG_A (€/kWh)	MG_B (€/kWh)
PV	0,390	0,254
WT	0,132	0,096
ESS	0,182	0,110
FC	0,144	0,186
EC	0,054	0,063
GRID	0,690	1,140
ST	0,130	-
EBOY	-	0,034
STHP	0,057	-

Table 2.5 *Actual values of LCOE of RES and DG in the interconnected scenario*

Compared to the scenario dealing with interconnected MG, the contributions of RESs (namely WT and ST) are equivalent to PEMFC-CHP. The exceeding thermal energy, which is not used and cannot be transferred to the other MG, is stocked in large tanks (Tank_Boiler, Tank_ST) by heating water as storage medium; hence the stored energy can be used at a later time.

The load-exceeding available electric energy supplied by PEMFC-CHP is given in sell-back to the utility grid. Thus, this optimized scenario does not consider large ESS. The demand of energy for MG_B of this second scenarios is satisfied with an approach similar to a traditional power system. In fact, the main source of electricity is the grid utility. The electric energy is then converted into thermal energy with an EBOY in combination with a HP.

In the third scenario, both thermal and electric loads are powered solely by the utility grid and EBOYs. This is a typical actual electric system, where loads do have not a peer-to-peer interconnection to RES through MG. The financial impact of the dispatching strategy is indicated in Table 2.6.

In conclusion, revenues of the interconnected scenario are higher than the other. In MG_A of this first scenario, 25% of the revenue stream is generated by the loads, 14% by water, and 54% by sell-back to the other MG. In MG_B, 57% of revenues comes from the loads and 39% to sell-back to the utility grid. The sale strategy implemented by SLSQP, allows to obtain the highest revenue streams with the lowest initial capital investment (CAPEX) in the interconnected scenario compared with that in the not interconnected one. Consequently, the contribution margin, calculated by deducing the

DER	Interconnected				Not Interconnected				Main Grid (Not MGs)			
	CAPEX MG_A	OPEX MG_A	CAPEX MG_B	OPEX MG_B	CAPEX MG_A	OPEX MG_A	CAPEX MG_B	OPEX MG_B	CAPEX A	OPEX A	CAPEX B	OPEX B
PV	2.087	332	1.152	183	3.500	525	1.100	175	0	0	0	0
WT	19.896	389	11.000	215	220.000	4.300	11.000	215	0	0	0	0
ESS	1.230	4	1.230	4	2.400	7	1.500	4	0	0	0	0
FC	230.000	162.252	6.900	1.372	187.000	109.704	7.000	2.190	0	0	0	0
EC	600	60	600	60	600	60	600	60	0	0	0	0
GRID	5.676	5.369	17.254	11.870	37.500	18.011	37.500	148.863	75.000	185.121	75.000	185.000
ITCEL	7.836	1.527	7.836	132.539	0	0	0	0	0	0	0	0
ST	1.291	202	-	0	55.000	8.499	11.000	1.750	0	0	0	0
EBOY	-	-	193	64	30.000	9.999	30.000	9.999	45.000	14.998	45.000	14.998
STHP	20.427	1.571	-	0	130	10	5.500	430	0	0	0	0
ITCTH	10.355	3.463	10.355	84.362	0	0	0	0	0	0	0	0
Tank EBOY	-	-	8.291	166	15.000	300	15.000	300	15.000	300	15.000	300
Tank ST	95	2	-	0	8.000	155	14.000	281	0	0	0	0
Tank CHP	18.000	300	-	0	-	-	-	-	-	-	-	-
TCO	**492.964**		**295.646**		**710.700**		**298.467**		**335.419**		**335.298**	
Revenue	**416.466**		**176.742**		**282.284**		**107.524**		**107.113**		**106.722**	

Table 2.6 *Rounded initial, yearly operational costs and revenue stream in € of the three scenarios*

total costs is considerably higher when the two MG are interconnected.

These considerations are finally synthesized in Table 2.7 with key financial ratios. The limited number of investments involving the first scenario leads to a very attractive IRR (54%) and a relevant amount for the NPV (calculated with discount rate of 5%). Actual LCOE resulting from the final calculation of CAPEX and OPEX as an aggregation of DER is much lower than actual grid purchase costs in Germany [38]. Payback (years to recuperate from operations in form of cash inflow the total amount invested) calculated for these MG is less than two years. In the other scenarios, the return of investments is null, and the cost-profit structure of the business leads to a negative NPV.

Financial ratio	**Interconnected**		**Not Interconnected**		**Only Main grid**	
	MG_A	**MG_B**	**MG_A**	**MG_B**	**MG_A**	**MG_B**
IRR	54%	65%	10%	0%	0%	0%
LCOE	0,16 €/kWh	0,14 €/kWh	0,19 €/kWh	0,43 €/kWh	0,49 €/kWh	0,5 €/kWh
RES factor	6%		51%		0%	

Table 2.7 *Key financial ratios of the three scenarios (25 years project lifetime, 5% discount rate)*

Finally, it should be noted that the RES fraction (calculated as the ratio between the energy generated by the RES and the load consumptions) in the interconnected MG, results in 6% of the entire generated energy. However, if the fraction of the on-site hydrogen production is added and moreover it is assumed that the further hydrogen demand is sourced by large wind and solar farms (green hydrogen), the contribution of RES is almost 100%. These simulations demonstrate that optimization strategies implemented via SLSQP algorithm in hybrid interconnected MG leads to a very attractive IRR and, short-term paybacks while contributing to strengthen the resilience of power systems. Optimal configurations of hybrid DER in multiple MG can operate at lower LCOE than the current tariff offered today from the utilities.

Thus, interconnected hybrid MG with SLSQP optimization techniques makes renewable and DER outcompeting. They are a viable route to foster the transition to the low-carbon energy paradigm and they can strand investments in fossil fuel generation.

2.7 Conclusions

This chapter has introduced an optimization method based on SLSQP to secure the best economic performances of interconnected hybrid MG. The algorithm minimizes at every time-step a piecewise-linear convex objective function that incorporates the weighted contributions in terms of costs and revenues of DG, loads, and MG interconnections.

The nominal LSOE are the weights for the revenues terms of the objective function. Thermal and electric energy balances are the non-linear constraint functions. The SLSQP algorithm finds efficiently at each iteration the global solution of this non-linear constrained convex optimization problem.

The optimizer is embedded into a techno-economic model designed to shape dynamically the boundaries of the objective function. Moreover, the algorithm computes the states of DER and at the end, it returns the actual values of the key financial ratios.

The proposed techno-economic model starts with the manipulation of climate datasets by combining FFT function with the IFFT. The aim is to achieve an accurate extrapolation of reanalyzed climate datasets issued by ECMWF over the project lifetime.

A method to identify linear correlations among coupled datasets has been developed to predict temperature from solar radiation with less computing resources. The climate datasets feed the stochastic models in forecasting renewable thermal and electric generation.

Subsequently, a stochastic model based on the Gauss Markov function has been introduced to simulate hybrid loads profiles. Similarly, load shedding and load shifting have been implemented to simulate the ED response to disturbances of the main grid.

The proposed tool has proven to be very effective in simulating innovative business scenarios in which multiple revenue streams are generated from the sales of energy to end-users, from further sales to the other energy networks and from deliveries of energy services to the grid utility.

In particular, the techno-economic simulator was used to analyze the financial performances of three different scenarios. The outcomes demonstrate the economic advantages of interconnected hybrid MG which are operated with an SLSQP algorithm.

The optimal scenario is compared to an alternative configuration of two not connected MG and another configuration where the loads are solely powered by the grid utility.

All these simulations deal with both thermal and electric loads profiles of household communities located nearby the city of Bremen. With a payback within two years and an IRR at 65%, the first scenario results in a LCOE of 0,14 €/kWh.

This value leads also to the conclusion that interconnected hybrid MG can operate at costs that are lower than a current typical utility tariff if an adequate mechanism of remuneration among prosumers and the utility grid is provided.

The overall results of this chapter demonstrate that the discussed multi-microgrids are very competitive options against the actual centralized large power networks.

2.8 References

[1] Eliasen E.,Machenhauer B., Rasmussen E., 1970, On a numerical method for integration of the hydrodynamical equations with a spectral representation of the horizontal fields. Report 2, Institut for Teoretisk Meteorologi, University of Copenhagen, https://ci.nii.ac.jp/naid/10003554485/en/

[2] Orszag S.A., 1970, Transform method for calculation of vector coupled sums: application to the spectral form of the vorticity equation. J. Atmos. Sci., 27, pp. 890–895, DOI: https://doi.org/10.1175/1520-0469(1970)027<0890:TMFTCO>2.0.CO;2

[3] Voldoire M.J.A., 2009, Role of the Gulf of Guinea in the inter-annual variability of the West African monsoon: what do we learn from CMIP3 coupled simulations?, Int. J. Climatol. 30 pp.1843–1856

[4] Kent E.C.,Fangohrb S.,Berrya D.I., 2013, A comparative assessment of monthly mean wind speed products over the global ocean. Journal of Climatology 33, pp.2520–2541

[5] Wang A.,Zeng X., 2015, Global hourly land surface air temperature datasets: inter-comparison and climate change, International Journal of Climatology, 35, 13, pp.3959-3968

[6] Amendola S., Maimone F., Pasini A.,Ciciulla F.,Pelinod V., 2017, A neural network ensemble downscaling system (SIBILLA) for seasonal. Meteorol. Appl. 24, pp 157–166

[7] Benjamin Y.H. Liu, Richard C. Jordan,The interrelationship and characteristic distribution of direct, diffuse and total solar radiation,Solar Energy,Volume 4, Issue 3,1960,Pages 1-19,ISSN 0038-092X, https://doi.org/10.1016/0038-092X(60)90062-1.

[8] Garg H.P.,Garg S.N., 1985, Correlation of monthly-average daily global, diffuse and beam radiation with bright sunshine hours, Energy Conversion and Management, Volume 25, Issue 4, pp. 409-417

[9] P.C. Jain, Estimation of monthly average hourly global and diffuse irradiation, Solar & Wind Technology, Volume 5, Issue 1, 1988, Pages 7-14, ISSN 0741-983X, https://doi.org/10.1016/0741-983X(88)90085-9.

[10] Konstantinos, K. 2017, Welcome to enlopy's documentation!, Version 0.1.dev9, https://enlopy.readthedocs.io/en/latest/

[11] Shouxiang Wang, Xiguang Fan, Liang Han & Leijiao Ge (2015) Improved Interval Optimization Method Based on Differential Evolution for Microgrid Economic Dispatch, Electric Power Components and Systems, 43:16, 1882-1890, DOI: 10.1080/15325008.2015.1057783

[12] Radosavljević J.,Jevtić M.,Klimenta D., 2015, Energy and operation management of a microgrid using particle swarm optimization,Journal Engineering Optimization, pp. 811-830

[13] Soares A., Gomes Á., Henggeler Antunes C. (2017) An Evolutionary Algorithm for the Optimization of Residential Energy Resources. In: Bertsch V., Fichtner W., Heuveline V., Leibfried T. (eds) Advances in Energy System Optimization. Trends in Mathematics. Birkhäuser, Cham. https://doi.org/10.1007/978-3-319-51795-7_1

[14] Jamaledini, Ashkan, Khazaei, Ehsan, Toran, Mehdi (2018): Modified Genetic Algorithm Framework for Optimal Scheduling of Single Microgrid Combination with Distribution System Operator, MPRA Paper No. 89411, https://mpra.ub.uni-muenchen.de/89411/

[15] Nagapurkar P., Smith, J.D., 2019, Techno-economic optimization and social costs assessment of microgrid-conventional grid integration using genetic algorithm and Artificial Neural Networks: A case study for two US cities, Journal of Cleaner Production, Volume 229, Pages 552-569, ISSN 0959-6526, https://doi.org/10.1016/j.jclepro.2019.05.005

[16] Cooley J.,Tukey, 1965, An algorithm for the machine calculation of complex Fourier series, Math. Comp. 19 (1965), 297-301, https://doi.org/10.1090/S0025-5718-1965-0178586-1

[17] Press W., Teukolsky S.,Vetterline W.T., Flannery B.P., 2007, Numerical Recipes: The Art of Scientific Computing, ch. 12-13. Cambridge Univ. Press, Cambridge, UK

[18] Khatib T.,Elmenreich W., 2015, A Model for Hourly Solar Radiation Data Generation from Daily Solar Radiation Data Using a Generalized Regression Artificial Neural Network, International Journal of Photoenergy, Volume 2015, Article ID 968024

[19] Raschka S., Python Machine Learning, 2015, pp.280-297

[20] Liaw A.,M.Wiener M. ,2002, Classification and Regression by random, Forest, Vol. 2/3, ISSN 1609-3631, pp.. 21-22

[21] Luque A.,Hegedus S., 2011, Handbook of Photovoltaic Science and Engineering, ed.2, pp. 1012-1016

[22] Breipohl A.M., Lee F.N., Zhai D.,Adapa R.,1992, A Gauss-Markov oad model for the application in risk evaluation and production simulation, Transactions on Power Systems, 7 (4) , pp. 1493-1499

[23] Lawson C., Hanson R., 1974, Solving Least Squares Problems, volume 161, SIAM

[24] Kraft D (1988) A software package for sequential quadratic programming. Tech Rep DFVLR-FB 88-28, DLR German Aerospace Center—Institute for Flight Mechanics, Köln, Germany

[25] Kiril D. Hristovski, Brindha Dhanasekaran, Juan E. Tibaquirá, Jonathan D. Posner, Paul K. Westerhoff; Producing drinking water from hydrogen fuel cells. Journal of Water Supply: Research and Technology-Aqua 1 August 2009; 58 (5): 327–335. doi: https://doi.org/10.2166/aqua.2009.103.

[26] Wright, Randy Ben, and Motloch, Chester George. Calendar Life Studies of Advanced Technology Development Program Gen 1 Lithium Ion Batteries. United States: N. p., 2001. Web. doi:10.2172/911512.

[27] Hydrogen Council, 2020, Path to hydrogen competitiveness - A cost perspective, https://hydrogencouncil.com/wp-content/uploads/2020/01/Path-to-Hydrogen-Competitiveness_Full-Study-1.pdf

[28] NREL. Technology brief: analysis of current-day commercial electrolyzers; 2004. Golden, CO NREL/FS-560-36705.

[29] Battelle Memorial Institute, 2016, Manufacturing Cost Analysis of 100 and 250 kW Fuel Cell Systems for Primary Power and Combined Heat and Power Applications. U.S. Department of Energy

[30] Fracas, P., Zondervan, E., 2019, Fast Fourier Transforms for Microgrid Climate Computing. Proceedings of the 29th European Symposium on Computer Aided Process Engineering, Eindhoven, The Netherlands, Elsevier 10.1016/B978-0-12-818634-3.50277-0

[31] P.I. Cooper, The absorption of radiation in solar stills, Solar Energy, Volume 12, Issue 3, 1969, Pages 333-346, ISSN 0038-092X,https://doi.org/10.1016/0038-092X(69)90047-4.

[32] Papoulis A, Pillai U. Probability, random variables and stochastic processes. 4th ed. New York: McGraw-Hill, 2001: 51-125pp.

[33] Wright, Randy Ben, and Motloch, Chester George. Cycle Life Studies of Advanced Technology Development Program Gen 1 Lithium Ion Batteries. United States: N. p., 2001. Web. doi:10.2172/911513.

[34] Virtanen, P., Gommers, R., Oliphant, T.E. et al. SciPy 1.0: fundamental algorithms for scientific computing in Python. Nat Methods 17, 261–272 (2020)

[35] NASA, Surface meteorology and Solar Energy (SSE) database, https://power.larc.nasa.gov.

[36] Lund, Henrik, & Thellufsen, Jakob Zinck. (2020, September 7). EnergyPLAN – Advanced Energy Systems Analysis Computer Model (Version 15.1). Zenodo. http://doi.org/10.5281/zenodo.4017214

[37] US Department of Energy, Levelized Cost of Energy (LCOE), 2015, https://www.energy.gov/sites/prod/files/2015/08/f25/LCOE.pdf

[38] Eurostat, https://ec.europa.eu/eurostat/statistics-explained/index.php/Electricity_price_ statistics

2.9 Units of measurement

$10si$	10 meter wind speed, m/s
E_{act}	Activation energy constant, kjoule/mole
$P_{ess\_aged\_capacity}$	Aged energy capacity of energy storage systems, kWh
R^2	Coefficient determination of performance of numerical methods
r	Discount rate
η_{eboy}	Energy conversion efficiency of electric boilers
η_{stph}	Energy conversion efficiency of heat pump combined to solar panels
η_{hp}	Energy conversion efficiency of stand alone heat pumps
$x_{c,r}$	Energy flow of the distributed energy resources, kWh
T_{amb}	Environmental temperature, K
$k_{shifted}$	Fraction of energy to shift
k_{hm}	Fraction of hours to shift
$k_{shedding}$	Fraction of load to cut
F_j	Fuel expenditures in a year, €
R	Gas constant, 8.315 joules/mole/K
T_{in}	Input mean temperature of solar collectors, K
C_j	Investment expenditures in a year, €
θ	Latitude, degree
$LCOE_c$	Levelized cost of energy of the c-distributed energy resource, €/kWh
$LSOE_r$	Levelized sales of the r-distributed energy resource, €/kWh
L_i	Lifetime of the distributed energy resources, year
ϕ	Longitude, degree
P_{max}	Maximum daily mean power of loads, kW
SOC_{ess_max}	Maximum state of charge
P_{min}	Minimum daily mean of electric power load, kW
O_j	Operations and maintenance expenditures in year, €
β_{opt}	Optimal tilt angle, degree
$P_{x,y}$	Pearson product-moment covariance coefficients
λ_s	Photovoltaic solar yield, kWh/kW_{peak}
υ_i	Power losses of solar thermal collectors
η_i	Power losses of wind turbine and photovoltaic panels

C_{fuel}	Purchase cost per liter of fuel, €/l
$P_{ess\_rated\_capacity}$	Rated energy capacity of a battery, kWh
δ	Solar declination, degree
ssr	Solar net surface radiation, kW/m^2
σ_{noise}	Standard deviation of electric power load
σ_g	Standard deviation of solar declination
SOC_{ess}	State of charge energy storage system
A_{pv}	Surface of the photovoltaic panel, m^2
A_{st}	Surface of the solar solar collector, m^2
$t2m$	Temperature at 2 meters from soil, K
β	Tilt angle, degree
t_s	time-step, hour
tcc	Total cloud cover, %
C_{trp}	Transportation cost of fuel, €/l
V_{ed_fuel}	Volumetric energy density of the fuel, kWh/l

CHAPTER 3: Machine learning models in techno-economic optimizations

Optimization with an SLSQP algorithm requires a large computing resource. In this chapter, three algorithms for the approximation of the analytical techno-economic model into machine learning (MLTE) based models are discussed. The first MLTE model, is based on a multiple linear regression (MLR), fitting a linear model with coefficients to minimize the residual sum of squares between the observed targets in the dataset (DERs sizes and geolocations), and the targets predicted (fitness values) by the linear approximation. A second model uses a 1-layer neural network (NN), whose input and output neurons are connected by weighed synapses. A third model is a deep neural network (DNN) where the NN is expanded into 3 dynamic layers. MLTE models require a dimensionality reduction of the feature space, training and testing before querying. Min-max, standardization-based scaling techniques have been used to reduce the dimensionality of the feature space. The MLTE models return R^2 lower than 0.2 with all the pre-processing methods. The stochastic behavior of CHP-MMG permits to MLTE to correlate solutions and fitness values similarly to ATE model, for fitness values nearby zero. This behavior can be used in combination with ATE-based optimization to tighten the search area of the best CHP-MMG siting and sizing.

3.1 Introduction to machine learning models for microgrids

With reference to the SLSQP algorithm and ATE model presented in Chapter 2, in this chapter, three alternative machine learning-based models to replace the analytical ATE model are introduced: 1) LR model 2) NN model 3) DNN Model.

Machine Learning algorithms have been already used for the optimization of microgrids since the inherent variability of large-scale renewable energy generation leads to significant difficulties in microgrid energy management.

Karim et al. in 2018 [14] proposed a system based on a machine learning algorithm to forecast the security of a standalone microgrid and to schedule multiple backup diesel generators. The underlying objective was to maintain the voltage stability with an optimized economic dispatch scheme, right after clearing of a critical three-phase short circuit fault.

In a further study [15] Lan et al. in 2021, proposed a machine learning-based approach for energy management in renewable microgrids considering a reconfigurable structure based on remote switching of tie and sectionalizing. The suggested method considers the advanced support vector machine for modeling and estimating the charging demand of hybrid electric vehicles.

In the work of Yaprakdal et al. [16] (2020), a bi-directional long short-term deep recurrent neural network model was designed to provide accurate aggregated electrical load demand and the bulk photovoltaic power generation forecasting results. The real-world data set was utilized to test the proposed forecasting model, and based on the results, they demonstrate that the neural network model performs better in comparison with other methods in the surveyed literature.

Fahim et al. [17] in 2020, presented a review on the MG fault diagnosis techniques with their limitations and proposes a machine learning model made of multiple layers with a restricted Boltzmann machine, which allows a probability reconstruction over its inputs and provide a precises solution for fault diagnosis of MG.

Yao et al. in 2020 [18] introduced a load predictor for microgrid operation based on the combination of machine learning with Ant Colony Optimization (ACO) algorithm and Particle Swarm Optimization (PSO) algorithm to improve the prediction accuracy. The experimental results showed that the prediction results were close to the actual

values and the error changes were stable, which verified the effectiveness of the improved algorithm. Moreover, the algorithm contributed to improve the accuracy of load prediction of the two communities and the optimal operation of the microgrid. Hence, it has a good applicability in the load prediction of microgrid.

Park et al. (2020) [19] proposed an energy storage system (ESS) operation scheduling model to be applied to virtual space when constructing a microgrid using digital twin technology. An ESS optimal charging/discharging scheduling was established to minimize electricity bills and was implemented using supervised learning techniques such as the decision tree machine learning-based techniques models instead of existing optimization techniques. Using the proposed model, it was found in a case study that the amount of electricity bill savings when operating the ESS is greater than that incurred in the actual ESS operation.

In this chapter, four different machine learning approaches are investigated to approximate the original techno-economic model of the CHP-MMG and thus reduce the computing time. The linear regressor (LR) has been the first method as one of the most common methods for industrial problems. Regression models are used to predict target variables on a continuous scale, which makes them attractive for understanding relationships between variables, evaluating trends, or making forecasts. An ordinary LR model has been selected among different methods (e.g., Bayesian Regression, Gaussian Process Regressor) as during the training LR model returns a better R^2.

To improve the R^2 of the LR model alternative methods based on NN and DNN models were employed. The aim was to compare if a multi-layer neural network architecture that connects multiple non-linear functions correlations with higher R^2 can be obtained.

The innovation content introduced in this chapter concerns: 1) the application of machine learning models to improve the performance of techno-economic optimizations; 2) the training method of the MLTE based on the ATE model of CHP-MMG.

3.2 Preprocessing datasets

Preprocessing the datasets has a relevant influence on the performance of the machine learning algorithm [1]. Raw data does not usually fit the form and shape of machine learning algorithms (i.e., LR, NN, DNN). Thus, it is required that the selected features are on the same scale for optimal performance, which is often achieved by transforming the features in the range [0, 1] or a standard normal distribution with zero mean and unit variance. Furthermore, some of the selected features may be highly correlated and therefore redundant. In those cases, dimensionality reduction techniques are useful for compressing the features onto a lower-dimensional subspace. Reducing the dimensionality of our feature space has also the great advantage to reduce the data storage space, and therefore the learning algorithms can run much faster.

Min-max scaling, standardization and arbitrary value-based scaling preprocessing techniques are evaluated in the following sections. The dataset that will be used later to train the machine learning models is generated with the ATE model.

3.2.1 Transforming the data into the right shape

The MLTE models require a dataset previously generated by the ATE model. The latter is used to feed the training and the validation dataset, hereafter called: *Q-dataset.* The *Q-dataset* comprise all the generated individuals and the corresponding fitness values. The *Q-dataset* are matrix with size: [*t, m*] where the index *t* represents the number of the array and *m* the feature (i.e., respectively the individual, the chromosomes and the fitness value in the evolutionary algorithm).

The quality and amount of the information that are contained in the *Q-dataset* are a paramount to assess the performance of these models. Therefore, it is necessary to examine and preprocess the datasets before feeding the learning algorithms.

First, individuals embedding error values in the raw data which typically appears with strings such as *NaN ("not a number")* are removed from the dataset entirely. Following the cleaning procedure, the resulting dataset is the following:

$$\check{Q} = \{q_i \in \quad R: \quad q_i \quad \neq \quad NaN\}, \qquad [3.1]$$

where q_i is the *i*-feature that does not contain errors.

If marginal outliers in the fitness column are found, a subset of individuals is selected from the resulting dataset in [3.1] as follows:

$$\hat{Q} = \left\{ q_j \in \quad R : \quad q_j \quad \leq \quad q_o \right\}, \qquad [3.2]$$

where q_o is the feature embodying the maximum fitness considered. Based on the structure of the fitness function described in Paragraph 4.4, higher values above a certain threshold are not useful to train a MLTE algorithm. Thus, a method that selects the features permits to speed up the training process without losing relevant information.

The resulting dataset is further subjected to feature scaling. This is a crucial step in the preprocessing to ensure that different values of the datasets are brought within the same scale and thus make it easier to optimize the weights of cost functions in each MLTE algorithm.

Two approaches are considered to bring different features onto the same scale: normalization (i.e., min-max method, common divisor) and standardization.

Normalization refers to the rescaling the features to the range [0, 1]. To normalize our data, the min-max scaling has been applied to each feature column, where the new value of a sample can be calculated as follows:

$$\hat{q}_{i,j}^{norm} = \begin{cases} \hat{q}_{i,j}^{min,j} \leq \hat{q}_{i,j} \leq \hat{q}_{i,j}^{max,j} \\ \dfrac{\hat{q}_{i,j} - \hat{q}_{i,j}^{min,j}}{\hat{q}_{i,j}^{max,j} - \hat{q}_{i,j}^{min,j}} \end{cases} . \qquad [3.3]$$

Standardization removes the mean, and scales the data to unit variance. The standard score of a sample is calculated as follow:

$$\hat{q}_{i,j}^{std} = \frac{\hat{q}_{i,j} - \quad \mu_j}{\sigma_j} \qquad , \qquad [3.4]$$

where μ is the mean of the training samples and σ is the standard deviation of the training samples.

Eq. 3.3 translates the features of each axis j, individually in the range [0,1] considering the bound as minimum and maximum of the axis.

In Eq. 3.5 each feature is transformed in a range within [0,1] considering as bound the whole minimum and maximum values of the *Q-array*.

$$\hat{q}_{i,j}^{norm} = \begin{cases} \hat{q}_{min} < \hat{q}_{i,j} < \hat{q_{max}} \\ \frac{\hat{q}_{i,j} - \hat{q}_{min}}{\hat{q_{max}} - \hat{q}_{min}} \end{cases} . \quad [3.5]$$

3.2.2 Training and testing machine learning algorithms

The transformed training datasets are next divided into *training* and *validation (i.e., test)* subsets to estimate the overall performance of the models. The training sets embed the known output, that the models use to tune the parameters in the learning phase. The test subset is utilized later to evaluate the performances of the model's predictions.

The *Scikit-Learn* library of Python® [2] and specifically the *train_test_split* method has been used. It permits to generate training and testing subsets with two dimensions's shape (i.e., *Q*). A further split is performed next to obtain a subset with the individuals (I.E., *X*) and another subset with the related fitness values (i.e., *y*) as follows:

$$\hat{Q}_{train}^{scaled}, \quad \hat{Q}_{test}^{scaled} \quad = \quad [X_{train}^{scaled}, \quad y_{train}^{scaled}], \quad [X_{test}^{scaled}, \quad y_{test}^{scaled}] . \quad [3.6]$$

3.2.3 Validation of results

After training the algorithms, the test dataset is used to assign a score to the models. The coefficient of determination R^2 as defined in Eq. 2.4 is used for this task. This indicator results from the ratio between the sum of the residual square error and the variance. The R^2 is usually affected by three general errors: bias, variance and noise. The bias has its average error for different training sets, the variance indicates how sensitive it is to varying training sets, and the noise is intrinsic to the data. Here, R^2 indicator evaluates whether the model is over-fitting or under-fitting with training and test data. If the training score and the validation score are both low, the estimator will be under-fitting. If the training score is high and the validation score is low, the estimator is overfitting. A low training score and a high validation score are usually not possible [3]. The algorithm overfits when it performs well on the training dataset but fails to perform on unseen or validation and test datasets.

3.3.1 Multiple linear regression

Linear regression is a statistical technique that can be used to predict target variables on a continuous scale, which makes it suitable for making forecasts for our fitness values. Multiple linear regression (MLR) captures the relationship between two or more input variables and a response observed variable by fitting a linear equation to observed data. In our case, the input variables: $X_{i,train}^{i,scaled}$, $X_{i,test}^{i,scaled}$, and the corresponding observed variables: $y_{i,train}^{scaled}$, $y_{i,test}^{scaled}$ which can be found from [3.6] and are used to train and validate the MLR model.

The relationship for the MLR is defined as follows:

$$f_i = \sum_{j=0}^{N} w_{i,j} \cdot x_{i,j} \,. \qquad [3.7]$$

Where $x_{i,j}$ is the element of the X_i individual; $w_{i,j}$ is the associated parameter that permits to obtain the correlation with the corresponding observed feature f_j.

The first step is to train the set of coefficients $w_{i,j}$; to do that, an objective function defined in Eq. 3.8, is iterated until the difference between the observed variables embedded in the training dataset, $y_{i,train}^{scaled}$ and the observed value $\hat{f}_i$, estimated with the linear Eq. 3.7 is minimized.

$$\min J(w_{i,j}) = \frac{1}{N} \sum_{i=0}^{N} \left(y_{i,train}^{scaled} - \hat{f}_i\left(w_{i,j}\right) \right)^2 \,. \qquad [3.8]$$

This method prevents cancellations between positive and negative values and thus it considers all residuals in the estimation of constants weights $w_{i,j}$. Another property of this cost function is that it is convex; i.e., the steepest descent method can be apply to find the weights that minimize our cost function. The trained model can then be used to predict the responses of new input variables that were not part of the training dataset.

3.3.2 Neural network

In this section, neural networks (NN) are briefly discussed as alternative method to MLR for predicting the fitness values. Similarly to MLR, the datasets obtained with the method described in Eq. 3.6 are used to train and then validate the NN model.

$X_{i,train}^{scaled}$ and $X_{i,test}^{scaled}$ are the inputs (explanatory variables) while $y_{i,train}^{scaled}$ and $y_{i,test}^{scaled}$ are the corresponding observed variables (fitness).

In a NN, information processing occurs, over simple elements called neurons. A neuron is a mathematical function that takes one or more input values and outputs a single numerical value. Neurons are organized in interconnected layers. Neurons of one layer are connected to neurons of another layer through connection links and they exchange signals among them.

Connection links between neurons can be stronger or weaker and this determines how information is processed. To determine the intensity of each incoming signal to the neuron (i.e., node), the input is combined to an optimized weight. In other words, the outcoming signal of the neuron has an internal state that is determined by all the incoming weighted connections from other neurons. Moreover, each neuron embeds an *activation function* that based on the internal state of the outcoming signal determines the output signal.

Similar to MLR, the neural network correlates the input array *I,* with the resultant output array *F,* using the matrix *W*.

The overall model of a NN is expressed as concisely as:

$$F_k = W_{k-1,k} \cdot I_{k-1} \,. \qquad [3.9]$$

Here the index *k* denotes the *k*-layer of a NN which incorporates *n* nodes and *l* layers.

Thus, F_k is the 1d-array with dimension [n,1] of the output signals of the k-layer. $W_{k-1,k}$ with dimension [n, n-1] embodies the weights of the interconnecting signals among nodes. Then, the elements of the input 1d-array I_{k-1} with dimension [n-1, 1] are the incoming signal to each neuron.

In this work a NN composed by 3 layers has been considered: the input layer, the hidden layer and the output layer.

The resultant matrix [F_k] of the k-layer becomes an input to the *sigmoid activation function* returning all the values between the interval 0 and 1:

$$O_k = \frac{1}{\left(1 + e^{-F_k}\right)}. \qquad [3.10]$$

Hence, the result is the 1d-array O_k, which contains all the outputs from the k-layer. Eq. 3.10 is applied to compute the outputs between one layer and the next layer.

The NN is first initialized with the number of input nodes corresponding to the chromosomes of each individual ($X_{i,train}^{scaled}$). Next, the intermediate layer has a number of hidden nodes equivalent to the number of input nodes. Finally, the output layer has one output node corresponding to the fitness value of the input individual.

The matrix of weights is constructed initially with a normal probability distribution function centered on zero and with a standard deviation that is related to the number of incoming links into a node. T. Rashid (2016) [4] proposed that the range of these values should be roughly the inverse of the square root of the number of links.

Some overly large initial weights would bias the activation function in a biased direction and very large weights would saturate the activation functions. The training of the NN is executed in two phases. In the first phase, the matrix of weights is trained by iterating the learning rate parameter and the epoch parameters to obtain their best values.

The learning rate is utilized to moderate the strength of the changes error slope during the training of matrix weight elements. The epoch parameter is the number of iterations of the training function. During the training phase, epochs and learning rates are used to set weights, which, will define the internal states for each neuron in the network. Epochs and learning rates parameters are optimized with an external "for-loop" over the training phase. The means square error (MSE) between target (training) and predicted data during the iteration of epochs and learning rates is the objective to minimize. For each $X_{i,train}$ data, the correspondent observed O_l value is computed by calculating the signals into the input, hidden, output layers with the Eq. 3.11. Then the error E_l given by the training data and the predicted data at the output nodes is calculated with the Eq. 3.11.

$$E_l = y_{i,train}^{scaled} - O_l \,. \qquad [3.11]$$

The propagation of the errors back (i.e., backward propagation) to the internal nodes are computed with the matrix Eq. 3.12 which split the output layer errors in proportion to the size of the connected link weights.

$$E_{k-1} = W_{k-1,k}^{T} \cdot E_k \,. \qquad [3.12]$$

Second, each weight matrix is updated with the gradient-descent optimization algorithm as described in Eq. 3.13.

$$W_{k-1,k} = \hat{W}_{k-1,k} - \alpha \cdot \frac{dE}{dw_{i,j}} . \quad [3.13]$$

The former elements of weight matrix $\hat{W}_{k-1,k}$ which determine the signals' intensity coming from the nodes of the layer *k-1* to the nodes of the layer *k*, are adjusted by the slopes of the errors gradient.

After the training phase, a NN query can be executed. Thus, as further discussed in the following Chapter 4 the evolutionary computation method can be used to iteratively improve the solution and obtain the probabilistic global solution by processing in parallel the NN algorithm, with the individuals constituting the population of each generation.

3.3.3 Deep neural network

Deep neural networks (DNNs) are neural networks with multiple hidden layers.

It is notable that a network's performance degrades if a single layer is removed (A. Krizhevsky et al., 2017) [5]. For example, removing any of the middle layers results in a loss of about 2% for the top-1 performance of the network. So the depth is important for achieving good results.

PyTorch [8][9] is a high-performance tensor library for the computation of deep learning tasks on GPUs (graphics processing units) and CPUs (central processing units). PyTorch is a machine learning and deep learning tool developed by Facebook's artificial intelligence division to process large-scale image analysis including object detection, segmentation and classification. However, it is not limited to these tasks. It can be used with other frameworks to implement complex algorithms.

In the PyTorch deep learning network tool, the most important layers, i.e., the linear layers, apply a linear transformation of signals with Eq. 3.9. Deep learning architectures used for solving real-world cases generally embeds multiple layers.

Each layer learns some kind of pattern that the later layers will build on. There is a problem in adding just linear layers together, as they fail to learn anything new beyond a simple representation of a linear layer. Hence, just stacking multiple linear layers will

not help the algorithm to learn anything new. To solve this problem, different non-linearity functions can be chosen. This aids the network in learning different relationships, rather than only focusing on linear relationships. There are different non-linear functions available in deep learning. PyTorch provides these non-linear functions as layers and they can be used the same way as the linear layer. Non-linear activations are functions that take inputs and then apply a mathematical operation and produce an output. One of the non-linear operations is the *ReLU* function. The latter was used in this work. *ReLU* has become more popular in recent years [10]. It has a simple mathematical formulation:

$$f(x) = \max(0, x) . \qquad [3.14]$$

ReLU resets any input that is negative to zero and leaves positive numbers as they are. *ReLU* helps the optimizer in finding the right set of weights sooner. More technically it makes the convergence of stochastic gradient descent faster. *ReLU* is computationally inexpensive, as it is just thresholding and not calculating anything like what is done for the sigmoid and tangent functions. *ReLU* has one disadvantage; when a large gradient passes through it during the backward propagation, they often become non-responsive. These are called dead neutrons, which can be controlled by choosing the learning rate factor. For the forward pass of the model, we randomly choose either 0, 1, 2, or 3 layers and reuse the middle linear layer that many times to compute hidden layer representations. Since each forward pass builds a dynamic computation graph (i.e., mathematical expressions described with a graph) normal loops are used when defining the forward pass of the model. Here it can be seen that the same module can be reused many times when defining a computational graph. The training of the model initiates with random learnable weights. The gradient descent optimization algorithm is applied to learn the weight coefficients of the model. In every epoch (i.e., pass over the training set), the weights are updated. In order to find the optimal weights of the model, an objective function based on the sum of squared errors (SSE) is minimized. Furthermore, the gradient is multiplied by a factor, the learning rate η, which is chosen to balance the speed of learning against the risk of overshooting the global minimum of the cost function [1].

3.4 Results and discussion

3.4.1 Results of data pre-processing

In this section, the results of preprocessing datasets by using the Sklearn preprocessing library of python [2] are discussed. The latter provides several common utility functions and transformer classes to change raw feature vectors into a representation that is more suitable for the downstream estimators.

The transformed datasets are used later by the three different supervised machine learning algorithms: Multiple linear regression, Neural Network and Deep Neural Network.

In the first step undefined NaN (i.e., not a number) are removed (Eq. 3.1-3.2); then, the cleaned datasets are scaled with normalization and standardization methods (Eq. 3.3-3.5). The transformed datasets are split in the two subsets train and tests (Eq. 3.6).

The three MLTE algorithms are trained with the first subset while the second subset is utilized to analyze the performances. Table 3.1 shows the genetic composition of the cracked population composed by [$X_{i,train}^{i,scaled}$, $X_{i,test}^{i,scaled}$] individuals, whose shape are 2d-array, comprising of 38 elements of the optimal solution of CHP-MMG (Appendix A). These datasets treated with the above mentioned preprocessing methods, are discussed in the following part of this paragraph. The trial starts with the two original correlated datasets, respectively:

$$X \in \mathfrak{R}^{368.594 \times 38} \text{ and } y \in \mathfrak{R}^{368.594 \times 1} . \quad [3.15]$$

Where the first array, X is the explanatory dataset which embeds all the individuals that has been generated with the analytical techno-economic model (ATE) and y is the 1d-array corresponding to the fitness values (observed datasets); to each X_i-individual with index i corresponds a fitness value y_i.

All the individuals with a fitness values lower than 2 are selected. The final dimension of our datasets is the following:

$$X \in \mathfrak{R}^{9.243 \times 38} \text{ and } y \in \mathfrak{R}^{9.243 \times 1} . \quad [3.16]$$

Only 2.5% of the original records has been considered to train the models. Upon of the tests carried out, it was found that, the dimension of the selected size improves the overall training process.

The impact toward the distribution of the datasets after preprocessing has been studied. Moreover, the performances obtained with the three machine learning algorithms (MLR, NN, DNN) fed with different scaled datasets, have been evaluated.

Among the variables indicated in Appendix A, we choose a couple of variables (FC_SIZE_MG_A vs WT_SIZE_MG_A), having a complementary role in the power generation.

Figure 3.1 shows the distribution of coupled unscaled explanatory datasets. It can be observed that a relevant portion of data are scattered in the upper right area of the plots. This behavior entails that several outliers may be present in the sets; they can degrade the predictive performance of many machine learning algorithms.

In Figures 3.2-3.4, the transformed features of the correlation between the size of FC and WT are plotted. The left plot shows the entire dataset and the zoomed-in right plot shows the dataset without the marginal outliers. Note that several marginal outliers (individuals embedding FC with size 100 kW and WT with 150 size) are still presents with all transformers.

The transformation in Figure 3.2 refers to the normalization of the individuals's datasets by scaling all the values of the dataset in the range [0,1] considering as divider a given arbitrary value common for all the genes.

The maximum value of the dataset (48.000) has been chosen as the common divisor. However, this transformation compresses all the inliers in a narrowed area the original data. This is due to the divisor chosen between values with different scale (e.g., DG, Tanks, GPS coordinates).

StandardScaler in Figure 3.3 removes the mean and scales the data to unit variance. Note in particular that the spread of the transformed data on each feature lies in the range [-2, 1]. The distribution of data is similar to the original unscaled datasets.

Figure 3.4 outlines the rescaling thru normalization of all feature values in the range [0, 1] with axis-independent dividers rescaling factors. This transformation, similarly as the others, keeps the distribution of data similar to the original datasets.

To conclude, in all the examples of the correlation between WT and FC are visualized outliers in transformed datasets which cannot be eliminated with any preprocessing technique. This behavior can origins a degradation of the predictive performance of the machine learning algorithms.

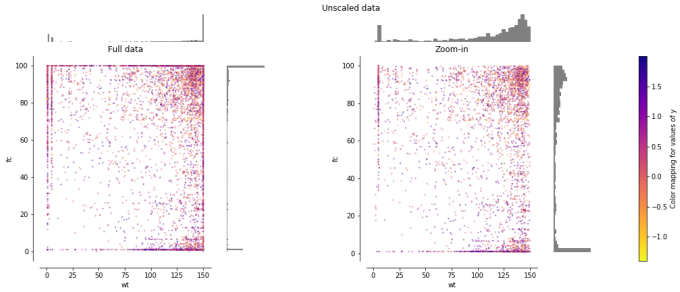

Figure 3.1 *spread of unscaled data of two coupled variables (FC_size, WT_size)*

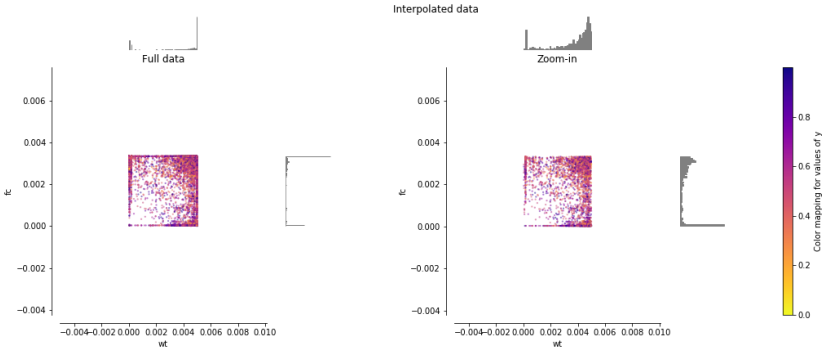

Figure 3.2 *spread of scaled data by common divisor method of two coupled variables (FC_size, WT_size)*

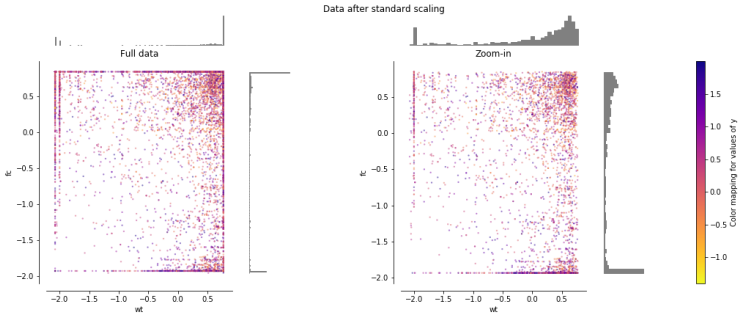

Figure 3.3 *spread of scaled data by standardization method of two coupled variables (FC_size, WT_size)*

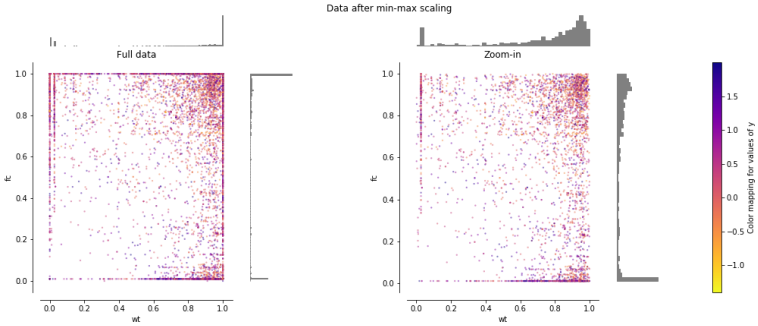

Figure 3.4 *spread of scaled data by min-max method of two coupled variables (FC_size, WT_size)*

3.4.2 Result of machine learning model training

After scaling, the transformed datasets are ready to train the MLTE algorithms. Thus, the matrices are split into random 50% training and 50% test subsets. The resulting size is the following:

$$X_{train}^{scaled} \in \mathfrak{R}^{4.621 \times 38} \qquad y_{train}^{scaled} \in \mathfrak{R}^{4.621 \times 1} \qquad [3.17]$$

$$X_{test}^{scaled} \in \mathfrak{R}^{4.622 \times 38} \qquad y_{test}^{scaled} \in \mathfrak{R}^{4.621 \times 1} \; . \qquad [3.18]$$

The learning phase has been conducted in a similar fashion by feeding all the models with the datasets transformed by normalization and standardization as described in the previous Paragraph 3.3.1. The effective size of the dataset to train MLTE algorithms is further restricted to the number of simulations that it has been possible to run with the ATE model so far. This may affect the overall robustness of the proposed approach. Figures 3.5 and 3.6 show how the transformations with the common divisor method affect the MLR algorithm during the phases of training and testing. The correlation between the predicted observed variable y^{scaled} of the vertical axis and the same variable generated with the ATE model (horizontal axis) is here depicted. Evaluated on the training data, the R^2 is 0,2. It should be noticed that R^2 keeps the same value for all pre-processing methods (standardization, min-max, common divisor).

It was also observed that the measured R^2 reflects into a concentrated horizontal cluster of predicting data (*y_pred*), meaning that a small number of predictions correspond to a large number of actual data. It is deemed that the delivered datasets are not able to properly train the MLR algorithm. Thus the independent *X-dataset* is not able to explain much in the variation of the dependent variable y - regardless of the variable significance. Based on the work of P. Yarnold (2019) [11] it has been assumed that this behavior indicates the existence of a high non-linear effect. To demonstrate this statement, further trials have been executed. The explanatory X and the observed variables y have been replaced with two stochastic arrays having the shape of the original datasets, but given in the half-open interval [0,0, 1.0) with a random samples generator which creates values from a continuous uniform distribution over the stated interval. When the random datasets are transformed and then they feed the MLR, the cluster confirms again a similar highly non-linear behavior as given with the original data.

Finally, the MLR model has been replaced with a NN and DNN models. To get the datasets in the shape for feeding the activation functions of the NN (i.e., sigmoid function) and DNN (i.e., *ReLU* function), the original datasets have been changed with min-max scaling method. This method avoids a null signal, when inputs are negative and it fosters a better distribution (e.g., Figure 3.2 vs. Figure 3.4) of the datasets within the range [0,1]; to this extent, the NN/DNN algorithms improve their ability to learn the weights [12][13]. Then, the shuffling has been applied similarly to MLR, before performing the split of train and test subsets.

As for MLR, the neural network and deep neural network algorithms utilize the training data to learn the weights and the other parameters (i.e., epochs, learning rates in NN). The results of the two models are similar. The outcome of the validation phase of DNN is reported in Figure 3.7. This scattered plot similarly to precedent Figure 3.5-3.6 shows a poor correlation among the observed values generated with ATE model *y_test* and the corresponding values *y_pred* obtained with the DNN. The simulations computed with DNN give a negative R^2 (-0,03). Similarly, the simulations executed with three-layer NN, return a negative R^2 values with X variables treated with the same transforming method. It should be noticed that even the extensions to large epoch ranges does not improve the R^2 performance. The negative R^2 score, reflects a non-linearity more pronounced than MLR. From the distribution of the scattered patterns in Figure 3.5-3.7, can be inferred that the correlation among predicting data (*y_pred*) and original data (*y_test*) is neglected.

3.4.3 Implications of machine learning models in techno-economic optimizations

The results coming out from the simulations described in the previous paragraph 3.3.2 are characterized by a R^2 lower than 0.20. Among the three different MLTE models, the highest R^2 value is obtained with MLR. Trials have been repeated with different parameterizations of MLR, NN and DNN algorithms and changing scaled training datasets. However, a result comparable to ATE for the whole domain of the observed variables has not been achieved. It is assumed that the R^2 performance indicates that any transformed independent variable X is not explaining in the variation of the dependent variable y - regardless of the variable significance. Hence, the correlation among X and y remains highly non-linear.

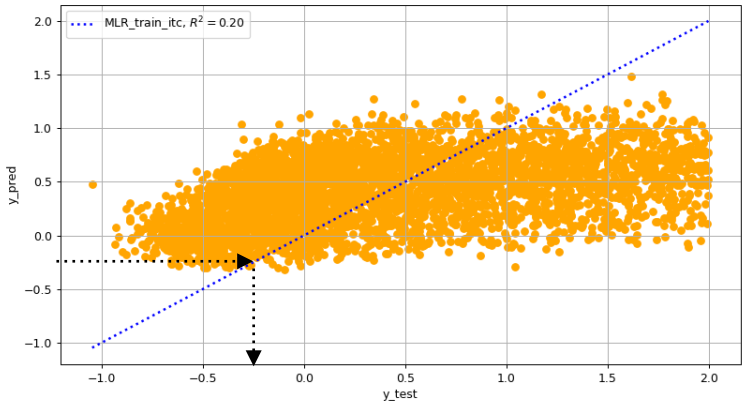

Figure 3.5 *Scatterplot of predicted vs test ATE-based values in MLR training. X-explanatory variable scaled by interpolation*

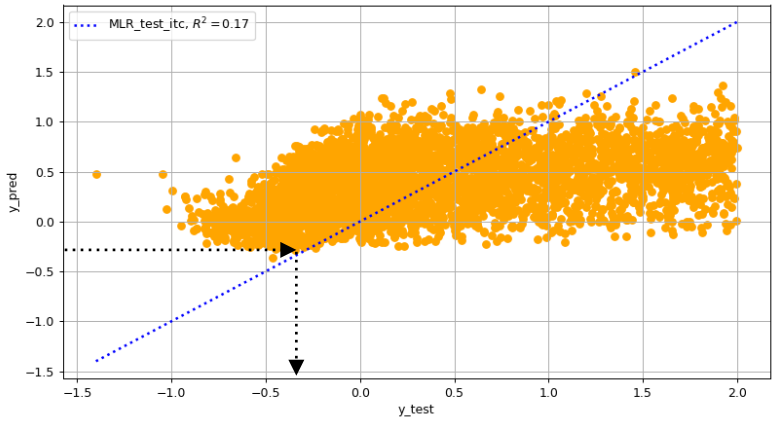

Figure 3.6 *Scatterplot of predicted vs test ATE-based values in MLR validation. X-explanatory variable scaled by interpolation*

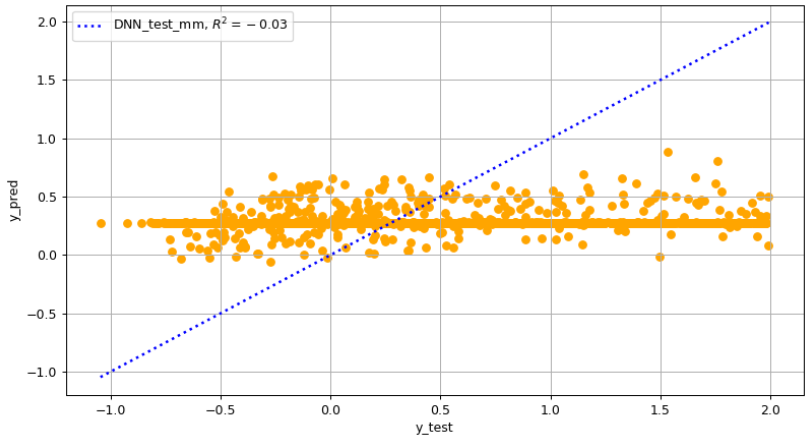

Figure 3.7 *Scatterplot of predicted vs testATE-based values in DNN validation. X-explanatory variable scaled by normalization with axis-1 min, max values*

This hypothesis has been investigated in a further campaign of simulations where the original explanatory variables X and the original dependent variable y have been replaced with stochastic matrices resulting from continuous uniform distributions. When a stochastic dataset is transformed and it feeds an ML algorithm, an highly non-linear correlation appears in a scattered plot. Neither MLR, NN, nor DNN are able to replace the ATE analytical techno-economic model in the overall domain of solutions.

The potential argumentation that justifies the non-linearity among the *X-explanatory* datasets and the *y-dependent* datasets has been investigated.

The ATE model that is used to generate the training and test datasets, embeds several stochastic relations that contribute to return different fitness values for the same solution: 1) cloudiness Eq. 2.10; 2) wind speed Eq. 2.21; 3) electric loads Eq. 2.27; 4) thermal loads Eq. 2.28; 5) demand response profiles Eq. 2.30; 6) grid outage Eq. 2.31.

These terms cause in the underlying fitness function to become noisy, in the sense that the boundaries condition applied to the SLSQP may vary for the same trial solution. The stochastic behavior is amplified by repeating the SLSQP optimization as the number of time-steps.

The scattered pattern shows in Figure 3.5-3.6 a restricted area (indicated by black arrows), in which *y_pred* (i.e., the fitness value predicted by ML) and y_test (i.e., the test fitness value) have the same value. It can be assumed that their correspondent solutions, although not yet the best, are within the optimal search area.

Hence, MLTE can be used in combination with ATE as follow: 1) compute the first query with MLTE to search the solutions until the corresponding fitness values is nearby zero, 2) execute further queries with ATE by constraining the high values of the boundaries with the elements of the solutions obtained with MLTE.

Optimizations based on MLTE have the great advantage to reduce the execution of a query from several hours to minutes. Thus, MLTE in combination with ATE (i.e., hybrid model) allows to shorten the computing time of optimizations based on multiple queries.

3.5 Conclusion

Three algorithms for the approximation of the analytical techno-economic model into MLTE based models have been discussed in this chapter. The first is based on MLR. A second algorithm is a 1-layer NN. A third model is a deep neural network where the NN is expanded into 3 dynamic layers.

Optimizations based on MLTE in combination with the ATE model have the great advantage to reduce the computing time from several hours to minutes while searching the global minimum.

The first query bases on MLTE can be used to tighten the search area of the best CHP-MMG siting and sizing. In order to preserve the quality of the results, the stopping criteria of the fitness function need to be set near zero. Then, the best solution obtained with MLTE must be utilized to override the boundaries of the subsequent search with the ATE-based model.

The combination of machine learning with analytical models is a novel contribution in the techno-economic optimization of CHP-MMG that is proposed by this work.

3.6 References

[1] Raschka S., Python Machine Learning, 2015, pp.11-12, 343-344

[2] Scikit-learn: Machine Learning in Python, Pedregosa et al., JMLR 12, pp. 2825-2830, 2011, https://jmlr.csail.mit.edu/papers/v12/pedregosa11a.html

[3] Andreas C. Müller and Sarah Guido, 2017, Introduction to Machine Learning with Python, O'Reilly Media, Inc., pp. 26-29

[4] T.Rashid, 2016, Make your own neural network, Amazon

[5] Alex Krizhevsky, Ilya Sutskever, and Geoffrey E. Hinton. 2017. ImageNet classification with deep convolutional neural networks. Commun. ACM 60, 6 (May 2017), 84–90. DOI:https://doi.org/10.1145/3065386.

[6] Pietro Perconti, Alessio Plebe, Deep learning and cognitive science, Cognition, Volume 203, 2020, 104365, ISSN 0010-0277, https://doi.org/10.1016/j.cognition.2020.104365

[7] Hazelwood, K., Bird, S., Brooks, D., Chintala, S., Diril, U., Dzhulgakov, D., ... Wang, X. (2018). Applied machine learning at Facebook: A datacenter infrastructure perspective. IEEE International Symposium on High Performance Computer Architecture (HPCA) (pp. 620–629).

[8]	Adam Paszke, Sam Gross, Soumith Chintala, Gregory Chanan, Edward Yang, Zachary DeVito, Zeming Lin, Alban Desmaison, Luca Antiga, Adam Lerer, 2017, Automatic differentiation in PyTorch, 31st Conference on Neural Information Processing Systems (NIPS 2017), Long Beach, CA, USA, https://openreview.net/forum?id=BJJsrmfCZ
[9]	Vishnu Subramanian, 2018, Deep Learning with PyTorch, Packt Publishing Ltd., pp. 9-84
[10]	He, Juncai; Li, Lin; Xu, Jinchao; Zheng, Chunyue, ReLU Deep Neural Networks and Linear Finite Elements, 2018, J. Comput. Math. 38(3), 2020, 502-527; doi:10.4208/jcm.1901-m2018-0160
[11]	Paul R. Yarnold, 2019, When to Evaluate a Non-linear Model, Optimal Data Analysis, LLC, Vol. 8 (January 15, 2019), 15-20
[12]	Bert Moons, Daniel Bankman, Marian Verhelst, Embedded Deep Learning, 2019, Springer Nature Switzerland AG
[13]	Steven J. Nowlan and Geoffrey E. Hinton, Simplifying Neural Networks by Soft Weight-Sharing, Neural Computation 1992 4:4, 473-493
[14]	Miftah Al Karim, Jonathan Currie, Tek-Tjing Lie, A machine learning-based optimized energy dispatching scheme for restoring a hybrid microgrid, Electric Power Systems Research, Volume 155, 2018, Pages 206-215, ISSN 0378-7796
[15]	Lan, T.; Jermsittiparsert, K.; T. Alrashood, S.; Rezaei, M.; Al-Ghussain, L.; A. Mohamed, M. An Advanced Machine Learning Based Energy Management of Renewable Microgrids Considering Hybrid Electric Vehicles' Charging Demand. Energies 2021, 14, 569. https://doi.org/10.3390/en14030569
[16]	Yaprakdal F, Yılmaz MB, Baysal M, Anvari-Moghaddam A. A Deep Neural Network-Assisted Approach to Enhance Short-Term Optimal Operational Scheduling of a Microgrid. Sustainability. 2020; 12(4):1653. https://doi.org/10.3390/su12041653
[17]	Fahim, S. R., Sarker, S. K., Muyeen, S. M., Sheikh, M. R. I., & Das, S. K. (2020). Microgrid fault detection and classification: Machine learning based approach, comparison, and reviews. Energies, 13(13). https://doi.org/10.3390/en13133460
[18]	Yao, T., Jiang, D., Xin, R., Wu, J., & Sun, S. (2020). Load prediction of microgrid optimal operation based on improved algorithm in machine learning. International Journal of Mechatronics and Applied Mechanics, 1(7). https://doi.org/10.17683/ijomam/issue7.18
[19]	Park, H. A., Byeon, G., Son, W., Jo, H. C., Kim, J., & Kim, S. (2020). Digital twin for operation of microgrid: Optimal scheduling in virtual space of digital twin. Energies, 13(20). https://doi.org/10.3390/en13205504

CHAPTER 4: Optimizations with evolutionary algorithms

This chapter addresses the optimal design, sizing and siting of CHP-MMG. This leads to a non-linear stochastic optimization problem, subjected to variety of uncertain climate variables, load profiles, grid outages. The fitness function is based on a techno-economic models describing the energy flows and costs of the distributed energy resources. ATE makes use of sequential least squares programming for the hourly optimizations of operation. The FF is used to measure the IRR and the LCOE for each solution. Two novel self-adaptive differential evolution algorithms (ADE, AIE) are proposed. In these algorithms, the genotype of each individual incorporates the site and size features of the candidate solution. In the ADE, a mutant and crossover factor is adapted according to the difference of best-so-far fitness values. In AIE the mutant vector is obtained with a normal random distribution driven by the diversity of population and fitness convergence. Mutant genes are randomly recombined with the target genes and external genotypes (horizontal gene transfer). A one-to-one survivor selection criterion is used to find the best individual. The adaptive approach enhances the search radius and increases the convergence of the algorithm. The results demonstrate that AIE performs 20% better on average. Moreover, the optimization tools have been used to execute a sensitive analysis of hydrogen costs in off-grid and on-grid contests. Both scenarios do not select the generation of hydrogen on-site as preferred choice. With CHP-MMG, energy production surplus is converted from electricity to heat and thus, an efficient swarm of energy permits to keep the LCOE lower than 18c€/kWh. The overall results show that at a hydrogen cost of 3€/kg, the optimal design returns an IRR of over 50%. Further simulations that consider on-site hydrogen production via plasma assisted decomposition of methane, led to similar outcomes as for green hydrogen.

Based on: P. Fracas, E. Zondervan, M. Franke, K. V. Camarda, 2021, Nature-inspired two-layer optimizations for interconnected heat and power multi-microgrids.

Published and presented at:

- 9th Global Conference on Global Warming, 1-4 August 2021, http://www.gcgw.org/gcgw2021/.
- TUBA World Conference on Energy Science and Technology, 8-12 August 2021, https://wcest.tuba.gov.tr.

4.1 Introduction

When two or more CHP-MG systems are interconnected into a CHP-MMG, they become flexible and counterbalance the variations required to match supply and demand at any time. Energy production surplus (i.e., exceeding the load demands and energy services) can be converted from electricity to heat and transferred to the nearby CHP-MG. As a consequence, the TCO for the installations is minimized, a better LCOE is achieved and the IRR is higher than stand-alone MG. Orecchini et al. in 2011 [1] proposed the concept of "intelligent energy network" as an intelligent management system that incorporates distributed energy sources, electricity, heat, hydrogen, biofuels and non-biofuels.

Unpredictable and variable climatic conditions make the production of the energy with RES, intermittent and not programmable. Matching the latter with load profile uncertainty, grid availability and flexible energy demand requires algorithms to solve stochastic optimization problems.

In this chapter, the techno-economic optimization of multiple interconnected heat and power microgrids is discussed. Two novel evolutionary computing methods are proposed to solve this stochastic optimization problem. They are designed to simultaneously find the best type (design optimization), size (sizing optimization) of DER, the best geo-location (siting optimization). The objective of the optimizations is to achieve the highest IRR and lowest LCOE depending on energy policies, cost and hydrogen type in on-grid and off-grid contexts.

4.1.1 Features of evolutionary algorithms

To find the optimal design, sizing and siting of CHP-MMG, a stochastic multi-objective optimization (MOP) problem has to be solved. This is a non-convex, non-linear problem that does not have a unique global solution. Many solutions with incommensurable quality, hereafter called “probabilistic best solutions” (PBS) can be identified. Metaheuristics are useful for solving MOP [2]. The term “metaheuristic” (F. Glover, 1986) [3] refers to a nature-inspired robust searching mechanism that may provide a sufficiently good solution.

EA are a family of random-based solution space search algorithms. An evolutionary algorithm is a special computation technique that draws inspiration from the principle of

natural evolution and survival of the fittest that are described by the Darwinian Theory. The Darwinian Theory explains the principle of natural selection, which favors the survival of species that are matched with their environmental conditions and explains the evolution of species as an outcome of random variations and natural selection. There are a wide variety of metaheuristics including genetic algorithms (GA), evolution strategies (EVS), evolutionary programming (EP), genetic programming (GP) and differential evolution (DE). Since EA deal with a group of candidate solutions, it seems natural to use them in optimization problems to find a group of promising solutions. Indeed, EA have proven very efficient in solving complex multi-objective optimization problems (Rodriguez, M. A. et al., 2020) [4]. EA have a direction-based search method that optimizes a problem by iteratively trying to improve a candidate solution with respect to a given measure of quality.

The metaheuristic EA method needs few or no assumptions about the problem and can search for solutions in very large spaces. Thus, EA are suitable when solving complex unconstrained global optimization problems. A population of target solutions evolves at each generation in new candidate solutions by combining existing ones and then keeping whichever candidate solution has the best fitness.

The optimization problem is treated as a “black box” that merely provides a measure of quality given by the candidate solution the gradient is not needed. In 1995, R.Storn and K.Price [5] proposed the Differential Evolution (DE) algorithm, a stochastic population-based search method, for solving non-linear, high-dimensional and complex computational optimization problems. DE uses a simple mutation operator based on differences between pairs of solutions (called hereafter vectors) to promote a search direction-based approach. It is worth noting that DE can support the contour matching, i.e., the vector population adapts such that promising regions of the objective function surface are investigated automatically once they are detected.

An important ingredient is the promotion of basin-to-basin transfer, where search points may move from one local minimum to another [6]. DE also utilizes a mechanism, where the newly generated offspring competes only with its corresponding parent (previous vector) and replaces it if the offspring has a higher fitness value.

4.2 State-of-art of evolutionary algorithms applied to microgrids

In recent years, EA have emerged as successful alternatives to more classical approaches for solving microgrid optimization problems. The applications of EA spun from optimization of management to scheduling of energy-efficient scheduling to optimal sizing of nominal power of generators and capacity of energy storage. Most research is dealing with specific sites of the energy systems. A number of methods are considered and applied to determine optimal size and location of MG. Such methods can be classified as single-objective and multi-objective sizing and siting optimization problems. Single-objective methods target to minimize the cost or maximize the profits.

Whereas multi-objective methods are used to determine Pareto optimal solutions of different objectives. For example, to ensure that the generation and consumption of energy are balanced at minimal operational costs, the emission of pollutions are minimized and the financial returns of investments (i.e., NPV, IRR) are maximized.

4.2.1 Evolutionary computing for optimal operations

Several works deal with the optimization of MG operations using different metaheuristics. Such methods search for solutions over a well-defined MG configuration and installation site. These methods incorporate voltage, current and power flow regulations, multi-grid dispatch, pollutant emissions, reactive power, energy scheduling and the cost of energy.

The work of H.Vahedi et al. in 2010 [7] focused on developing a cost optimal operational strategy for a single MG using a differential evolution to meet the customer demand and ensuring system safety. M. Hemmati et al. in 2014 [8] presented a comprehensive operational model for MG in the islanded mode. A new learning-based differential evolution algorithm is presented to solve the operational problem of various DER. W. Gu et al. in 2014 [9] presented a review of the energy management of CHP-MG with distributed cogeneration units and renewable energy sources which yield an effective solution to energy-related problems, including high energy demand, costs, supply security, and environmental concerns. J. Zhang et al. in 2016 [10] proposed an optimal day-ahead scheduling model for a microgrid system based on a hybrid harmony search algorithm with differential evolution (HSDE). S.Reddy et al. in 2016 [11]

discussed a power scheduling approach for standalone MG. The proposed scheduling problem is solved using a hybrid differential evolution and harmony search (HSDE) algorithm. M. Marzband et al. in 2016 [12] developed an algorithm for an energy management system (EMS) based on multi-layer ant colony optimization approach (EMS-MACO) to schedule energy in MG. This algorithm can be used to determine the required load demand with minimum energy cost in a local energy market. The performance of MACO is compared with EMS and particle swarm optimization. N. Nikmehr et al. in 2017 [13] applied a PSO method to minimize the costs of multi-microgrids concept. A stochastic model of both a small-scale energy resource as well as a load demand profile at each microgrid is developed to determine the best economic operation for each MG, based on the power transaction between the MG and main grids. The proposed methods allow to regulate the power demand and power transaction between each MG and the main grid.

M. Hossain et al. in 2018 [14] demonstrated an application of PSO for real-time energy management of a community microgrid. The complexity of time-varying electricity prices, stochastic energy sources and power demand is managed to save costs and minimize energy waste. Yang Li et al. in 2019 [15] have investigated how to coordinate several scheduling objectives from the perspective of cost, environment and users with a multi-objective dynamic dispatch model. An evolutionary algorithm is used to find a set of Pareto-optimal solutions. The results demonstrated the effectiveness of the suggested approach.

Willian M. Et al. in 2020 [16] proposed a multi-objective optimization method structured in multi-layers to operate DER that needs to be connected unevenly throughout the phases of a microgrid. The MOP, based on an EA, maximizes the active power generation by single-phase distributed energy resources and it minimizes the reactive power flow through the grid and grid currents unbalance at the point of common coupling. The results of microgrid operation demonstrated the effectivity of the proposed approach to steer grid power flow and prioritize active power injection or compensation of currents unbalance.

4.2.2 Evolutionary computing for optimal siting and sizing

Similar to the optimization of operation problems, in the last ten years, metaheuristics have been proposed to solve multi-objective siting of MG. Notably, multi-microgrid optimization problems are rarely investigated. Sizing problems are usually combined with a low-level management of operations, which are usually solved as MILP.

H. Doagou-Mojarrad et al. in 2013 [17] introduced an interactive fuzzy method, to solve the problem of optimal placement and sizing of DG in a distribution network. The multi-objective function based on electrical energy losses, cost and pollutant emissions is handled by an evolutionary algorithm. B. Li et al. in 2017 [18] proposed a combined sizing and energy management methodology, formulated as a leader-follower problem. The leader problem focuses on sizing and selects the optimal size for the microgrid components. The energy management issue is translated into a unit commitment problem and is solved as a mixed-integer linear program. Uncertainties are considered using a robust optimization method. Several scenarios are modeled and compared via simulations to show the effectiveness of the proposed method. Mohseni S. et al. in 2017 [19] investigated a novel multi-agent based method applied to the sizing of the components of an islanded combined heating and power residential microgrid that includes hydrogen refilling demands of the fuel cell electric vehicles (FCEV). The proposed architecture consists of five agents, namely a generation agent, an electrical- and thermal loads agent, a FCEV refilling station agent, a control agent, and a design agent. The design is the main agent that according to its interactions with the control agent and by minimizing the total costs of the system through PSO finds the optimal sizes of the system's components. In 2017 A. Kaabeche et al. [20] proposed a hybrid RES sizing method taking into account the combination between the RES, the ES capacity, and a given load profile. This optimization method is based on the Firefly Algorithm (FA), considering a load dissatisfaction rate criterion (LDR), the electricity cost indicator for power reliability and system cost. J. Jung et al. in 2017 [21] developed a technique for the planning and design of hybrid renewable energy systems in MG. A Distributed Energy Resources Customer Adoption Model (DER-CAM) determined the optimal size, type of DER and operating schedules. The electrical grid of the Brookhaven National Laboratory campus was used to demonstrate the effectiveness of

this approach. A.M. Ramli et al. in 2018 [22] optimized the size of hybrid microgrid system components, including storage, to determine system cost and reliability. The optimal sizing of a PV/wind/diesel HMS with battery storage was conducted using a Multi-Objective Self-Adaptive Differential Evolution algorithm. The objectives have been treated simultaneously and independently leading to a reduction in computational time. Results showed that a set of design solutions could assist researchers in selecting the optimal MG configuration. N. Ghorbani et al. in 2018 [23] presented a hybrid genetic algorithm based on PSO applied for the optimal sizing of an off-grid house with photovoltaic panels, wind turbines, and batteries. The minimization of the total costs of ownership was the main goal of this study. D. Prathapaneni et al. in 2020 [24] proposed a leader-follower based design optimization method for microgrids where the management of load demand is incorporated into the sizing process. A microgrid powering a desalination plant has been considered to evaluate the performances of the proposed method. The results demonstrated that the proposed coordinated sizing is cost-effective, and it provides better operational flexibility.

4.3 The two-layer optimization method

A two-layer algorithm to simultaneously find the optimal design, site, sizing and operation of CHP-MMG is proposed. The inner layer is a convex piecewise-linear problem and is solved with the sequential least squares programming method. The outer layer simultaneously solves a non-linear, non-convex problem with two novel evolutionary methods (i.e., ADE, AIE). The fitness values are generated by an analytical techno-economic model. A detailed description of ATE is reported in Chapter 2 and in the publication of the author (P. Fracas et al., 2021 [25]).

Figure 4.1 shows the flowchart of the algorithm. ATE incorporates a set of DER models, SLSQP algorithm, the associated objective function, energy balances and boundaries dictated by outer ADE/AIE methods and state of health of DER. The whole ATE model is described in Chapter 2 and discussed in [25]. The SLSQP method ensures that the generation and consumption of energy are balanced each time-step (i.e., hour) at minimal operational costs and highest revenues streams. The objective function of the dispatch problem to solve with SLSQP can be defined as:

$$min \quad f(x) = \sum_{c=1}^{N} LCOE_c \cdot x_c(t_s) - \sum_{r=1}^{R} LSOE_r \cdot x_r(t_s). \qquad [4.1]$$

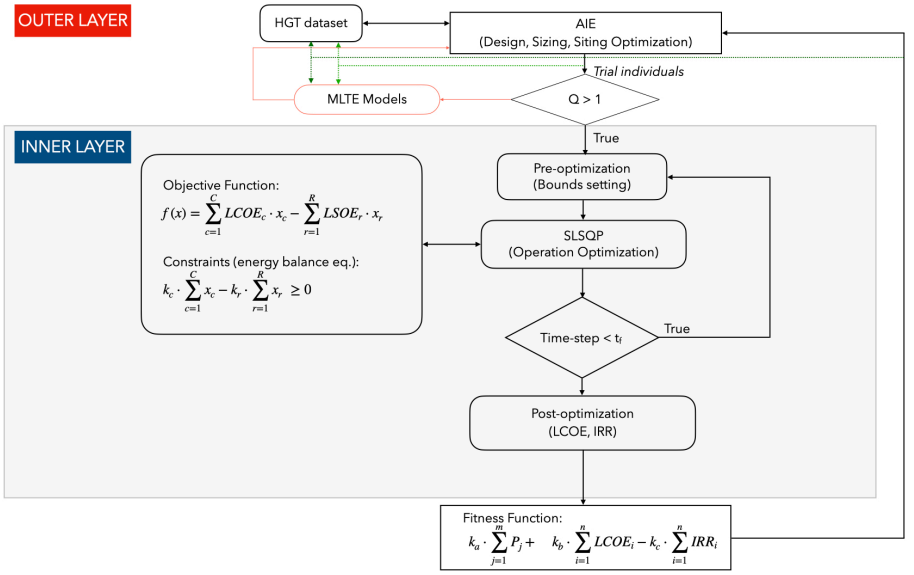

Figure 4.1 *Framework of the two-layer optimization algorithm*

Where x_c, x_r are the elements of the X-array candidate solution (i.e., respectively the energy flows of DERs consuming and generating energy). The LCOE is the ratio between the TCO and the energy generated along the lifetime of the DER. Similarly, the LSOE is the selling price deducted from the LCOE of the microgrid's products. While minimizing at each time-step the cost-revenues, the electric, the thermal generation of each microgrid and interconnections should balance the demands surplus DER and networks losses. To avoid energy under-flows and improve the convergence, the constraints are inequalities both for the thermal and electric energy flows of the DER and equalities for the exchanged energy flows between the two MG:

$$\begin{cases} \left(\left(\sum_{i=1}^{N} g_i^{der}(t_s) \right) \cdot k_d \right) - \left(\left(\sum_{j=1}^{M} g_j^{load}(t_s) \right) \cdot k_l \right) \geq 0 \\ \sum_{h=1}^{2} g_h^{itc}(t_s) = 0 \end{cases} . \qquad [4.2]$$

Where the terms g^{der} and g^{load} are the energy flows of the DER and are the energy flows between the MG. The index *i, j* and *h* specify each generator (i.e., DER), consumer of energy (i.e., load) and device to interconnect the MG, respectively. The k_d and k_l are parameters to calibrate the contribution of the two terms and hence, to set the size of the overflow. The latter permits the algorithm to improve the capability to converge. The DER models dynamically adapt the boundaries and computes the states of DERs after the elaboration of SLSQP. At the end of the iterations, ATE exits the SLSQP loop and computes the actual key financial ratios (LCOE, IRR, NPV) over the lifetime of the installation. The evolutionary algorithm at the upper generates the size of DER's size, the latitude and the longitude. The setting is used by the ATE model for the boundaries of SLSQP algorithm.

4.3.1 Introduction to self-adaptive evolutionary algorithms

Two novel self-adaptive differential evolution algorithms ADE and AIE have been developed to identify in the search space the setting of two CHP-MMG. Before proceeding to discuss the overall structure of the algorithms, the candidate solutions within the search area (i.e., the objects) are defined. An individual is a term used to denote the objects. The individual is composed by chromosomes; each of them embodies several elements named genes. The genotype is the set of genes. The phenotypes are the set of characteristics of an individual, as they result from the expression of its genotype. In our problem, the phenotype expresses the observable behavior of individuals interacting with local stochastic environmental conditions (e.g., radiation, wind speed, load profile, grid outages).

As described in Appendix A (Table A.2), in our problem, the individual is composed of 38 genes. The genotype contains two chromosomes: the first (chromosome of siting) embeds two genes describing the geo-spatial location (i.e., latitude, longitude) of the CHP-MMG configuration; the second (chromosome of sizing features) is composed of 36 genes that are describing the size of each DER. The two chromosomes (genotype) are the first property of the individual; the second property is the measure of its quality (fitness value). The individual can also be defined as a list of data having one dimension. Thus, for the latter is also used the term "population vector", "vector", "1d-array".

In our evolutionary computing problem, a population embedding 12 individuals is considered. An initial population is randomly generated according to a uniform distribution. After initialization, the EA enters a loop of evolutionary operations: adaptive mutation, crossover and selection. At each generation, a mutation vector is created with three individuals, named parents, randomly selected in the mating pools. The target vector is perturbed with the differences of the parents. The resulting difference vector is scaled down with a mutant factor which is self-adapted to the difference vector based on the latest best-so-far fitness values. This approach enables optimization of the search radius and increases the convergence of the algorithm. In AIE the mutant vector is obtained with a normal random distribution where standard deviation and mean are driven by the diversity of population and fitness convergence. Chromosomes of the mutant are randomly recombined with the target individual and with individuals randomly chosen in a dataset (horizontal gene transfer). In ADE the genes of the mutant individual are mixed and recombined with the target individual to obtain a trial individual. The intensity of crossover is adapted to the difference vector based on the best-so-far fitness values.

In both algorithms, a one-to-one survivor selection criterion is used to find the best individual. The selection criterion is based on the fitness values. The trial individual competes with the target vector. The individual with the lowest fitness value survives into the next generation. The selection procedure selects the better one between the target vector and the trial vector. Individuals with higher quality have a higher probability of being selected into the mating pool so that the good ones will have more chances to breed. Then the newly generated population replaces the old one and another generation starts. In the development of the ADE and the AIE algorithms, the above mentioned techniques keep the genotype diversity within an optimal bandwidth. The implementation is based on adapting the mutant, crossover parameters and a switching strategy to generate the mutant vectors and to transfer the genetic code during the recombination phase.

4.3.2 Self-adaptive differential evolution algorithm (ADE)

The self-adaptive differential evolution algorithm proposed method is based on DE. Compared to the original version introduced by Storn at al. in 1995 [5] here, the mutant

and crossover parameters are adapted according to the difference of the best-so-far fitness values. In other words, the best fitness value of the latest (e.g., n = 7) i-generations are saved in a vector and the difference is calculated.

The i-individual is represented by a vector embedding the chromosome of sizing with 36 genes ($x_{i,h,g}$, $h=1,\ldots,36$) and the chromosome of siting composed by 2 genes ($x_{i,k,g}$ k=1,2). A group of individuals represents the g-population. The index g denotes the generation counter. The maximum value of g (g_{max}) is the stop criterion. Thus, the g-population of n individuals is a matrix (2d-array) of vectors as follows:

$$X_g = \begin{bmatrix} x_{1,1,g} & \cdots & x_{1,38,g} \\ \vdots & \ddots & \vdots \\ x_{n,1,g} & \cdots & x_{n,38,g} \end{bmatrix} . \qquad [4.3]$$

The dimension n of the population is hereafter named as *popsize*.

Based on that, the DE algorithm starts to randomly generate the initial *0*-population according to a uniform distribution.

$$X_{i,0} \quad = \quad rand_{i,0}[0,1) \cdot \left(B_{i,0}^{U} - B_{i,0}^{L} \right) + B_{i,0}^{L} . \qquad [4.4]$$

The two initialization vectors: $B_{i,0}^{U}$ and $B_{i,0}^{L}$ of the individual $X_{i,0}$, indicate respectively the initial upper and lower bounds of the genotype $X_{i,0}$. The boundaries - which are input values of the algorithm - represent the limit of genotype space to search. The random number generator: $rand_{i,0}[0,1)$ returns a uniformly distributed random number within the range $0 \leq rand[0,1) \leq 1$. The index i indicates that a new random value is generated for each parameter. The main idea after initialization is that DE enters a loop of evolutionary computations *mutation* and *crossover*, generating a set of trial parameter vectors. Then, the loop ends with the *selection* of the best individual between the trial and the target vector. The original mutation strategy (DE/rand/1) is based on three vectors uniformly chosen from population set. The mutation vector is generated with the perturbation of a base vector $X_{1,g}$ by using a difference vector based mutation.

The difference vector distribution usually adapts to the landscape of the objective function. During the trials, it has been observed that a single difference vector limits the potential perturbation possibilities for a base vector and hence stagnation in a certain

search area may occur which leads to solutions away from the global optimum. Perturbation of the base vector by mutation has been treated very early and has led to various variants of DE. To enhance genotype diversity, the original mutation strategy is modified by perturbing the base vector $X_{1,g}$ with three difference vectors whose intensity is adapted. The goal is to generate more distributed difference points without increasing the number of population members and thus enhance the contour matching property.

The following variant of the original mutant equation is proposed:

$$V_{i,g} = a_{i,g}^{par} \cdot \quad X_{1,g} + a_{i,g}^{dith} \cdot (X_{2,g} - X_{3,g})/3 + \cdot a_{i,g}^{dith} \cdot (X_{1,g} - X_{2,g})/3 + \cdot a_{i,g}^{dith} \cdot (X_{1,g} - X_{3,g})/3 , \quad [4.5]$$

where $a_{i,g}^{par}$, $a_{i,g}^{dith}$ are the parameters to adapt *and* k_1, k_2 are constants.

To set $a_{i,g}^{par}$, $a_{i,g}^{dith}$ a 1d-array is created with the subset of the latest best-so-far fitness values as follow:

$$F_g = [f_k^{bsf}, \ldots, f_g^{bsf}], \quad [4.6]$$

where k is the *index* denoting a subset of g. Then the corresponding *1d*-array with the differences is calculated as follow:

$$S_{i,g} = \left[(f_k^{bsf} - f_{k-1}^{bsf}), \ldots, \left(f_g^{bsf} - f_{g-1}^{bsf} \right) \right]. \quad [4.7]$$

The difference vector ($S_{i,g}$) is used to self-adapt the parameters $a_{i,g}^{par}$, $a_{i,g}^{dith}$, and thus, to maintain an optimal population diversity.

$$a_{i,g}^{dith}, \quad a_{i,g}^{par} \quad c_{i,g} = \begin{cases} rand(v_{min}, v_{max}) & if \quad each \quad S_{i,g} \quad \in \quad S_{i,g} > 0 \\ rand(w_{min}, w_{max}) & if \quad otherwise. \end{cases} . \quad [4.8]$$

Eq. 4.8 shows that the mutant $(a_{i,g}^{dith}, a_{i,g}^{par})$ and crossover parameters $(c_{i,g})$ are uniformly distributed over intervals whose range is subjected to intensity and versus of the elements of $S_{i,g}$.

Notably, v and w have been empirically set within the interval: 0.54 - 0.98. It has been observed that queries based on this bandwidth allow to obtain a suitable genotype diversity. The mutation vector $V_{i,g}$ is then mixed with the so-called target vector $X_{i,g}$ (where $i \neq 1,2,3$) through the classic variant of diversity enhancement, the crossover,

which allow to properly mix the parameters of the mutation vector $V_{j,g}$ to generate the trial vector $U_{i,g}$.

The crossover is defined as:

$$U_{i,g} = \begin{cases} v_{j,i,g} & if \quad (randj[0,1) \leq c_{i,g}) \\ x_{j,i,g} & otherwise \end{cases} . \qquad [4.9]$$

The parameter $c_{i,g}$ is uniformly distributed over intervals whose range is subjected to the value of $S_{i,g}$. As for the mutant factor, the crossover parameter, is generated with Eq. 4.8. Here the amplitude of the random intervals is chosen between 0.5 and 0.98 to modulate the intensity of the vector mix and thus keep an optimal genotype diversity. The situation where: $U_{i,g} = X_{i,g}$ is avoided with at least one element of the array $U_{i,g}$ is taken from the mutation vector $V_{i,g}$.

The crossover has the potential to destroy the directional information provided by the difference vectors and thus, it can reduce genotype diversity. It happens when strong crossover is used (e.g., $c_{i,g} \leq 0{,}30$). In this case, DE has a strong tendency to search along the target points; in contrast to a weak cross over (e.g., $c_{i,g} \geq 0.90$) which addresses the DE to search far away from the target, i.e., nearby the mutant.

The role of the parameter $S_{i,g}$ is to enhance the control of the diversity over all the process of generation of the trial vector. The trial vector $U_{i,g}$ is finally utilized to compete against the target vector $X_{i,g}$ as follow:

$$X_{i,g+1} = \begin{cases} U_{i,g} & if \quad f\left(U_{i,g}\right) \leq f\left(X_{i,g}\right) \\ X_{i,g} & otherwise \end{cases} . \qquad [4.10]$$

The one between the trial and target vector that yields the lowest objective function result (fitness value) will survive and become a member of the next generation g+1. For each generation, the individual within the *g*-population having the best fitness i.e., the best-so-far (BSF) value, is preserved to keep track of the progress that is made during the minimization process. Figure 4.2 shows the overall framework of the AIE.

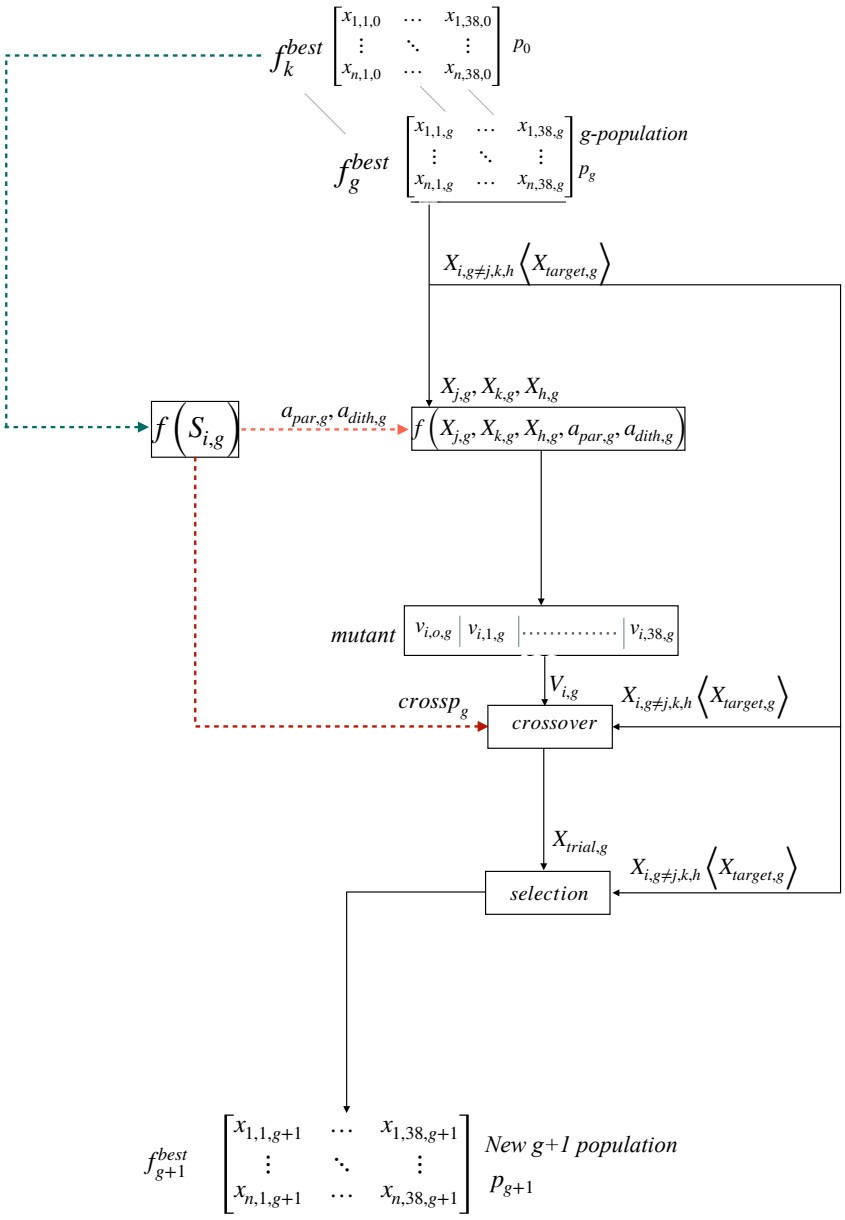

Figure 4.2 *Flowchart of self-adaptive differential evolution algorithm*

4.3.3 Self-adaptive artificial immune algorithm (AIE)

In 2020 our life has been deeply influenced by the corona virus disease (COVID-19). The spread of this pandemic across the globe was an inspiration to imitate how the immune system fights harmful viruses that enter the body. The basic function of the immune system is to identify and destroy the virus. The pathogen is recognized by special structure molecules, known as an antigen. An early example of an autoimmune algorithm has been proposed by De Castro et al. in 2002 [27].

Their algorithm mimics the clonal principle. In artificial immune algorithms, the term of "individuals" (in ADE represented as a "vector") is replaced by "antibodies", the objective function is replaced by "antigen", the fitness values with the term "affinity measure", the population with the "repertoire" and the mutation with somatic "hypermutation".

An innovative version of the EA, hereafter named *self-adaptive artificial immune evolutionary algorithm* (AIE) is proposed. In the early generations, a mutant antibody is created with a random generator. In the later number of generations, a difference vector-based mutant is randomly recombined with external antibodies. The latter is randomly chosen by the horizontal gene transfer (HGT) and vertical gene transfer (VGT) techniques. The first method to create a mutant object mimics the early stage mechanisms to generate an antibody to unknown antigens. The subsequent method is based on the difference between a couple of antibodies. It imitates a more sophisticated mechanism to evolve an antibody in the acquired immune system. The recombination method (HGT/VGT) imitates the improvement of the immunity deriving from external genetic pieces (i.e., RNA) having beneficial properties. The initialization is performed with an equivalent method as described in Paragraph 4.3.2. The parameters i.e., popsize, generations, boundaries are assigned to the matrix repertoire described in Eq. 4.3. Then, the main loop is repeated until the stop criterion (e.g., maximum generation, minimum affinity measure) is reached.

In the AIE loop, the mutant is generated by following two different methods. The selection of the methods is correlated to the generation g (i.e., $g < g_{ade}$, where $g_{ade} = 20$) and *g-diversity of repertoire* (D^R_g) obtained by computing the standard deviation of the g-repertoire. The parameter D^R_g measures the genetic diversity of the g-repertoire.

Thus, at the early generations or if $D^R_g < 0.4$, the mutation vector is drawn from the parameterized normal distribution of Eq. 4.11, then it switches to ADE method.

$$V_{i,g+1} = \begin{cases} V_{i,g} = N\left[\mu_{i,g}, \sigma_{i,g}\right] & if \quad f\left(D^R_g, g\right) \quad = \quad False \\ Eq.\ \ 4.5 \quad otherwise \end{cases}. \qquad [4.11]$$

It has been observed that the early populations affect the investigation of the promising regions of the best-so-far fitness values obtained later. The purpose of the AIE-based mutant strategy in Eq. 4.11 is to enhance the initialization phase.

Switching after the first 20 generations to the differences vector-based mutant of Eq. 4.5, allows enhance the search with the direction-based method. The elements of mutant are within the normal range: $0 \leq v_{i,j,g} \leq 1$. The parameters $\mu_{i,g}, \sigma_{i,g}$ are respectively the mean and the standard deviation of the *i*-mutant.The term $\mu_{i,g}$ is set equal to the mean of the i-individual. The term $\sigma_{i,g}$ is self-adapted based on the value of *i-convergence of antibody* ($C^A_{i,g}$) and D^R_g. $C^A_{i,g}$ is obtained by computing the standard deviation of the 1d-array that embeds the i-affinity measure of the i-genotype and the *i-best-so-far affinity*, minus a constant ($k_c \cong 0{,}3$) chosen to strengthen the tendency toward the convergence. This term gives an indication of the location of the antibody in the space area. The correlation between D^R_g and $C^A_{i,g}$ is an indicator of the convergence toward a local minimum. It is used to adapt $\mu_{i,g}, \sigma_{i,g}$ and determine the crossover parameter.

To tune the adaptive parameters, the AIE has been executed for 100 queries. From the best 60 queries, it has been observed that if the D^R_g remains within a bandwidth from 0.30 to 0.44 , and the C_A gets down from a high value (i.e., 0.90) to a lower one (i.e., 0.1), the trial vector population adapts to search the most promising regions of the search area.

The scatter pattern in Figure 4.3 shows the three clusters of pair-wise data obtained in 5.741 generations, corresponding to the optimal 60 queries. The upper cluster embeds the features of early generations of each query (brown dots). The cluster of yellow dots is the features of the intermediate generations. The lower cluster groups the final generations whose j-convergence is centered on 0.10 while the corresponding value for the *j*-diversity is 0.38. The centers of the three clusters (large orange dots in Figure 4.3) have been obtained with the *KMeans* clustering method to separate samples in groups of

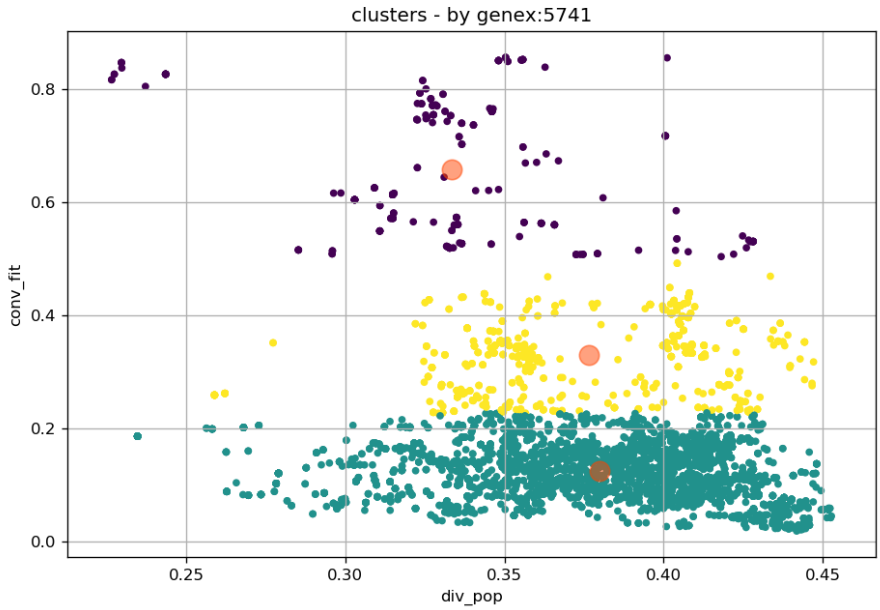

Figure 4.3 *Clusters of fitness convergence and genes diversity by KMeans algorithm*

equal variance [28]. The cluster centroids are used to adapt $\mu_{i,g}, \sigma_{i,g}$ in Eq. 4.11. The cluster centroids are further employed to parametrize the crossover to further control the diversity of the repertoire. A strong crossover is set when the C_A is between 0.15 and 0.30 and the $D^R{}_g$ is between 0.30 and 0.40 (i.e., the affinity measure is keeping a moderate convergence while the repertoire still remains diverse). If these conditions are not respected, the search is moving away from the most promising area and the crossover is set to weaker values. After setting the mutant and crossover parameters, a somatic hypermutation is performed. Here the mutant antibody is randomly recombined with the target antibody (VGT) or with pieces of an external genotype (HGT). The external vector is randomly chosen within a dataset of optimal solutions obtained from previous queries. HGT technique, imitates the imaginary alien organisms (e.g., spike proteins) that latch on to antibodies and prevents the virus from getting into cells, stopping the virus from causing disease (i.e., minimization of the affinity measure).

HGT has been recently recognized to play a relevant role in the evolution of living organisms in combination to vertical transfers of genes. In biological eukaryotic and prokaryotic organisms share a large portion of non-coding DNA/RNA transferred with

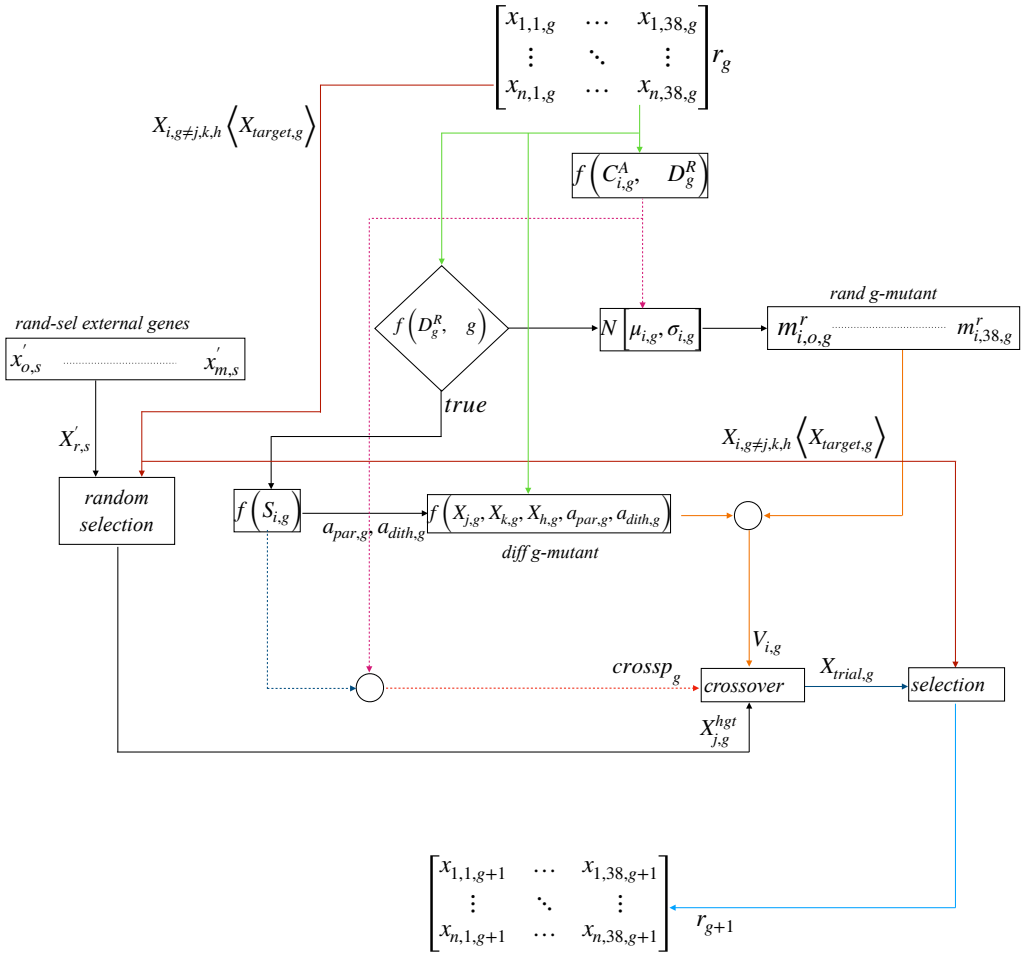

Figure 4.4 *Flowchart of self-adaptive artificial immune algorithm*

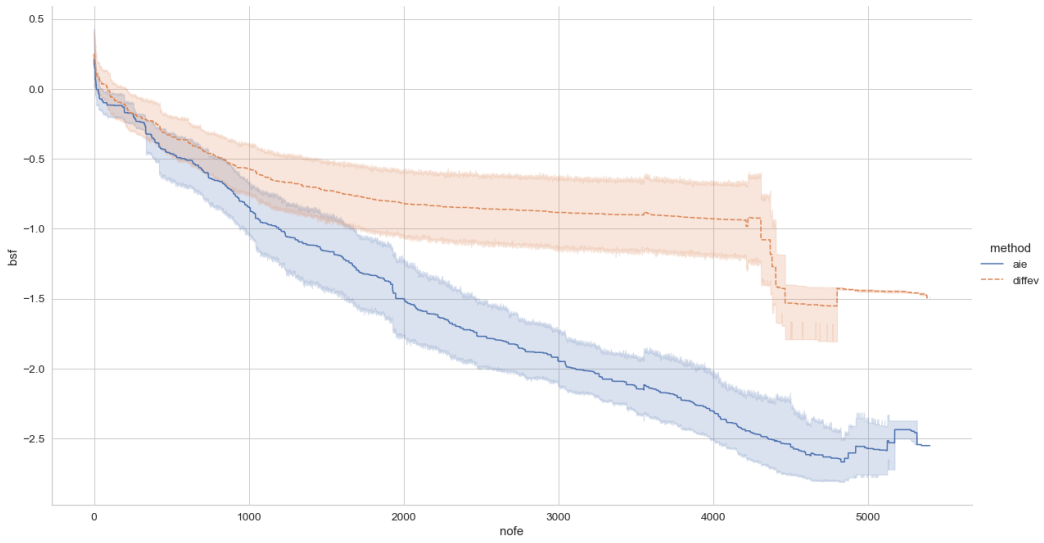

Figure 4.5 *Comparison of the fitness spread, 350 generations, AIE and DE (original algorithm by Storn) with objective function based on ATE*

lateral mechanisms (e.g., virus). Parts of DNA/RNA from a dead, disintegrated organism can, in some rare cases, penetrate the cellular organism wall and be incorporated into living cell DNA. Rafajłowicz W. in 2018 [29] proposed HGT to transfer genes from a random individual in old repertoire. Numerical results indicate the usefulness of HGT when applied to optimization problems of moderate size. When the vertical/horizontal recombination is executed, the affinity measure is computed and hence, the loop ends. Hence, the *j*-trial antibody vector and the *j*-target antibody are evaluated according to Eq. 4.9, returning the minimum affinity measure. Figure 4.4 shows the overall framework of AIE.

Figure 4.5 shows the comparison between AIE and the original DE algorithm proposed by Storn [6] in which the mutant factor is set $F = 0.5$ and crossover $C_r = 0.8$. The plot is based on 24 queries (i.e., 12 queries with AIE and 12 with DE) to search the optimal configuration and size of DER in a CHP-MMG located in Bremen.

The correlation between the slope of the standard deviation of the affinity measures and the slope of the D_R has been used as stopping criterion. The results for AIE are represented with blue bandwidth and for DE with the red bandwidth. The vertical axis indicates the best-so-far fitness values found by the algorithm for each evaluation in each query. The horizontal axis indicates the number of fitness evaluations (NOFE). The curves aggregate the measurements at each iteration for the mean and the 95% confidence interval around the mean. The behavior of the curves demonstrates an overall better quality of solutions with AIE. The gap between the means values of the AIE (dashed blue line) and DE (dashed red line) widens since 120 generations.

The plot in Appendix B is obtained with 20 queries (i.e., 10 queries with AIE and 10 with DE). The quality of the best-so-far fitness values of AIE is still better than ADE but the deviation between the bands is less marked. Thereby, the adaptation of mutant parameters even without HGT, contributes to improve the quality.

The overall results demonstrate the effectiveness of the strategy implemented in AIE. At the beginning, the random mutant enhances the initialization phase, then the mutant based on ADE combined with the HGT/VGT crossover enhances the search direction. The AIE method avoids that parents suffer from a loss of diversity, and thus it prevents that populations are stalled in a low-fitness valley. After the initial generations, the search area is in a better position where it proceeds with the differential mutant vectors. The initial control of mutant and crossover enhances the exploration of wide regions of the search space.

Therefore, the risk that a repertoire converges a local optimum is mitigated. HGT gives a contribution to accelerate the search and it attenuates the fitness error. The method mimics antibodies that randomly mutate and casually recombine thru HGT with external organisms. This approach strengthens the ability to confer protection against an aggressive antigen that evolves over the RNA. The mutation of the antigens in this case, is represented by the stochastic terms in the fitness function [25]. The aleatory recombination with pieces of external RNA secretes quicker and better repertoire of antibodies. These mechanisms enable to successfully evolve generation by generation to improve faster the affinity measures and to effectively converge into global minimum locations.

4.4 The fitness function

Each solution (i.e., the *j*-individual) of the *g*-population has associated a performance indicator: the fitness value. The latter is derived from a fitness function (FF) that is designed to search for the most profitable solution among a mix of DER type (design objective), size (sizing objective) and geo-locations (siting objective). FF is a multi-objective relation that combines three terms: the levelized cost of energy, the internal rate of return, and penalties on unusual configurations and energy unbalances. The IRR is used to rank the profitability of the potential investment in the j-solution. The latter measures the rate of return on an investment, calculated from the discount rate that equates the present value of future cash inflows to the CHP-MMG's total cost of ownership. The LCOE gives the cost of generating electric and thermal energy for the CHP-MMG including the cost of the energy-generating system, including all the costs over its lifetime, initial investment, operations and maintenance (O&M), cost of fuel, and cost of capital [25]. The LCOE is a measure of the marginal cost (the cost of producing one extra unit) of electricity and heating over an extended period. The combination of these two objectives and the penalties (P) associated to undesired configurations is given in the following relation:

$$f(x_{j,i,g}) \quad = \quad k_a \cdot \sum_{j=1}^{m} P_j + \quad k_b \cdot \sum_{i=1}^{n} LCOE_i - k_c \cdot \sum_{i=1}^{n} IRR_i \ . \qquad [4.12]$$

Where k_a, k_b, k_c are different constant empiric weights. They are set with trials and their role is to balance the contribution of each term (i.e., LCOE, IRR, P). LCOE is widely used to compare the economic competitiveness of the energy mix (S. Sung et al. , 2019 [29]). This term is easy to understand and straightforward to apply which is the reason why it preferred by many energy policymakers. However, the method is not exhaustive from the business point of view. The LCOE approach does not consider revenues. Additionally, the LCOE does not consider equity, loan which influence the economic attractiveness of an investment. LCOE and IRR are not in conflict, but they are not necessarily proportionally correlated. LCOE is correlated to the total cost of ownership per energy generated, while IRR is subjected to the contribution of each product to the revenue stream. Eq. 4.12 measures both the financial objectives (i.e., LCOE and IRR) and penalties (P) associated to undesired configurations and underflow energies (i.e., unbalanced energy flows). The penalties, discourage the selection of

individuals with unusual configurations (i.e., generators without tanks and vice-versa) and thus contribute to accelerate the search of the best LCOE and IRR. The weighted sum method gives to the decision-maker the possibility to assign the importance for each objective with the calibration of the weights. The correlation between the standard deviation of fitness array and population's genes reflects the quality of the sought design and this correlation can be used as stop criterion. Moreover, the FF incorporates stochastic terms (i.e., climate variables, grid outage, load profiles) [25]. Hence, this problem returns clusters of global solutions (i.e., PBS) having a similar fitness value. To find the best configuration, the optimization must be repeated until the standard deviation of the PBS genotypes reach the desired value. The PBS having the lowest fitness value can be assumed as the candidate of being the "best of the best probabilistic solution". The final task is to verify with the sample average approximation method [30] if the latter solution returns the best expected performance over all the uncertain scenarios. This approach can be defined as "simulation-optimization" [2] [31].

4.5 Results and discussion

The first part of this work is addressed to investigate how the geographical location affects the size and performance of CHP-MMG configurations in on-grid and off-grid scenarios. Moreover, the study investigates how the cost and type of hydrogen impact the selection of the CHP-MMG settings.

Three options for the supply of hydrogen are discussed. The first is the on-site production by electrolyzers embedded into the CHP-MMG. The second is hydrogen sourced from large renewable-to-hydrogen (*R2H2*) plants. The third deals with on-site production by plasma assisted decomposition of methane.

R2H2 links WT and PV to electrolyzer stacks which pass the excess electricity through water to split it into hydrogen and oxygen. In our simulations, hydrogen delivered by R2H2 plants, is stored at the CHP-MMG site for later use with FC. R2H2 is the most promising scenario for generation of green hydrogen over the coming decade. For regions where renewable energy costs are on average higher, e.g., Northern Europe, there are areas with favorable conditions for large scale renewable energy. This makes it possible to produce hydrogen at lower-than-average costs and site selection for renewable hydrogen production becomes critically important. A.Ochoa Bique et al. [32]

Location	Lat	Long	Cost of Hydrogen	
			actual	future
Bremen	53.07	8.80	13€/kg	3€/kg
Catania	37.50	15.08		

Table 4.1 *cost of fuel and geolocations for the simulated scenario*

show how mathematical modeling and mixed integer linear optimization allow to identify optimal decentralized green hydrogen production fields, infrastructure pathways and supply chain networks. In the present study, the green hydrogen is outsourced to FCs thru R2H2 fields is not counted into the fraction of energy generated with RES. The RES factor contemplates only the portion of energy generated by the RES locally integrated in the CHP-MMG. Although in the on-grid scenario both choices for the hydrogen supply are considered, configurations with hydrogen generation on-site are not selected (i.e., the size of EC in Table 4.3 is zero). Hence, it is inferred that the optimal CHP-MMG's configurations are those that store electric energy or convert in thermal energy or exchange it with other grids rather than converting electricity into the hydrogen.

Two sites displaced in different area of Europe has been considered to examine the impact of the geo-location. Their geo-coordinates and costs for the delivered fuel are indicated in Table 4.1.

4.5.1 The on-grid scenario with green hydrogen

This first scenario considers two CHP-MMG connected to the main grid. Each MG can embed a PEMFC-CHP powered with hydrogen generated on-site and green hydrogen supplied by R2H2. The optimization is executed with the ADE using a population of 12 individuals evolving over 220 generations. In Appendix A the boundaries of the 38 genes of each individual are listed.

The fitness values are computed for 85% of the generation in "low resolution" (LR). Namely, the time series are sliced to select one day each month. Hence SLSQP executes only 288 loops (i.e, 24 time-steps/month). The remaining generations (15%) are computed in "high-resolution" (HR); it means that SLSQP executes 8760 loops. Before switching in HR, the algorithm recalculates the fitness values of the latest population to

Service	Grid-tied	Off-grid
Electric energy to user	38 c€/kWh	45 c€/kWh
Thermal energy to user	22 c€/kWh	22 c€/kWh
Sellback of electric energy among MG	5 - 28 c€/kWh	23 c€/kWh
Sellback of thermal energy among MG	5 - 18 c€/kWh	12 c€/kWh
Sellback of electric energy to grid utility	*11 - 18 c€/kWh*	
Demand response to grid utility	*-5 - 28 c€/kWh*	
Water	15 c€/lt	15c€/lt

Table 4.2 *Price structure of the services offered in isolated CHP-MMG*

check the consistency of the best-so-far solution. It is remarkable to note that LR computes in 3 minutes a generation instead of 12 minutes/generation in HR.

In Table 4.2 the price's structures of products (heat, electricity and water of FC), which are sold to the nearby MG and of the delivered energy demand services to the main grids (GRID) are listed. The boundaries applied to the ADE algorithm are indicated in Appendix A (Table A.1). Based on these assumptions, the best solutions (optimal design and sizing) of the best query obtained in the southern (Catania - Italy) and northern (Bremen - Germany) sites are computed.

Table 4.3 shows the results for the scenarios in each location with the different cost structure of hydrogen. It can be observed, that in South Europe, the increase of the hydrogen costs does not affect the optimal mix of RES: the role of PV, WT, ST remains marginal in all cases. Here, a cost of hydrogen 1-3 €/kg boosts FCs to lead the production of electricity and heat. On the contrary, with the actual cost of hydrogen (i.e., 13 €/kg), the optimal supplier of energy still remains the GRID with tariff rates ranging between 0,24 and 0,36 €/kWh. The cost of hydrogen heavily impacts the financial performance (IRR) of the optimal CHP-MMG. IRR almost halves when the hydrogen costs doubles. This is mainly due to substantial differences in CAPEX but a similar structure for revenues in the two scenarios.

In Northern Europe, a high supply cost of hydrogen causes a consistent increment of the PV and WT sizes while FC are still replaced by the main grid. The RES factor, a ratio that correlates the energy generated by RES installed into the MG with the energy

	1,00 € / kg_{H2}		3,00 € / kg_{H2}				13,00 € / kg € / kg_{H2}			
	Bremen (GE)		Bremen (GE)		Catania (IT)		Bremen (GE)		Catania (IT)	
DER Size	**MG_A**	**MG_B**	**MG_A**	**MG_B**	**MG_A**	**MG_B**	**MG_A**	**MG_B**	**MG_A**	**MG_B**
PV	5 kW	5 kW	5 kW	8 kW	5 kW	5 kW	29 kW	141 kW	9 kW	5 kW
WT	3 kW	3 kW	3 kW	3 kW	3 kW	3 kW	140 kW	131 kW	3 kW	3 kW
ESS	-	-	100 kWh	14 kWh	-	-	-	-	-	-
FC	12 kW	18 kW	41 kW	40 kW	13 kW	10 kW	-	2 kW	-	-
EC	-	-	-	-	3 kW	-	-	-	-	-
OG	-	-	-	-	-	-	-	-	-	-
GRID	-	-	-	-	-	-	100 kW	100 kW	22 kW	100 kW
ITCEL	100 kW	100 kW	6 kW	6 kW	3 kW	3 kW	3 kW	3 kW	3 kW	3 kW
ST	-	5 kW	5 kW	5 kW	-	5 kW	5 kW	-	-	5 kW
EBOY	-	-	-	157 kW	23 kW	70 kW	26 kW	126 kW	121 kW	-
HP	300 kW	300 kW	-	300 kW	81 kW	-	281 kW	281 kW	242 kW	-
STHP	-	-	300 kW	-	-	98 kW	-	-	-	243 kW
ITCTH	5 kW	5 kW	5 kW	5 kW	5 kW	5 kW	5 kW	5 kW	5 kW	5 kW
LCOE	0,15	0,161	0,155	0,223	0,136	0,116	0,114	0,165	0,164	0,172
IRR	***32,7%***	***31,7%***	***19,7%***	***12,6%***	***51,1%***	***55,4%***	***19,9%***	***12,4%***	***27,4%***	***28,3%***
NPV	***542.586***	***596.401***	***461.218***	***240.464***	***622.123***	***841.975***	***849.888***	***434.543***	***434.533***	***401.888***
RES_factor	2,9%	2,9%	3,4%	2,9%	2,4%	3,3%	100%	100%	3,2%	3,3%

Table 4.3 *DER size, key financial ratios in different scenarios (25 years project lifetime, 5% discount rate)*

to sell, from 3% jumps up to 100%. The IRR drops by almost 50% if the hydrogen costs raise from 1,00 to 3,00 €/kg €/kg_{H2}

From 3,00 to 13,00 €/kg_{H2}, the IRR is almost the same. This result can be explained by a similar structure of net cash flows, which does not produce any substantial change in IRR.

It can be concluded that cost of hydrogen and availability of local renewables resource both deeply influence the optimal design, sizing of DER and their IRR. Contrarily, LCOE assumes a similar value in each location and scenario. Moreover, the outcomes demonstrate that in different locations it is always possible to find an optimal mix of DER that keeps the cost of energy at the same level. Hence, these simulations prove the versatility of CHP-MMG technology which can adapt to different climate conditions of Southern and Northern Europe. However, this flexibility affects the return on investment. The simulations indicate that the optimal location in Southern Europe.

While the precedent optimizations refer to fixed geo-locations (i.e., Bremen, Catania), a further study was conducted by setting the boundaries of geo-locations in Northern Europe centered in Bremen +/- 7 decimal degree both for latitude and longitude and the same in Catania for South Europe. The scope was to search the best siting and design of CHP-MMG in two regions of Europe with different climate conditions.

These further optimizations were performed with AIE, the same inputs, with the exception of fuel cells for which a more realistic operating condition was set. The start-up/shut-down procedures have been constrained as follows: at startup, the FC supply a maximum 10% of nominal power and then they have to run for at least 1 hour before executing the shut-down. Additionally, an average random grid outage at 10% is assumed. It is noted that these conditions affect the search area in both European regions. The sell-back to the main grid accounts for over 80% of the overall revenue streams in both regions. Thus, remuneration of energy demand response services has a relevant role in the IRR. When sell-back policies are not in place, IRR is null and thus there is not any payback of the investments.

Within the cluster of best solutions, the AIE selects in Denmark the best siting of Northern Europe for CHP-MMG. This region has favorable wind conditions and thus WT are the best choice for RES coupled with FC and the main grid. Thermal energy is generated with heat pumps and exchanged between the MG. Similarly, in Southern Europe the best configurations comprise a mix of PV with WT associated with FC and the main grid. Here the best siting from Catania is the East part of the Mediterranean Area (i.e., Greece) where the combination of solar radiation, wind speed and cloudiness conditions are more favorable.

These simulations have brought out a scheme of collaboration between the two microgrids (i.e., ‘swarm effect’, Chapter 6) fostering the overall efficiency, energy resilience to uncertainty, and optimal financial performance [25]. Interconnections are used to permit crossflows of thermal and electrical energies.

Notably, a fraction of the exceeding electrical energy (i.e., not used to feed the loads or charge batteries), flows via the interconnections back and it is converted into thermal energy. Thus, a portion of heat swarms to the other microgrid.

4.5.2 The off-grid scenario

The analysis in this paragraph is extended to off-grid. It is assumed that the CHP-MMG does not have access to hydrogen refilling as well to the main grid. The refilling of OG is still considered. To simulate the off-grid scenarios, the boundaries of AIE indicated in Appendix A / Table A.1 have been set to zero for the GRID_SIZE genes (i.e., MG are disconnected to the main grid). At the initial start-up of the plant, the thermal storage tanks and hydrogen fuel tanks are empty and the initial state of charge of the lithium battery is 30%. Based on these harsh conditions it is intended to simulate the resilience of the CHP-MMG at the beginning of the operations, and the financial sustainability of the entire off-grid configurations in Europe.

It is relevant to note that as indicated in Table 4.2 the price structures for off-grid (i.e., third column) are set equal to the on-grid except for: 1) the tariff rates of electricity to the end-users which has been set slightly higher (i.e., 18%) than on-grid; 2) the sell-back tariffs of thermal and electric energy which are exchanged between MG are reduced.

The off-grid optimization problem has been solved by EA in two queries without slicing the time series (i.e., high-resolution). The first query has processed 120 generations. In the second query, 90 generations were enough as the boundaries have been narrowed values nearby the best solutions given in the first run. The overall results are presented in Table 4.4.

AIE has selected a similar mix of DER in both sites. It is worth noting that the range of LCOE in off-grid (i.e., 0,11 - 0,16 €/kWh) is narrower than to in on-grid scenarios (0,11 - 0,22€/kWh). The optimal configuration combines WT, ESS, the electrical interconnection among MG, direct thermal energy generation with ST and its heat hump (STHP). This MG setting is demonstrated to be an effective solution to overcome the missing refilling of hydrogen and the electricity supplied by the main grid.

It is noted that both locations do not include FC and OG. The AIE penalizes candidate configurations generating on-site hydrogen with EC or OG (i.e., diesel gensets). In Northern Europe, the TCO is lower than on-grid scenarios where the hydrogen cost is 3 - 13 €/kg.

The revenues are slightly lower as the demand response services are not furnished. However, with the price of selling electricity and heat indicated in Table 4.2. On the

contrary, in Southern Europe, TCO are higher than the correspondent on-grid cases depicted in Table 4.3. This is explained by the different sizes of RES which have lower specific yields than in Northern Europe. In both locations, the deprivation of income given by energy demand services and sell-back to a main grid in on-grid, lower the financial performances. However, the effect is marginal. The IRR still remains with 13% in South Europe and 22% in North Europe attractive. Besides, it is noted that RES factor is not 100% as it should be expected in off-grid contests, without any external outer energy contribution. Indirect generation of energy by STHP thru RES is not considered.

These simulations have demonstrated the resilience of the off-grid CHP-MMG system. The SLSQP algorithm is able to perform a full balance of both thermal and electric energies with the PBS. No thermal and electric energy underflows have been computed during the whole time horizon (i.e., 8760 hours). It can be concluded that with a structure of energy tariffs somewhat higher than on-grid CHP-MMG, islanded systems ensure a reliable, regular supply of energy with highly attractive IRR, and convenient LCOE.

DER Type	Bremen (DE)		Catania (IT)	
	MG_A	MG_B	MG_A	MG_B
PV	10 kW	45 kW	10 kW	11 kW
WT	60 kW	79 kW	111 kW	109 kW
ESS	49 kWh	45 kWh	41 kWh	50 kWh
FC	-	-	-	-
EC	-	-	-	-
OG	-	-	-	-
GRID	-	-	-	-
ITCEL	21 kW	21 kW	74 kW	74 kW
ST	59 kW	114 kW	109 kW	300 kW
EBOY	-	-	-	-
HP	-	-	-	-
STHP	272 kW	300 kW	259 kW	262 kW
ITCTH	-	-	74 kW	74 kW
LCOE	0,11€/kWh	0,12€/kWh	0,16€/kWh	0,15€/kWh
IRR	24,70%	22,70%	13,60%	14,00%
NPV	657.634 €	756.342 €	391.721 €	475.883 €
RES_factor	57%	68%	81%	100%

Table 4.4 *Size of DER, key financial ratios for off-grid CHP-MMG (25 years project lifetime, discount rate of 5%, no daily refilling of hydrogen)*

4.5.3 Scenario with fuel cells powered by blue hydrogen

Another set of optimization-simulations has been conducted replacing green hydrogen with blue hydrogen in combination with FC. Although green hydrogen leads to the lowest greenhouse gas (GHG) emissions, networks, infrastructures for storage and transport of hydrogen are not yet established. On the contrary, the infrastructure of natural gas containing methane is available worldwide and hydrogen is already produced industrially from steam methane reforming (SMR). The drawback of SMR is the generation of significant carbon emissions. Thus, this type of hydrogen is known as "grey" hydrogen. In the cleaner version (SMR with CCS) named as "blue hydrogen", carbon emissions are captured and stored, or reused. These processes emit few GHG because the reaction from methane to hydrogen yields only solid carbon and no CO_2. S.Timmerberg et al. in 2020 [33] have assessed the life-cycle GHG emissions and the levelized costs for hydrogen provision from three types of methane pyrolysis (plasma, molten metal, and thermal gas).

The results of these configurations have been then compared to electrolysis and SMR with and without CO_2 capture and storage (CCS). In methane pyrolysis, GHG are between 43 and 97 g $CO_{2\text{-eq.}}$/MJ which is mainly caused by the primary energy source.

They have concluded that the lowest emissions are obtained with the combination of plasma-based methane decomposition with renewable electricity. This configuration shows lower GHG emissions compared to the "classical" SMR (99 g CO_2-eq./MJ), but similar emissions to the SMR with CCS (46 gCO_2-eq./MJ). Two types of plasma can be applied to methane decomposition: cold and thermal (hot) plasma. Cold plasma processes typically show lower conversion efficiencies compared to hot plasma processes.

Hence, a further optimization study based on Southern Europe has been launched again. The latter work intends to analyze the financial performance of optimal CHP-MMG embedding PEMFC-CHP and on-site hydrogen generation thermal plasma (TP) systems operating on-grid.

Table 4.5 shows the comparison between two optimal on-grid CHP-MMG configurations delivered by AIE after 350 generations. The first comprises PEMFC-CHP powered by green-hydrogen (i.e., hydrogen supply by remote R2H2) and the other

	On-grid with blue hydrogen		On-grid with green hydrogen	
	MG_A	**MG_B**	**MG_A**	**MG_B**
Energy to loads	33.815 €	33.265 €	33.912 €	33.880 €
Energy services to main grid and microgrid	111.553 €	49.802 €	67.130 €	64.033 €
Water by FC	21.370 €	- €	33.097 €	31.498 €
Carbon by TP	142.465 €	- €	-	-
Total revenues	***309.203 €***	***83.067 €***	***134.139 €***	***129.411 €***
Total costs of ownership	1.053.678 €	320.379 €	268.224 €	273.174 €
LCOE	0,28€/kWh	0,16€/kWh	0,21€/kWh	0,21€/kWh
NPV	478.297 €	239.528 €	280.000 €	297.199 €
IRR	9,80%	12,20%	17,90%	17,90%

Table 4.5 *Key financial ratios of the on-grid scenarios in North Europe (Bremen) with green hydrogen at 3€\kg (0,25€\Nm³) and blue hydrogen at 0,85 €\Nm³, 25 project lifetime, 5% discount rate, revenues and TCO refer to the first year*

powered by blue-hydrogen (i.e., hydrogen supplied by local TP systems). Both are located in Northern Europe, nearby Bremen. In the latter, the carbon black is generating a revenue stream being a valuable by-product produced during methane decomposition.

The outcomes are in agreement with the techno-economic analysis prepared by T. Keipi et al. in 2016 [34] and by Dagle R. et al. [35] in 2017, concerning the carbon dioxide-free production of hydrogen using natural gas to make solid carbon and hydrogen.

These studies investigate the impact of the production of solid carbon as byproducts. Carbon black produced, so far, is used in tires and other rubber products as reinforcing fill – among others – increasing the abrasion resistance of the product. Market prices for carbon black products range from 0.40 to > 2,00 €/kg_C and it can be higher for graphite, carbon nanotubes (CNT). In our CHP-MMG problem, the selling price for carbon products is set at 2,50 €/kg_C. It should be noted that the TP-based methane decomposition subsystem, yields additional total costs of ownership. Thus the overall

CAPEX of FC integrated with TP are assumed to be: 3.500€/kW instead of 2.200€/kW (fuel cell powered directly with TP).

Assuming the cost of methane to 1,20 €/kg_{CH4} (0,85 €/Nm^3), electricity tariff at 0,38 €/kWh, consumption of methane 223 MJ/kg_{H2}, 13,90 kWh_{el}/kg_{H2} of electricity [33] TP leads to a net hydrogen cost of 2,59 €/kg_{H2} (i.e., cost of productions deduced of the selling price of carbon). The operational costs are also affected by the unfavorable energy conversion efficiency (from methane to electricity) that drops with CHP-PEMFC power with blue hydrogen from 44% to 21%.

Under this assumption and the remaining input data equivalent to those indicated in Paragraph 4.5.1, the outcome of the CHP-MMG simulations in grid-on configuration does not show any reduction of LCOE versus a fuel cell-powered with outsourced green hydrogen at 3,00 €/kg_{H2}. Nonetheless, the TP yields 3 kg_C/kg_{H2} which contributes to the revenue stream.

The result shows that the overall financial performances (IRR) although lower than the configuration based on green hydrogen are still very attractive. Thus TP should be considered as a viable technology until *R2H2* will not be massively diffused.

4.6 Conclusions

Techno-economic optimizations of multiple interconnected heat and power microgrids require to solve stochastic optimization problems subjected to uncertain, different local climatic conditions that make energy generation by RES not programmable, unpredictable loads, grid availability, flexible energy. In this chapter, a two-layer optimization method combining SLSQP with novels self-adaptive evolutionary algorithms is proposed to solve this problem. The latter is able to simultaneously identify the optimal design, configurations and siting of heat and power multi-microgrids while the power dispatch balance is delivered at each time-step. The multi-objective function is formulated to obtain the highest IRR to investors and the lowest LCOE for users. The candidate configuration generated with evolutionary algorithms feeds the analytical techno-economic model. Two novel self-adaptive evolutionary algorithms based on different mutant and crossover strategies are proposed. The results show that AIE performs 70% better on average than ADE. The optimization tool has been used to conduct sensitivity analysis of hydrogen costs in two locations placed in different latitudes. In Southern Europe, the optimal mix of RESs is selected in

combination with FC if the cost of hydrogen is 3 €/kg_{H2} or lower, otherwise, the main grid replaces the FC.

The overall analysis demonstrates that the cost of hydrogen and the availability of renewable resources affects the optimal design and sizing of CHP-MMG and IRR. The study of CHP-MMG in off-grid scenarios shows that can be obtained optimal configuration with LCOE similar to on-grid scenarios. Finally, these optimization-simulations demonstrate the resilience of the off-grid CHP-MMG systems: the selected best configurations do not exhibit energy underflows. Further optimizations have been carried out with on-site hydrogen generation by TP methane decomposition. This technology leads to a substantial increment of the revenue stream if carbon black is taken into account.

The optimal on-grid CHP-MMG configuration with TP, deliver an IRR: 17% to 21%; this performance leads to the conclusion that it can be considered as a viable bridge hydrogen generation technology. The whole study brings out the versatility of CHP-MMG technology.

Different settings of operating conditions, costs of fuels, energy demand price policies, locations, are not obstacles to achieve optimal configurations, sizing, and siting of CHP-MMG delivering high-quality energy and attractive financial performances.

4.7 References

[1] F. Orecchini and A. Santiangeli, "Beyond smart grids – The need of intelligent energy networks for a higher global efficiency through energy vectors integration," Int J Hydrogen Energy, vol. 36, no. 13, pp. 8126-8133, 2011.

[2] C. Schmidt, in Evolutionary computation in stochastic environments., Universitätsverlag Karlsruhe, 2007, pp. 2-9.

[3] F. Glover, M. Laguna and R. Marti, "Advances in evolutionary computation: theory and applications," p. 519–537, 2003.

[4] M. A. Rodriguez, D. F. Lopez, S. F. Contreras, C. A. Cortés and J. M. A. Myrzik, "Performance evaluation of the MOEA/D algorithm for the solution of a microgrid planning problem.," Proceedings of the 2020 Genetic and Evolutionary Computation Conference Companion, no. 173-174, 2020.

[5] R. Storn and K. Price, "Differrential evolution-a simple and efficient adaptive scheme for global optimization over continuous spaces, Technical report," International Computer Science Institute, vol. 11, 1995.

[6] R. Storn, "Differential Evolution Research – Trends and Open Questions," Advances in Differential Evolution, vol. SCI, no. 143, pp. 1-31, 2008.

[7] H. Vahedi, R. Noroozian and H. Hosseini, "Optimal management of MicroGrid using differential evolution approach," in 7th International Conference on the European Energy Market, Madrid, 2010.

[8] H. M. Amjady and M. Nima Ehsan, " Islanded Micro-grid modeling and optimization of its operation considering cost of energy not served by an enhanced differential search algorithm," Energy Engineering Management, pp. 2251-8061, 2014.

[9] W. Gu, Z. Wu, R. Bo, W. Liu, G. Zhou, W. Chen and Z. Wu, "Modeling, planning and optimal energy management of combined cooling, heating and power microgrid: A review,," International Journal of Electrical Power & Energy Systems, vol. 54, pp. 26-37, 2014.

[10] Y. W. Jingrui Zhang, Y. Guo, B. Wang, H. Wang and H. Liu, "A hybrid harmony search algorithm with differential evolution for day-ahead scheduling problem of a microgrid with consideration of power flow constraints,," Applied Energy, vol. 183, pp. 791-804, 2016.

[11] S. Surender Reddy, J. Y. Park and C. M. Jung, "Optimal operation of microgrid using hybrid differential evolution and harmony search algorithm," Front. Energy, vol. 10, p. 355–362, 2016.

[12] M. Marzband, E. Yousefnejad, A. Sumper and J. L. Domínguez-García, "Real time experimental implementation of optimum energy management system in standalone Microgrid by using multi-layer ant colony optimization,," International Journal of Electrical Power & Energy Systems, vol. 75, pp. 265-274, 2016.

[13] N. N. and R. N.S., "A study on optimal power sharing in interconnected microgrids under uncertainty,," International Transactions on Electrical Energy Systems, pp. 208-232, 2016.

[14] M. A. Hossain, H. R. Pota, S. Squartini and A. F. Abdou, "Modified PSO algorithm for real-time energy management in grid-connected microgrids,," Renewable Energy, vol. 136, pp. 746-757, 2019.

[15] Z. Li Yang, Z. Dongbo, L. Hangtian, C. Bai and L. Shaoyan, "Incorporating energy storage and user experience in isolated microgrid dispatch using a multi-objective model," ET Renewable Power Generation., 2019.

[16] W. M. Ferreira, I. R. Meneghini, D. I. Brandao and F. G. Guimarães, "Preference cone based multi-objective evolutionary algorithm applied to optimal management of distributed energy resources in microgrid," Applied Energy,, vol. 274, 2020.

[17] D.-M. Hasan, B. G. Gevork, R. Hassan and Olamaei Javad, "Optimal placement and sizing of DG (distributed generation) units in distribution networks by novel hybrid evolutionary algorithm," Energy, vol. 54, 2013.

[18] B. Li, R. Roche and A. Miraoui, "Microgrid sizing with combined evolutionary algorithm and MILP unit commitment," Applied Energy, vol. 188, pp. 547-562, 2017.

[19] S. Mohseni and M. S. M. Tafreshi, "A Multi-Agent Approach to Optimal Sizing of a Combined Heating and Power Microgrid.," in The 5 Iranian Conference on Renewable Energy & Distributed Generation (ICREDG2017), Rasht, 2017.

[20] A. Kaabeche, S. Diaf and R. Ibtioue, "Firefly-inspired algorithm for optimal sizing of renewable hybrid system considering reliability criteria," Solar Energy, vol. 155, pp. 727-738, 2017.
[21] J. Jung and M. Villaran, "Optimal planning and design of hybrid renewable energy systems for microgrids," Renewable and Sustainable Energy Reviews, vol. 75, 2017.
[22] M. A. Ramli, H. Bouchekara and A. S. Alghamdi, "Optimal sizing of PV/wind/diesel hybrid microgrid system using multi-objective self-adaptive differential evolution algorithm.," Renewable Energy, vol. 121, pp. 400-411, 2018.
[23] N. Ghorbani, A. Kasaeian, A. Toopshekan, L. Bahrami and A. Maghami, "Optimizing a hybrid wind-PV-battery system using GA-PSO and MOPSO for reducing cost and increasing reliability," Energy, vol. 154, pp. 581-591, 2018.
[24] D. R. Prathapaneni and K. Detroja, "Optimal design of energy sources and reverse osmosis desalination plant with demand side management for cost-effective freshwater production," Desalination,, vol. 496, 2020.
[25] P. Fracas, K. V. Camarda and E. Zondervan, "Shaping the future energy markets with hybrid multimicrogrids by sequential least squares programming," Physical Sciences Reviews, 2021.
[26] D. Sudholt, "The Benefits of Population Diversity in Evolutionary Algorithms: A Survey of Rigorous Runtime Analyses," in Theory of Evolutionary Computation. Natural Computing Series. , Springer, 2020.
[27] D. C. L. and Z. F.V., "Learning and optimization using the clonal selection principle," IEEE Transactions on Evolutionary Computation, vol. 6, no. 3, pp. 239-251, June 2002.
[28] P. Stuart, "Least square quantization in PCM," IEEE Transactions on Information Theory, vol. 28, no. 2, pp. 129-137, March 1982.
[29] S. Sung and W. Jung, "ompetitiveness Evaluation of the Energy Sources: Comparison between a Financial Model and Levelized Cost of Electricity Analysis.," Energies, vol. 12, no. 21, p. 4101, 2019.
[30] A. J. Kleywegt, A. Shapiro and T. Homem-de-Mello, "The Sample Average Approximation Method for Stochastic Discrete Optimization," SIAM Journal on Optimization, vol. 12, no. 2, pp. 479-502 , 2002.
[31] Y. Carson and M. Anu, "Simulation Optimization: Methods and Applications," in Proceedings of the 29th Conference on Winter Simulation, Atlanta, Georgia, USA, 1997.
[32] A. O. Bique, L. K. Maia, F. L. Mantia, D. Manca and E. Zondervan, "Balancing costs, safety and CO2 emissions in the design of hydrogen supply chains," Computers & Chemical Engineering, vol. 129, no. 106493, 2019.
[33] S. Timmerberg , M. Kaltschmitt and M. Finkbeiner , "Hydrogen and hydrogen-derived fuels through methane decomposition of natural gas – GHG emissions and costs," Energy Conversion and Management: X, vol. 7, no. 100043, 2020.
[34] T. Keipi, V. Hankalin, J. Nummelin and R. Raiko, "Techno-economic analysis of four concepts for thermal decomposition of methane: Reduction of CO2 emissions in natural gas combustion," Energy Conversion and Management, vol. 110, pp. 1-12, 2016.
[35] R. Dagle, V. Dagle, M. Bearden, J. Holladay, T. Krause, S.Ahmed and e. al, "Opportunities for Development of Natural Gas Conversion Technologies: for Co-Production of Hydrogen and Value-Added. Solid Carbon Products.," 2017.
[36] W.Rafajłowicz, "Horizontal Gene Transfer as a Method of Increasing Variability in Genetic Algorithms," in Artificial Intelligence and Soft Computing. ICAISC 2018. Lecture Notes in Computer Science, vol 10841, vol. 10841, Springer, 2018.

CHAPTER 5: Techniques enhancing computing performance

Due to the nature of uncertainty, the CHP-MMG problem returns clusters of solutions. The challenge is to find the solution returning the best fitness value over the most probable scenarios. The correlation between the gradients along the generations of the standard deviation of fitness values and the population's genes reflects the quality of the sought design and it can be used as a stopping criterion. In the first section, a method based on this interrelationship is discussed. Moreover, a criterion to select the best probabilistic solution and verify the globally optimal setting with the sample average approximation method is discussed. The second section discusses different strategies to overcome the drawback of required computing resources. Multiprocessing computing is used to efficiently parallelize tasks and thus to shorten the elaboration time. The next step is to extend the approach by slicing the time series. Searching globally optimal configurations with the ATE model requires several hours if the time series are not sliced. In the latter case, the quality of the results is worse if the sizes of the boundaries are too large or if the optimization is addressed to off-grid scenarios. Moreover, for the early queries ATE can be replaced with MLTE. The training is fast and the run of a query takes just a few minutes. The overall optimization with MLTE can be considered as a first step in solving our optimization problem.

5.1 Methods for searching global minimum in uncertain landscape

In Chapter 2 the techno-economic model (ATE) for the optimization problem of combined heat and power multi-microgrids (CHP-MMG) has been discussed. The ATE incorporates a subset of stochastic models of thermal-electric weather-dependent distributed renewable power generators, loads and unpredictable grid outages.

The electrical and thermal operation of the distributed energy resources (DER) embedded in the ATE are optimized in each time-step with Sequential Least Squares Programming. At the upper level, the self-adaptive differential evolutionary algorithms (ADE/AIE) simultaneously identify the best configurations and siting of the CHP-MMG. This multi-objective optimization minimizes an objective function based on the ATE to obtain the highest IRR for investors and the lowest LCOE for users. Due to the stochastic terms in the ATE , the fitness function is subject to noise.

B. Doerr et al. in 2020 [1] have investigated noise models in the area of the theoretical analysis of evolutionary computation. In their work, it has been highlighted that the fitness function returns a value that differs from time to time for the given solution, because of the disturbance. Similarly, in the problem of interest, it is observed that the noise causes a severe un-linearity among the candidate solution and the fitness value.

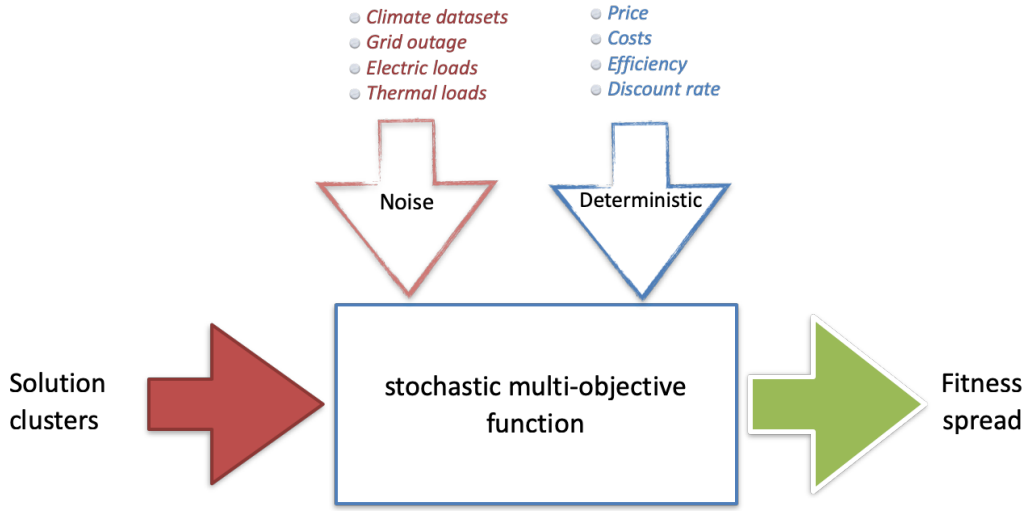

Figure 5.1 *Overall framework of the stochastic CHP-MMG optimization problem*

In Figure 5.1 the main categories of deterministic- and stochastic variables causing noise, for the ATE model are listed. The direct consequence of noise is a stochastic objective function that returns for each candidate solution, a distribution of fitness values. On the contrary, a fitness value is bonded to a cluster of solutions. Thus, AIE/ADE has to search for optimal solutions in an uncertain landscape. In such environment, the problem of finding the global minimum is cumbersome as the noise misleads the search of each computing run. The final objective is to find the configuration for a CHP-MMG that delivers the best performance for all random scenarios.

Friedrich T., et Al. (2010) [2] have proven that simple evolutionary algorithms behave very well when facing a stochastic optimizations problem. Moreover, Akimoto et al. in 2015 [3] proposed that the evaluation of a solution of noisy fitness functions must be repeated k-times. The algorithm then should take the average of the k-noisy values as the fitness value of the solution. The aim of such an approach is to obtain a robust (i.e., "uncertainty-immunized") solution to the optimization problem.

In this chapter an approach to find a probabilistic global minimum is based on the following method is proposed consisting of five steps: 1) run an optimization computation with multiple queries (k-time); 2) search the best probabilistic solution of each query; 3) identify a cluster of best probabilistic solutions having a genotype diversity lower than a defined target; 4) select the best of the best probabilistic solution in the cluster (e.g., best probabilistic solution returning the lowest fitness value); 5) check if the best of the best probabilistic solution (i.e., probable global solution) delivers the expected performance over all the scenarios.

To find the best probabilistic solution of a query, the tendency of the standard deviation of fitness values (i.e., the convergence of the fitness) associated to the individuals of the population is correlated to the population's genes diversity in the latest generations.

Figure 5.2 shows the slopes of the diversity's genotypes (i.e., divX_pop) and the correspondent slope of the fitness's convergence (i.e., divY_fit) for 281 generations. In this plot, the latest values of divY_fit gradually converge to similar values while the values of divX_pop increase from 0,30 to 0,40. In other words, despite AIE/ADE trying to keep population diversity high, the fitness values tend to assume similar values. This behavior in the latest generations indicates that the flat depression region of the global minimum has been reached.

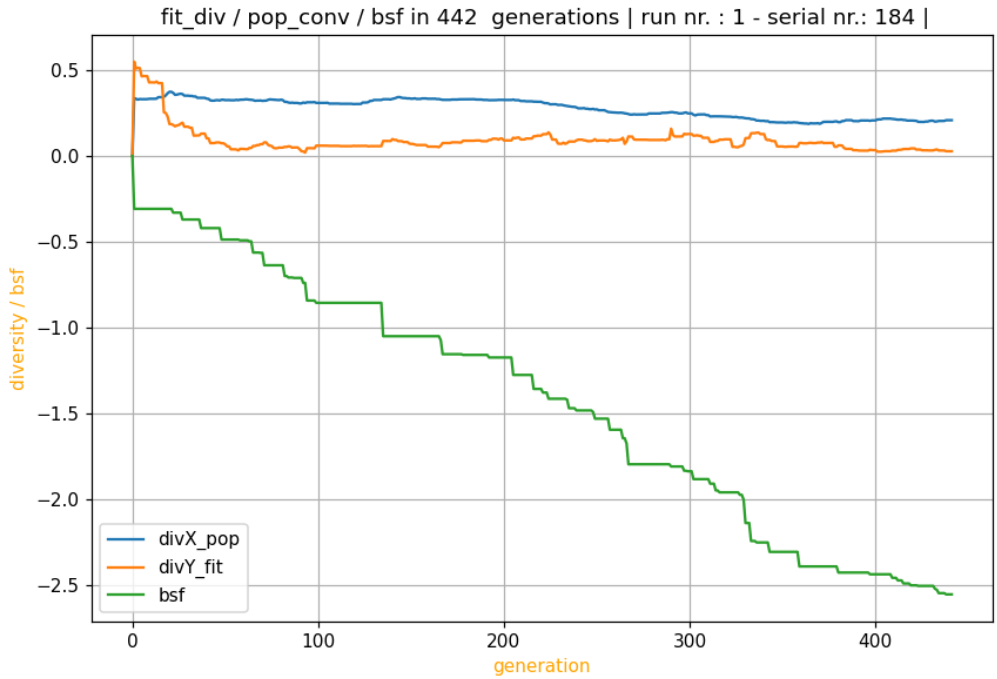

Figure 5.2 *Slope of population's diversity (divX_pop) and fitness convergence (divY_fit) and bsf's fitness (bsf) along 163 generations*

The CHP-MMG stochastic optimization problem must be repeated k-times until the spread of fitness values associated to the best probabilistic solutions are within the desired target (e.g., < 0,005).

It has been observed that 3 queries (i.e., k = 3) are enough to obtain a spread of fitness values < 0,005 when in the latest 5-10 generations of each query the gradient of divY_fit remains negative, while the gradient of divX_pop remains null or positive. It is worth noting that with datasets of reduced-size a number of generations, g > 400 for grid-tied scenarios (i.e., genes of grid power size, not null) and g > 1500 in case of off-grid scenarios are usually sufficient to obtain this correlation between the gradients. Furthermore, the latter condition is usually indicative of clusters of solutions with small dimensions.

Subsequently, two methods are investigated to select the "best of best probabilistic solution" of the cluster (i.e., probable global solution): 1) take the mean values of the best solutions or 2) select the solution having the best fitness value. The second choice demonstrates to be the most effective in most of the cases. The validation of a solution

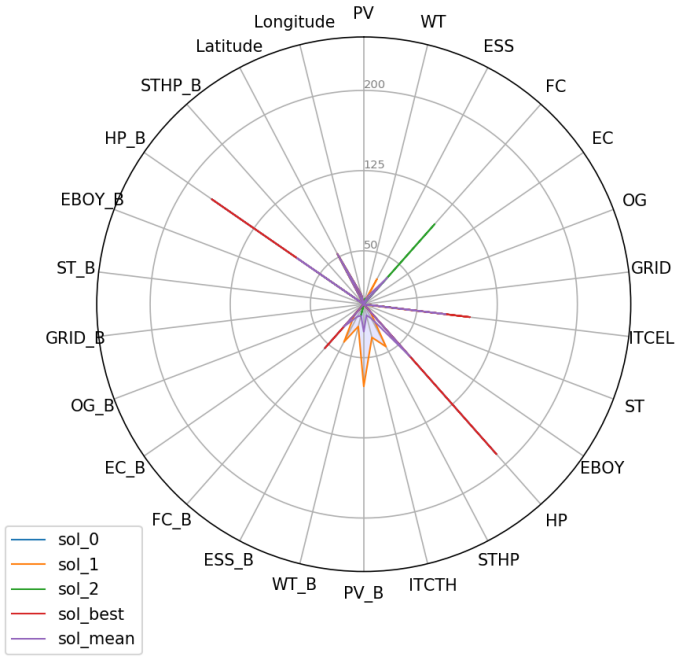

Figure 5.3 *Radar plot of a cluster embedding three best probabilistic solutions, mean and selected solutions*

array based on the mean values usually returns a fitness value much larger than those associated the best probabilistic solutions.

The radar-plot in Figure 5.3 provides the outlook of the best probabilistic configurations and the mean of 3 queries, 400 generations each. The boxplot in Figure 5.4 shows the spread from the lower to upper quartile of the genes of the same solutions. Both graphical representations support the evaluation of the quality of the results. It is worth noting that if the cluster embeds individuals with similar genes, the overall lines in the radar overlap and the rectangular body of the boxplot is shrunk.

The quality of the selected "probable global solution" must be measured by repeating the simulation *N*-times. The number *N* of queries (N) should be representative of the whole domain of stochastic scenarios. The objective is to verify that the selected setting is performing similarly over all scenarios.

To find the optimal value of *N*, the sample average approximation method (SAA) proposed by A. J. Kleywegt et al., 2002 [4] is used. For SAA, to achieve an optimal

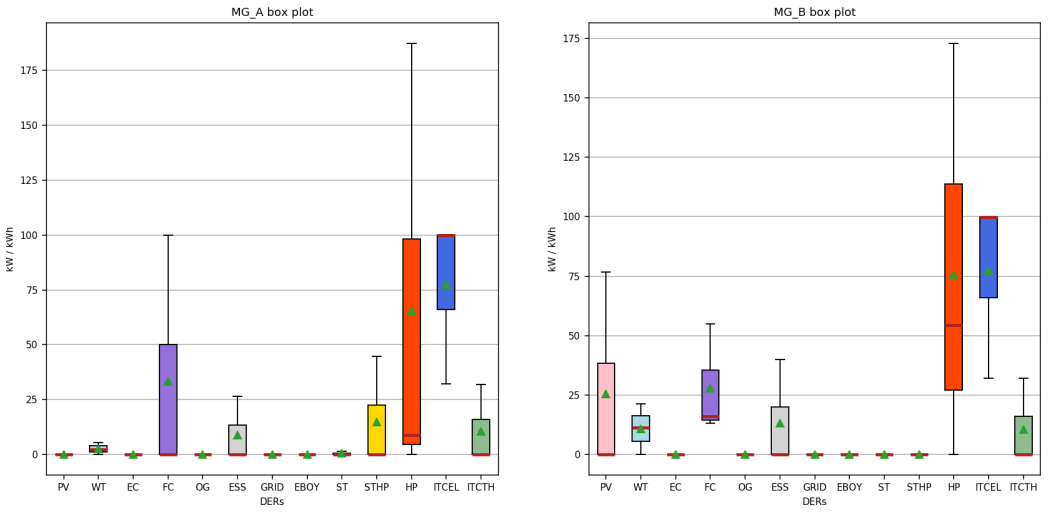

Figure 5.4 *Box-plot of cluster of probabilistic best solutions (3 queries)*

solution with probability at least: $1-\alpha$, the problem should be iterated:

$$N \geq \frac{3\sigma^2}{(\varepsilon-\delta)^2}\log\left(\frac{1}{\alpha}\right), \qquad [5.1]$$

where σ^2 being the variance, ε the deviation of the fitness values assigned to the selected solution of the problem and δ a number such as: $0 \leq \delta \leq \varepsilon$.

Optimization-simulation of off-grid scenarios which are computed with 3 queries, 1500 generation each, a target variance's value sufficiently small (e.g., $\sigma^2 < 0{,}002$), $\delta \cong 0{,}05 \cdot \varepsilon$, the global solution have a probability at least 99,00%, to be achieved in $N \geq 12$.

5.2 Performances of machine learning, analytical models with full and reduced datasets

The performances of the ATE model and MLTE models have been evaluated in 170 simulations. In Table 5.1, the quality of results, the computation times in relation to the

different methods and time series approximations are summarized. A common route to all the computing methods is running in parallel processing the tasks of each generation. Parallel processing is a mode of operation where the task is executed simultaneously in multiple processors on the same computer.

It is meant to reduce the overall processing time. The algorithm (Appendix C) has been structured with python standard multiprocessing libraries [10][11]. They efficiently parallelize tasks by creating child processes and thus it allows to fully leverage multiple processors on a given machine. The Pool class has been used. The pool distributes the tasks to the available processors using a first-input first-output (FIFO) scheduling. It maps the input to the different processors and collects the output from all the processors. After the execution of the code, it waits for all the tasks to finish and then returns the output. The processes in execution are stored in memory and other non-executing processes are stored out of memory. The Pool class synchronizes the calculation of the fitness values of the entire population before proceeding to the selection phase.

Two methods have been used to compute OP with the ATE model: 1) hybrid-resolution mode that consists in slicing in 85% of generations the yearly time series into a set of representative daily periods, notably 248 time-steps (12 day / year), then switch to full datasets (360 days / year) for remaining 15% of the query; 2) high-resolution mode that is based on full datasets of 8760 time-steps (360 days / year).

As discussed in Chapter 3, optimization based on the MLTE models can be combined with ATE-based models to tighten the search area. Moreover, as demonstrated in Chapter 4, the use of the AIE algorithm instead of ADE improves the quality of results and reduces the elaboration time.

In hybrid-resolution, the AIE algorithm solving the ATE fitness function has the ability to find clusters of solutions for on-grid scenarios in 350-400 generations with a population size of 12 individuals. The computing time is about 8 hours each query. In on-grid, the hybrid-resolution is satisfactory to achieve a high quality of the results as thermal- and electric storage components play a minor role than continuous power sources (e.g., FC, OG, main grid). It is worth noting that boundaries must have limited values. A good practice is to launch the first set of trials with large boundaries (e.g., with MLTE) and then shrink the bandwidth.

The hybrid-resolution permits to collapse the computation time of each generation from 10-15 minutes of high-resolution mode to 1-3 minutes. However, off-grid

scenarios simulated with sliced datasets, the configurations that combine renewable energy sources with energy storage can return misleading results. In fact, stochastic climate variables impact the calculation of cumulative energy storage.

In off-grid scenarios, the number of generations should be extended at values higher than 1500 otherwise queries in high-resolution with at least 200 generations are preferred.

Moreover, it is noteworthy to consider the computing resources required to solve the CHP-MMG optimization problems. For Example, a query of 1500 generations executed in hybrid-resolution requires 28 hours with an iMac with 8 microprocessors 3,6 GHz Intel Core i7 quad-core. The corresponding consumption of energy is 3,67 kWh. The estimated $C0_2$ emissions are 1,01 kg and the costs of electricity are 0,85 € (based on the energy mix of Italy). This example explains why a research effort has been devoted to investigating efficient approaches to save computation time in microgrids optimization.

K. Fahy et al., in 2019 [5] proposed a method to save computational time in optimization models that scales with the number of time steps. To save computing time, the solver resolution is reduced and input data are down sampled into representative periods such as one or a few representative days per month. However, such data reduction can come at the expense of solution accuracy. In their work, the impact of reduction of input data is systematically isolated considering an optimization that solves an energy system using representative days. A new data reduction method aggregates annual hourly demand data into representative days which preserves demand peaks in the original profiles. The proposed data reduction approach is tested on a real energy system and real annual hourly demand data where the system is optimized to minimize total annual costs. Compared to the full resolution optimization of the energy system, the total annual energy cost error is < 0,22% when peaks in customer demand are preserved. Errors are significantly larger for reduction methods that do not preserve peak demand. In another recent work issued in 2020, Zachary K. et al. [6] proposed a novel hybrid optimization framework to study power resilience to macro-grid outages. In their work, hybrid approaches to microgrid techno-economic planning are used. A reduced model is used to optimize DER sizing. A full model optimizes operation and dispatch.

Although these hybrid models save relevant computation time, during grid outages, these models are susceptible to infeasibility, when the size of the DER is insufficient to

meet the energy balance with full model. The authors counter this problem by executing the same optimization problem twice, where the second solution using full data is informed by the first solution using representative data to size and select DER.

T/E Models	Optimization	Pre-processing	Generations	Time	Results
MLR	*ADE/AIE*	*normalization, standardization*	*30-50*	*3 minutes*	*Training ultra-fast. Query ultra-fast with fitness limit setting. Fair results.*
DNN	*ADE/AIE*	*normalization, standardization*	*30-50*	*10 minutes*	*Training very-fast. Query fast, poor results.*
NN	*ADE/AIE*	*normalization, standardization*	*30-50*	*45 minutes*	*Training time consuming. Query fast, poor results.*
ATE (high-resolution)	*SLSQP/ADE*	*-*	*70-200*	*12 - 18 hours*	*Query time consuming. Good quality of results.*
ATE (hybrid-resolution)	*SLSQP/ADE*	*-*	*400-2000*	*10 - 30 hours*	*Query time efficient. Information lost in off-grid with minimum generations. Good quality of results.*
ATE (high-resolution)	*SLSQP/AIE*	*-*	*50-1500*	*6 - 24 hours*	*Query very efficient. Information lost in off-grid with minimum generations. Results better than ADE.*
MLTE / ATE (hybrid-resolution)	*SLSQP/AIE*	*normalization*	*50-120*	*6 - 12 hours*	*Query ultra-efficient. Information lost in off-grid scenarios with minimum generations. Good quality of results.*

Table 5.1 *comparison among different models, computing methods and optimization algorithms*

5.3 Conclusions

The techno-economic optimization of the CHP-MMG is a stochastic problem. If multiple queries are executed, clusters of best solutions are obtained. In this chapter, a five-step method suitable to identify the best solution within such clusters is discussed. It is based on the following steps: 1) run an optimization computation with multiple queries; 2) search the best probabilistic solution of each query; 3) identify a cluster of best probabilistic solutions having a genotype diversity lower than a defined target; 4) select the best of the best probabilistic solution in the cluster; 5) validate performance over all the scenarios of the best probabilistic solution. Moreover, it has been demonstrated that the correlation between the standard deviation of both fitness values and genotype over the generations is an effective stopping criterion for a query.

The execution of techno-economic optimization of the CHP-MMG is a complex task that requires relevant computing resources. Multiple strategies have been put in place to overcome this problem. Multiprocessing computing has been used to efficiently parallelize tasks and thus to shorten the elaboration time. Moreover the elaboration of the algorithm's time-series has been sliced from 8760 to 288 (i.e., 24 time-steps for each month).

Finally, to further speed up the computation, ATE can be substituted for MLTE for first runs. The optimization with MLTE can be considered as a first step in solving the problem. The optimal solution given by MLTE can be utilized to override the boundaries of a subsequent search with the ATE-based model.

The overall approaches proposed in this chapter provide an innovative contribution to the techno-economic optimization of CHP-MMG.

5.4 References

[1] Doerr, B., Doerr, C., Ebel, F., 2015, From black-box complexity to designing new genetic algorithms. Theor. Comput. Sci. 567, 87–104

[2] Friedrich, T., He, J., Hebbinghaus, N., Neumann, F., Witt, C. ,2010, Approximating covering problems by randomized search heuristics using multi-objective models. Evolutionary Computation 18(4), 617–633

[3] Akimoto, Y., Morales, S.A., Teytaud, O. 2015, Analysis of runtime of optimization algorithms for noisy functions over discrete codomains. Theoretical Computational Science 605, 42–50

[4] Anton J. Kleywegt, Alexander Shapiro, and Tito Homem-de-Mello, 2002, The Sample Average Approximation Method for Stochastic Discrete Optimization, SIAM Journal on Optimization 2002 12:2, 479-502

[5] Kelsey Fahy, Michael Stadler, Zachary K. Pecenak, and Jan Kleissl, 2019, Input data reduction for microgrid sizing and energy cost modeling: Representative days and demand charges. J Renewable Sustainable Energy; https://doi.org/10.1063/1.5121319.

[6] Zachary K. Pecenak, Michael Stadler, Patrick Mathiesen, Kelsey Fahy, Jan Kleissl, 2020, Robust design of microgrids using a hybrid minimum investment optimization, Applied Energy, Volume 276, 115400, ISSN 0306-2619, https://doi.org/10.1016/j.apenergy.2020.115400

CHAPTER 6: Conclusions and outlook

6.1 Lessons learned and outcomes achieved

The increase of energy demand and environmental issues are fostering a clean energy revolution across the world, underlined by the steady expansion of the renewable energy sector. The microgrid is the technology of choice to speed up this scenario. The latest information and communication technologies are instrumental to the roll-out of the distributed energy resources, e.g., wind turbines, photovoltaic panels. The new energy paradigm will lead to the deployment of intelligent microgrids to ensure peer-to-peer connectivity of decentralized, uncertain renewable systems. The microgrids embody the generation, transmission, distribution and consumption of energy as a whole. They enable an interaction among all nodes of the system to secure demand-side flexibility and the optimum operation, while maintaining second-to-second power balance, quality and security of the supply. There is a tremendous opportunity to deliver innovative, sustainable and efficient energy systems with microgrid.

This groundbreaking technology can step-up investments, fostering the transition to a low-carbon competitive economy. However, its design and management must meet multiple challenging requirements. The minimum cost of energy, the highest profitability and the highest power quality must be achieved by matching the uncertainty of energy subjected to the weather conditions and the variability of the load profiles. The choice of the distributed generators and the geographical sites have a great impact on the economic and technical performance of MG. The long useful life of installations (e.g., 20 to 40 years for PV and 20 years for WT) may cause lock-in situations until payback is not reached. The combination of DG may influence their lifetime and overall efficiency.

Stakeholders look at the problem from different perspectives. The investors look for projects with the lowest cost of the installations, operations, the most favorable environmental condition and local power policies (i.e., utility grid's price, incentives, demand response compensations), to obtain the most attractive financial performance (i.e., IRR). The users look for an energy supply with the most convenient tariff and the best reliable services. The energy providers aim to predict and balance correctly the energy demand to fulfill the user's requirement at lowest cost.

To find the best siting, sizing, and operation of the MG, the simulation of a large number of configurations is required. It is noteworthy that this is a stochastic problem as it contains uncertain parameters (i.e., weather forecast, user's demand).

In this thesis, a novel two-layer optimization method based on the combination of self-adaptive differential evolution algorithms with the SLSQP optimization method has been proposed to solve the latter problem. Moreover, several techniques (i.e., parallel processing, slicing datasets) have been applied to reduce the computing time.

The overall approach has allowed to achieve the optimal design, configuration and siting of heat and power multi-microgrids simultaneously while the power dispatch balance is satisfied at each time-step. The candidates of the DER configuration and the geo-coordinates of the evolutionary algorithms are represented by an individual having two properties: genotype and its quality. The genotype embeds two chromosomes (the first composed of 36 genes and the second 2 genes. The quality of the individual is the fitness value.

Twelve individuals of a population undergo a number of evolutions to mimic genetic gene changes and search the solution space. In the self-adaptive differential evolution algorithm (ADE), the mutation factor and cross-over, are adapted to the variation of the fitness value to optimize the search radius and converge faster. In the self-adaptive artificial immune algorithm (AIE) the mutant vector is obtained with a normal random distribution whose standard deviation and mean are driven by the diversity of population and fitness convergence. A crossover is obtained by applying horizontal and vertical gene transfer techniques.

The stochastic multi-objective function (i.e., fitness function) is formulated to obtain the highest IRR for investors and the lowest LCOE for users. The candidate configuration generated with evolutionary algorithms feeds a techno-economic model that measures the quality of the trial configuration. Due to the stochastic nature of this problem, clusters of global solutions, namely PBS, of similar quality are obtained. To find the best setting, the optimization must be repeated until the standard deviation of the PBS's genotypes reaches the desired value. The solution associated with the lowest fitness value can be assumed as the candidate of being the best probabilistic solution. The final task is to verify if the latter solution returns the best expected performance over all the uncertain scenarios.

The thesis discussed four different versions of the objective fitness function. The first is an analytical model (ATE). The others are different versions of machine learning algorithms (MLTE). The ATE uses the SLSQP method to balance at each time-step the energy flows and minimize a cost-revenues function inferred by the DER equations.

The machine learning models, in particular, the MLR can be used to quickly compute the fitness function. It should be noted that MLTE returns low-quality solutions from a narrow domain; however, MLTE model-based optimizations can be combined with ATE-based models to tighten the search area and thus further reduce computation time.

The simulation-optimization tool proposed in this thesis will lead to recommendations regarding the best configurations of CHP-MMG in Southern Europe (Catania, IT) and Northern Europe (Bremen, GE). The outcomes are subsequently used to examine the impact of the location of the sites, the costs of the fuels, the price policies and their financial implication. It has been observed that with a cost of the fuel fixed at 3,00 €/kg_{H2}, hydrogen-powered fuel cells are selected to be a predominant source of electricity and heat; whenever the cost raises to 13,00 €/kg_{H2}, the utility grid turns into the principal supplier, and the high fuel cost causes a substantial increment of the PV and WT. Nevertheless, LCOE values are comparable in almost all scenarios. By setting the boundaries of geo-locations covering for Northern Europe a region with its center in Bremen +/- 7 decimal degree both for latitude and longitude and Catania for Southern Europe, the best siting and design of CHP-MMG in two regions of Europe with different climate conditions could be found.

Within the cluster of best solutions, AIE selects in Denmark the best siting of Northern Europe for CHP-MMG. This region has favorable wind conditions and thus WT are the best choice coupled with FC and the macro-grid. Thermal energy is generated with heat pumps and exchanged between the microgrids.

In Southern Europe, the best configurations comprise a PV combined with WT, FC and the main grid. Here the best siting, if the search start from Catania, is the East part of the Mediterranean Area (i.e., Greece). Here, the combination of solar radiation, wind speed and cloudiness conditions are more favorable.

These simulations have brought out a scheme of collaboration between the two microgrids (i.e.,‘swarm effect’, Paragraph 6.2.5) fostering the overall efficiency, energy resilience to uncertainty, and optimal financial performance. Interconnections are used to permit crossflows of thermal and electrical energies. Notably, a fraction of the

exceeding electrical energy (i.e., not used to feed the loads or charge batteries), flows via the interconnections back and it is converted into thermal energy. Thus, a portion of heat swarms to the other microgrid.

Subsequent optimization dealing with off-grid scenarios, has demonstrated that LCOE can remain aligned to grid-tie scenarios. Revenues streams deprived of incomes delivered with energy demand services do not consistently affect IRR that still remain attractive (e.g., IRR reaches 20% if the cost of hydrogen is setup at 1,00 €/kg_{H2}). The optimal DER configurations even with unfavorable initial conditions craft a full balance of both thermal and electric energies.

Considering blue-hydrogen on-site generation with TP-based methane decomposition technology leads to a substantial increment of the revenue stream as compared to green hydrogen, if carbon black as a by-product is taken into account. These results exhibit how blue hydrogen can be a bridging technology to make CHP-MMG profitable.

The whole study demonstrates the versatility of CHP-MMG technology. In every latitude and longitude, with different settings of operating conditions, cost of fuels, and energy demand price policies, the self-adaptive evolutionary algorithms (AIE, ADE) are always able to find - for different space search regions - the optimal configurations, sizing and siting in which an interconnected heat and power microgrid can deliver a good quality of energy, attractive financial performance, and out-competing costs' drawbacks.

This thesis has extended the state-of-art in techno-economic analysis of multiple interconnected microgrids that aggregate a wide variety of electrical, thermal and interconnection devices. Innovative business scenarios with CHP-MMG acting as virtual power and manufacturing plant have been investigated. They showed that thermal and electrical energy exchanged between the MG, DER, utility grids and further by-products e.g., water, carbon black produced by the fuel cells and hydrogen made by electrolyzers provide a high return on investment (e.g., IRR> 50%).

The techno-economic model embeds several methods to correlate climate datasets issued recently by ECMWF, giving the ability to investigate locations all over the globe. Three alternative machine learning models have been also setup to speed up the computing time. A procedure to identify the valid domain of solutions furnished by highly non-linear numerical models was proposed.

Moreover, two-novel two-layers optimization algorithms and the computing methods to speed-up the code's execution were developed. They have successfully demonstrated that simultaneous multi-objective optimization of CHP-MMG is possible including a method for detecting the global probabilistic solution over all the uncertain.

6.2 The innovation content

The techno-economic study of this thesis considers two interconnected combined heat and power microgrids aggregating a wide variety of electrical, thermal systems and interconnection devices.

Due to the high computing resources required to research optimal CHP-MMG configurations, a newly developed simulation-optimization framework is proposed and validated with experimental data. The proposed framework is capable of performing simultaneously:

- **design and sizing optimization** of the interconnected heat and power microgrids (i.e., to search optimal DER configurations in a certain site, giving the most profitable return of investment, the lowest cost of energy);
- **siting optimization** (i.e., to find the most suitable location of DER configurations with a global geo-resolution);
- **optimization of operation** (i.e., to minimize at each time-step the cost-revenues while ensuring the balance of the thermal and electrical energy flows).

Overall, there are **four major contributions** introduced by this thesis in the area techno-economic optimization of a microgrid:

- First, novel methods based on *Fast Fourier Transform (FFT) and polynomial regression to manipulate climate datasets issued by the European Centre for Medium-Range Weather Forecasts (ECMWF) for accurate prediction of climate variables is presented.* The latter represent a valuable and relevant contribution as the climate variables have a strong impact on the selection of DER, their sizing, siting choice, optimization of operations.
- Second, a *novel two-layer stochastic optimization algorithm is introduced.* The lower level is a time-step optimization of cost-revenues while constrained electric and thermal energy flows are balanced. The outer level of simultaneous design, sizing and siting optimizations are solved with *two novel evolutionary computing*

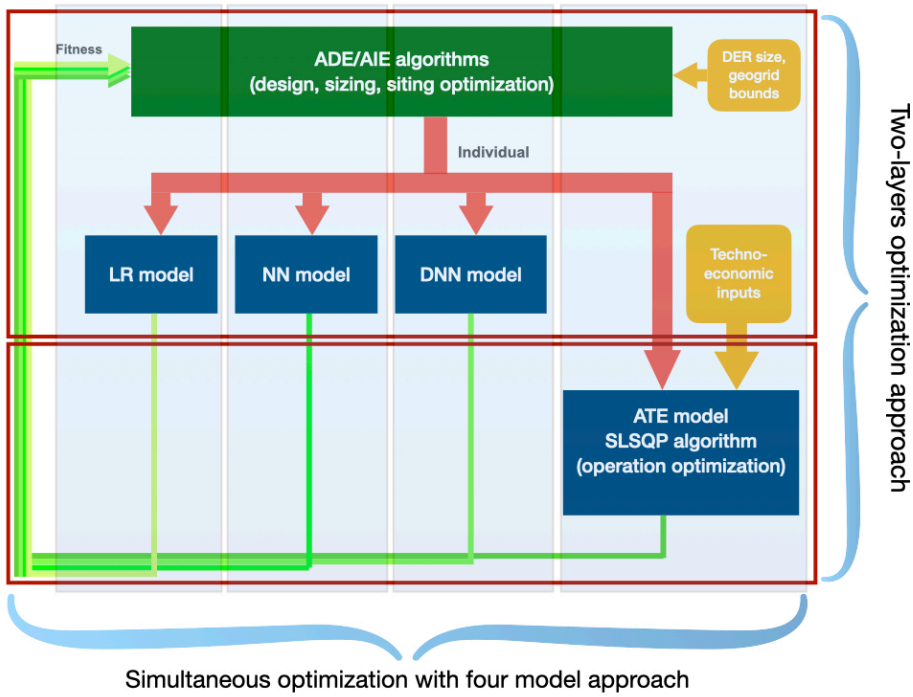

Figure 6.1 *Overall simulation-optimization framework based on ATE and MLTE models*

algorithms (ADE, AIE). As summarized in Figure 6.1 this represents the horizontal dimension of the optimization procedure.

- Third, *three novel machine learning models (MLTE) are proposed to improve the overall computational performance of the technical-economic optimizations.* These algorithms represent the vertical dimension of the optimization flow shown in Figure 6.1. The training of machine learning LR/NN/DNN algorithms is based on the results of a SLSQP algorithm embedded into the ATE deterministic model. The stochastic behavior of CHP-MMG permits MLTE to correlate solutions and fitness values similarly to ATE model, for fitness values nearby zero. MLTE used in combination with ATE-based optimization allows tightening the search area of the best CHP-MMG siting and sizing. Such a hybrid approach allows to exploit on one side the accurate prediction of an ATE analytical model, and at the same time exploit the fastest computation and performance that is offered by machine learning algorithms. This approach allows to find solutions that have the highest quality by minimizing the computing resources.

- Fourth*, all methods have been used to investigate novel scenarios of energy services and to conduct sensitivity analysis of hydrogen costs in two locations placed in different latitudes.* The whole study highlights the versatility of CHP-MMG technology. Different settings of operating conditions, costs of fuels, energy demand price policies, locations, are not obstacles to achieve optimal configurations, sizing and siting of CHP-MMG delivering high quality of energy, attractive financial performance, outcompeting costs' drawbacks.

As a further relevant aspect, the analytical techno-economic model proposed in this thesis covers a large variety of different DER, since all the following DG systems have been considered: internal combustion engines (OG), fuel cells (FC), photovoltaic panels (PV), wind turbines (WT), thermal solar collectors (ST), electric boilers (EBOY), standalone heat pumps (HP) and integrated with solar thermal-collectors (STHP). Lithium-ion batteries (ESS) and thermal water tanks (TES) are the ES considered in the MG configurations of this work. The cases discussed in Chapters 2 to 5 evaluate the best combinations and location of these DER.

Moreover to the writer's best knowledge, interconnected heat and power microgrids have not yet been fully investigated in the literature. Furthermore, techno-economic simultaneous optimization of siting, sizing, and operation of CHP-MMG has still not been addressed so far in detail by other scientific studies. This constitutes another relevant contribution of this thesis.

A more detailed description of the above scientific and original contributions is reported in the following paragraphs.

6.2.1 Novel methods for accurate climate variables prediction

A novel climate model based on recent data released by the European Centre for Medium-Range Weather Forecasts (ECMWF) which provides access to locations all over the globe is proposed in this work. Fast Fourier Transform (FFT) and polynomial regression are used to manipulate the climate datasets for accurate prediction of climate variables. The climate model is embedded into the ATE model of two interconnected hybrid microgrids whose electricity and thermal dispatch strategies are managed with SLSQP optimization technique. The ATE model allows to combine a large variety of thermal and electric power generation, transmission, and distribution systems as a whole

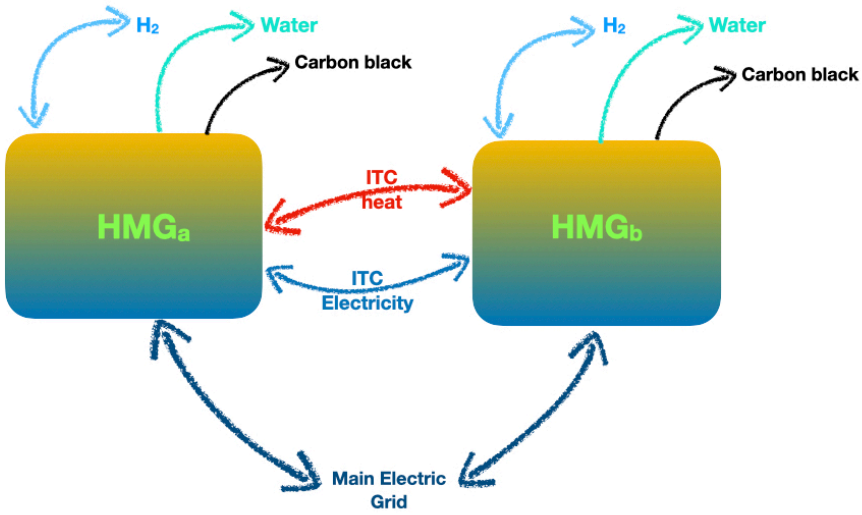

Figure 6.2 *Framework of exchange of energy among two microgrids and the main grid*

with weather-dependent distributed renewable generators and multiple stochastic load profiles.

The ATE model considers the inner- and outer exchanges of thermal, electric energy as indicated in Figure 6.2. Hydrogen is taken into consideration as the energy carrier next to heat and electricity. It stems from the inner generation by an electrolyzer and is also transported from outer generation fields. Water is a reaction product of fuel cells. Moreover, if fuel cells are coupled on-site with a hydrogen generation system based on methane decomposition with thermal plasma (TP), the reaction will yield carbon black. Hence, water and carbon black are side products from the fuel cell systems.

6.2.2 Two-layer optimization approach

Typical optimal techno-economic optimizations of MG deals usually with minimizations of the costs; stochastic models are approximated with linear models representing different scenarios. The simplified models are usually solved with mixed-integer linear programming (MILP) with a top-down approach (i.e., from the scenario to the solution).

Several papers address the optimization of MG with this approach [1],[2],[3],[4]. E.g., in their latest publication [5]. M.A. Hannan et al. provided a review of optimal

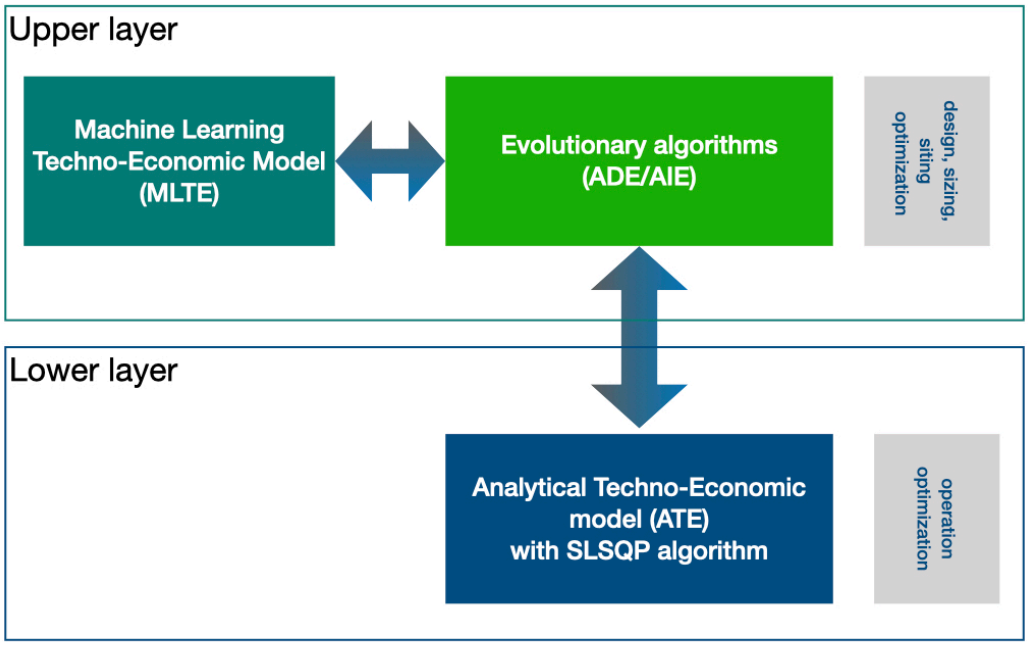

Figure 6.3 *Scheme of the two-layer algorithm and its interrelations with the ATE and MLTE models*

methods for sizing energy storage, outlining how typically used methods make use of stochastic properties of the forecasting error, i.e., mean, standard deviation and confidence intervals, for optimizing ESS sizing. M. Cao et al., (2019) [6] proposed a MILP (mixed-integer linear programming) methodology to optimize the sizing of the energy storage systems and the hourly dispatch by transforming stochastic constraints to deterministic ones. D. Wu et al. in 2020 [7] proposed to convert the two-stage (operation and sizing) stochastic problem into a finite number of possible realizations (scenarios) to solve with MILP methods.

In this work, the two-stage stochastic optimization problem is solved without approximations in finite scenarios by implementing a novel two-layer optimization and a further method to validate the best solution over all scenarios.

Figure 6.3 shows the two-layer optimization framework and the overall interrelations among the optimization methods, the analytical techno-economic model (ATE), and the machine learning models (MLTE). The lower level is a time-step optimization of cost-revenues while constrained electric and thermal energy flows are balanced. This convex not-linear problem is solved by the SLSQP (Sequential Least Squares Programming)

method. The upper level of simultaneous design, sizing and siting optimizations are solved with two novel evolutionary computing algorithms (ADE, AIE). Due to the stochastic nature of this problem, clusters of probabilistic best solutions (PBS) of similar quality are obtained. To find the best configuration, the optimization must be repeated until the standard deviation of the PBS reaches the desired fitness value. Then, the PBS having the lowest fitness value can be assumed as the candidate of being the PBS. The final task is to verify with the sample average approximation method if the latter solution returns the best-expected performance over all the scenarios. The results shows that AIE performs over 70% better than the original version of Differential Evolution (DE) introduced by Storn at al. in 1995 and it is well suited to compute complex CHP-MMG optimizations and obtain high quality of solutions validated over all the scenarios.

6.2.3 Simultaneous optimization with the hybrid model approach

In this work, a hybrid model approach based on the combination of an analytical technical-economic model with different machine learning models is proposed to further speed up the computing time. ATE model incorporates the techno-economic models of a large variety of thermal and electrical DER used in 1) the objective function of the SLSQP algorithm, 2) the energy balance equations, 3) the financial models that at the end, return the fitness value of the MG trial settings.

Three algorithms have been developed and tested to approximate the ATE model with machine learning (MLTE). The first MLTE model is based on a multiple linear regression (MLR), fitting a linear model with coefficients to minimize the residual sum of squares between the observed targets in the dataset (DER sizes and geolocations), and the targets predicted (fitness values) by the linear approximation. A second algorithm uses a 1-layer neural network (NN), whose input and output neurons, connected by weighed synapses. A third algorithm is a deep neural network (DNN) where the NN is expanded into 3 dynamic layers.

The stochastic behaviour of CHP-MMG permits MLTE to correlate solutions and fitness values similarly to ATE model, for fitness values nearby zero. MLTE can be used in combination with ATE-based optimization to tighten the search area of the best CHP-MMG siting and sizing.

6.2.4 Validation in innovative case studies

As a further result, the two-layer algorithms were used in this work to simulate innovative business scenarios for residential communities where the CHP-MMG fulfill electrical and thermal loads and provides energy services to the utility grid.

Synergies established by electric and thermal DER installed in stand-alone CHP-MG are investigated. The latter configurations are compared with interconnected CHP-MG; crossflows of energies among interconnected MG are investigated.

Moreover, it has been particularly useful to investigate how prices' policies of energy services and the cost, type of hydrogen impacts the competitiveness of CHP-MMG in different geographical sites, both in on-grid and off-grid contests.

6.2.5 The swarm effect

The results of simulations carried on in this thesis have highlighted a scheme of collaboration between CHP-MMG which has been called: *swarm effect*. With this term is intended optimal conversions and exchanges of thermal, electrical, chemical energies among MG that improve their efficiency, energy resilience to uncertainty, and best financial performances.

Figure 6.4 shows an example of the swarm effect between two CHP-MMG operating in islanded mode. The optimal setting has been obtained in 1 query, 150 generations with AIE running in high-resolution mode. The CHP-MMG configuration comprises in MG_A as primary power generation WT.

The exceeding electric energy not consumed by the load and not stored in ESS is transferred from MG_A to MG_B (i.e., ITCEL).

The latter is added to the electricity produced by WT. This electric energy is used to supply the electric load and to convert it in heat with HP. Finally, the exceeding thermal energy not consumed by the load is transferred back from MG_B to MG_A.

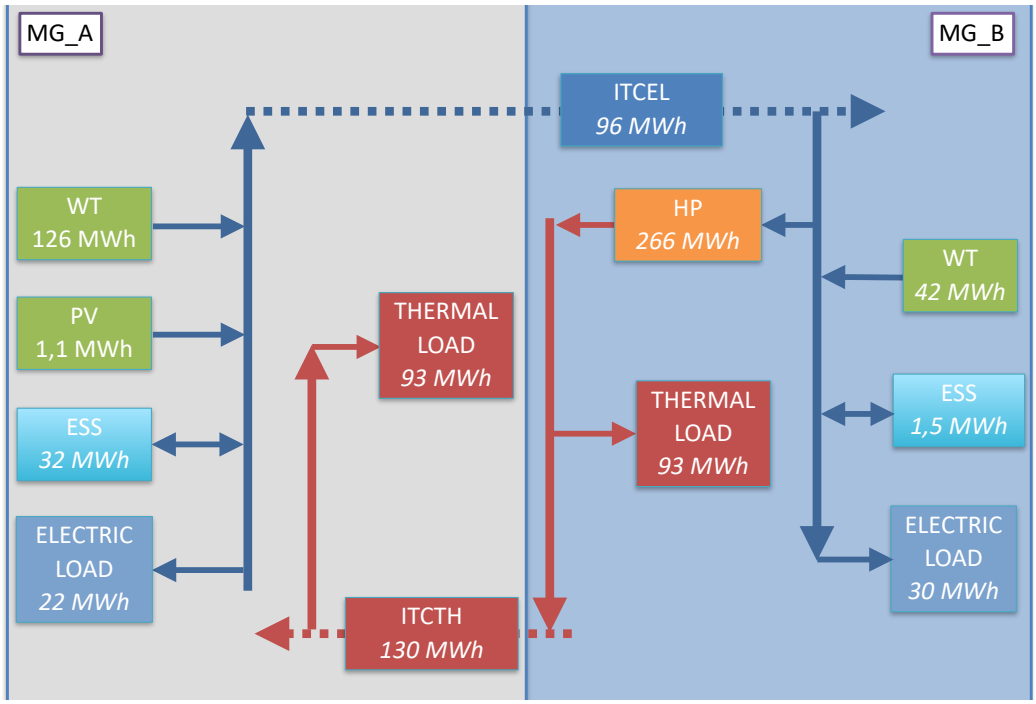

Figure 6.4 *Example of swarm effect between two CHP-MMG operating in islanded mode*

6.3 Future research directions

The results of this thesis indicate three further research topics for a better understanding of CHP-MMG role in future energy systems.

The first concerns the impact of solar radiation, temperature changes on energy yields of renewables systems under different greenhouse gas emissions scenario (e.g., RPC 4.5 and 8.5). The Representative Concentration Pathways (RCP) form a set of greenhouse gas concentration and emissions pathways designed to support research on impacts and potential policy responses to climate change. The RCP - RCP2.6, RCP4.5, RCP6, and RCP8.5 – are labelled after a possible range of radiative forcing values in the year 2100 (2.6, 4.5, 6.0, and 8.5 W/m^2, respectively). RPC 2.6 is associated to the most stringent mitigation scenario while RCP 4.5 is an intermediate scenario, where emissions peak around 2040, then decline. The RCP8.5 combines assumptions about high population and relatively slow income growth with modest rates of technological change and energy intensity improvements, leading in the long term to high energy demand and GHG emissions in absence of climate change policies. Compared to the total set of Representative Concentration Pathways, RCP8.5 thus corresponds to the pathway with the highest greenhouse gas emissions [8].

The solar radiation incident on the Earth's surface in this thesis is based on historical datasets. However, with changes in climate and air pollution levels, solar resources may no longer be stable over time and undergo substantial decadal changes. Observational records covering the past decades confirm long-term changes in this quantity. Wild et al. [9] examine how the latest generation of climate models used for the 5th IPCC report projects potential changes in surface solar radiation over the coming decades, and how this may affect, in combination with the expected greenhouse warming, solar power output from photovoltaic (PV) systems. J. Wu et al. [10] provide a scientific basis for the policies for the development of wind energy and towards the goal of carbon neutrality in China and local governments, changes in wind energy potential over China using the RCP2.6, RCP4.5 and RCP8.5 emission scenarios. The results of this work indicate that the implementation of newly developed wind power technology should consider the impact of changes in wind energy in different sub-regions.

However, the state of the art does not include any study addressing the impact of RPC scenarios in microgrids' techno-economic optimizations.

A second future area of investigation concerns the extension of number of microgrids. The idea is to study multiple interconnected residential- and industrial microgrids installed nearby. Further work should be focus on research on optimal configurations of a wide network of interconnected hybrid microgrids to achieve a higher quality of energy, financial performance, and lower cost of energy than an actual vertical electrical grid (utility grids) and stand/alone thermal systems. In such new energy framework, multiple industrial production and residential users of districts will act as virtual power plants. The improved optimization tool will permit to evaluate scenarios where each microgrid energy provider can decide dynamic pricing policies in response to the power demand of neighbors to maximize its rewards. A sort of peer-to-peer game to be settled at each time-step according to potential synergy schemes to dynamically establish the Nash Equilibrium [11] between the energy supplier and the users of each microgrid. Shunping et al. in 2021 [12] proposed a structure of a microgrid based on multi-agent system. A game-theory-based optimization model is proposed for the capacity configuration of these agents. The economic interests between the agents and their actions are analyzed by the game model. The Nash Equilibrium of the game is worked out by particle swarm optimization, as the reference for the configuration of the agents. Aihua et al. in 2021 [13] proposed a two-stage optimization approach on the optimal strategies to maximize the peer-to-peer (P2P) energy sharing trading of the prosumer within a community. In the first-stage optimization model, the decision on whether to participate in the P2P energy sharing trading is obtained based on the maximization of social utility function. The second-stage optimization problem is based on a payment bargaining model. They demonstrate that the customers who participate in P2P energy sharing trading can improve their utilities compared with an individual optimization method based on a case study. Zhenhao et al. [14] presented a novel day-ahead power market for distribution systems. Based on the linearized AC power flow model, the distribution locational marginal price for coupled active and reactive power is calculated and decomposed into different components (e.g., energy price, loss price, congestion price, and voltage support price) which can provide price signals for distributed generator and aggregator in a distribution system to respond. The nodes of the smart grid can trade with each other and optimize their profit based on distribution locational marginal prices. Game theory is applied to solve the energy trading payment problem. The latter recent research works inspire the adoption of the multi-agent

approach for setting the optimal trading policies among multiple nearby heat and power microgrids.

Moreover, a third innovative area of investigation concerns the fault-tolerant design optimization of microgrids to power manned lunar bases. Future steps in human space exploration foresee the deployment of a permanently manned moon base, an endeavor that is fully dependent on lightweight, efficient, scalable, resilient heat- and power systems. There are only a few publications in literature that are focused on microgrids in space environments. The current state-of-the-art of power systems architectures follows centralized schemes with redundancies. Such approaches, however, lead to increased budget and pre-set fault tolerance. Furthermore, power systems are not designed in a scalable manner. Thus, these established practices may not be sufficient for future exploration missions, which may demand gradual module-wise deployment. A. Bintoudi et al. in 2019 [15] proposed a meshed grid topology to satisfy the high reliability requirements of a manned space mission and, at the same time, to reduce the mass/ volume budget of the mission.

A series of microgrid-related technologies are suggested, covering all levels of grid design, control and protection; however, this works limits the DER to PV and ES sizing. In the proposed future work, terrestrial dataset for solar radiation should be replaced with moon surface radiation data. The available solar energy is a key information to allow the search of the ideal base location for future explorations and missions in the moon soil. Moreover, the techno-economic analysis could be extended to hydrogen microgrids' configurations in which hydrogen is delivered from the earth and generated on-site. The search of optimal moon siting should compare the availability of crude fuel (i.e., ice, hydrogen) [16][17][18] and the related cost to convert hydrogen with the option to transport a fuel from the earth. Additionally, the novel concept of heat and power multiple-microgrid applied to the moon contest [19][20][21]22] could be investigated under the scope of maximizing the energy reliability with specific irradiance of different base siting.

6.4 References

[1] A. K. V, A. Verma, and R. Talwar, “Optimal techno-economic sizing of a multi-generation microgrid system with reduced dependency on grid for critical health-care, educational and industrial facilities,” Energy, vol. 208, 2020, doi: 10.1016/j.energy.2020.118248.

[2] A. K. V. and A. Verma, “Optimal techno-economic sizing of a solar-biomass-battery hybrid system for off-setting dependency on diesel generators for microgrid facilities,” Journal of Energy Storage, vol. 36, 2021, doi: 10.1016/j.est.2021.102251.

[3] E. A. Martínez Ceseña, N. Good, A. L. A. Syrri, and P. Mancarella, “Techno-economic and business case assessment of multi-energy microgrids with co-optimization of energy, reserve and reliability services,” Applied Energy, vol. 210, 2018, doi: 10.1016/j.apenergy.2017.08.131

[4] B. Li, R. Roche, and A. Miraoui, “Microgrid sizing with combined evolutionary algorithm and MILP unit commitment,” Applied Energy, vol. 188, pp. 547–562, Feb. 2017, doi: 10.1016/j.apenergy.2016.12.

[5] M.A. Hannan, M. Faisal, Pin Jern-Ker, R.A. Begum, Z.Y. Dong, C. Zhang, 2020, Review of optimal methods and algorithms for sizing energy storage systems to achieve decarbonization in microgrid applications,Renewable and Sustainable Energy Reviews, Volume 131, 110022, ISSN 1364-0321, https://doi.org/10.1016/j.rser.2020.110022

[6] Minjian Cao, Qingshan Xu, Jilin Cai, Bin Yang,2019,Optimal sizing strategy for energy storage system considering correlated forecast uncertainties of dispatchable resources, International Journal of Electrical Power & Energy Systems, Volume 108, Pages 336-346, ISSN 0142-0615, https://doi.org/10.1016/j.ijepes.2019.01.019

[7] Di Wu, Xu Ma, Sen Huang, Tao Fu, Patrick Balducci, 2020, Stochastic optimal sizing of distributed energy resources for a cost-effective and resilient Microgrid, Energy, Volume 198, 117284, ISSN 0360-5442, https://doi.org/10.1016/j.energy.2020.117284

[8] Riahi, K., Rao, S., Krey, V., Cho, C., Chirkov, V., Fischer, G., Kindermann, G., Nakicenovic, N., Rafaj, P. (2011), RCP 8.5-A scenario of comparatively high greenhouse gas emissions. Climatic Change, 109(1). https://doi.org/10.1007/s10584-011-0149-y.

[9] Wild, M., Folini, D., Henschel, F., Fischer, N., Müller, B., Projections of long-term changes in solar radiation based on CMIP5 climate models and their influence on energy yields of photovoltaic systems, 2015, Solar Energy, Vol.116, pp. 12-24.

[10] Jia Wu, Zhen-Yu Han, Yu-Ping Yan, Chao-Yang Sun, Ying Xu, Ying Shi, Future changes in wind energy potential over China using RegCM4 under RCP emission scenarios, Advances in Climate Change Research, 2021, https://doi.org/10.1016/j.accre.2021.06.005.

[11] Charles A. Holt, Alvin E. Roth, The Nash equilibrium: A perspective, Proceedings of the National Academy of Sciences Mar 2004, 101 (12) 3999-4002; DOI: 10.1073/pnas.0308738101

[12] Shunping Jin, Shoupeng Wang, Fang Fang, Game theoretical analysis on capacity configuration for microgrid based on multi-agent system, International Journal of Electrical Power & Energy Systems, Volume 125, 2021, 106485, ISSN 0142-0615, https://doi.org/10.1016/j.ijepes.2020.106485

[13] Aihua Jiang, Huihong Yuan, Delong Li, A two-stage optimization approach on the decisions for prosumers and consumers within a community in the Peer-to-peer energy sharing trading, International Journal of Electrical, Power & Energy Systems, Volume 125, 2021, 106527, ISSN 0142-0615, https://doi.org/10.1016/j.ijepes.2020.106527

[14] Zhenhao Li, Chun Sing Lai, Xu Xu, Zhuoli Zhao, Loi Lei Lai, Electricity trading based on distribution locational marginal price, International Journal of Electrical Power & Energy Systems,Volume 124,2021, 106322,ISSN 0142-0615, https://doi.org/10.1016/j.ijepes.2020.106322

[15] Angelina D. Bintoudi, Christos Timplalexis, Goncalo Mendes, Josep M Guerrero, Charis Demoulias, 2019, Design of Space Microgrid for Manned Lunar Base: Spinning-in Terrestrial Technologies, European Space Power Conference (ESPC) Juan-les-Pins, France 2019 Sept. 30 - 2019 Oct. 4

[16] Ariel N. Deutsch, James W. Head, Gregory A. Neumann, Analyzing the ages of south polar craters on the Moon: Implications for the sources and evolution of surface water ice., Icarus, Volume 336, 2020, 113455, ISSN 0019-1035,https://doi.org/10.1016/j.icarus.2019.113455.

[17] Feldman, W. C., Lawrence, D. J., Elphic, R. C., Barraclough, B. L., Maurice, S., Genetay, I., and Binder, A. B. (2000), Polar hydrogen deposits on the Moon, J. Geophys. Res., 105(E2), 4175– 4195, doi:10.1029/1999JE001129.

[18] V.R. Eke, L.F.A. Teodoro, R.C. Elphic, The spatial distribution of polar hydrogen deposits on the Moon, Icarus, Volume 200, Issue 1, 2009, Pages 12-18, ISSN 0019-1035, https://doi.org/10.1016/j.icarus.2008.10.013.

[19] D. Tan, D. Baxter, S. Foroozan and S. Crane, "A First Resilient DC Dominated Microgrid for Mission-Critical Space Applications", IEEE J. Emerg. Sel. Top. Power Electron., vol. 4, no. 4, pp. 1147-1157, Dec. 2016.

[20] M. D'Antonio, C. Shi, B. Wu and A. Khaligh, "Design and optimization of a solar power conversion system for space applications", 2018 IEEE Ind. Appl. Soc. Annu. Meet. IAS 2018, no. c, pp. 1, 2018.

[21] Z. Khan, A. Vranis, A. Zavoico, S. Freid and B. Manners, "Power system concepts for the lunar outpost: A review of the power generation energy storage Power Management and Distribution (PMAD) system requirements and potential technologies for development of the lunar outpost", AIP Conference Proceedings, 2006.

[22] A. M. McNelis et al., "Simulation and Control Lab Development for Power and Energy Management for NASA Manned Deep Space Missions", 12th International Energy Conversion Engineering Conference, 2014.

APPENDIX A

Gene	Minimum	Maximum	Gene	Minimum	Maximum
Latitude	53	53	PV_SIZEB	0	200
Longitude	66	66	WT_SIZEB	0	150
PV_SIZE	0	200	FC_SIZEB	0	100
WT_SIZE	0	150	OG_SIZEB	0	100
FC_SIZE	0	100	ESS_SIZEB	0	100
TKFC_SIZE	0	30.000	TKFC_SIZEB	0	30.000
TKCHP_SIZE	0	30.000	TKOG_SIZEB	0	20.000
EC_SIZE	0	100	EC_SIZEB	0	100
OG_SIZE	0	100	EBOY_SIZEB	0	300
TKOG_SIZE	0	20.000	TKEBOY_SIZEB	0	30.000
ESS_SIZE	0	100	ST_SIZEB	0	300
GRID_SIZE	0	100	TKST_SIZEB	0	30.000
EBOY_SIZE	0	300	STHP_SIZEB	0	300
TKEBOY_SIZE	0	30.000	HP_SIZEB	0	300
ST_SIZE	0	300	TKHP_SIZEB	0	30.000
TKST_SIZE	0	30.000	GRID_SIZEB	0	100
STHP_SIZE	0	30.000	TKCHP_SIZEB	0	30.000
HP_SIZE	0	300	ITCEL_SIZE	0	100
TKHP_SIZE	0	30.000	ITCTH_SIZE	0	300

Table A.1 *Boundaries of the genotype. The term 'SIZE' and 'SIZEB' refers to nominal power (kW) of PV, WT, FC, OG, EC, GRID, EBOY, ST, STHP, HP and capacity of ESS (kWh), TKFC (l), TKCHP (l), TKOG (l), TKEBOY, (l), TKST,(l), TKHP(l), respectively of MG_A, MG_B*

Genotype		Nr. Genes
Chromosome siting	*Latitude*	*1*
	Longitude	*2*
Chromosome sizing	PV SIZE	1
	WT SIZE	2
	FC SIZE	3
	TKFC SIZE	4
	TKCHP SIZE	5
	EC SIZE	6
	OG SIZE	7
	TKOG SIZE	8
	ESS SIZE	9
	GRID SIZE	10
	EBOY SIZE	11
	TKEBOY SIZE	12
	ST SIZE	13
	TKST SIZE	14
	STHP SIZE	15
	HP SIZE	16
	TKHP SIZE	17
	PV SIZEB	18
	WT SIZEB	19
	FC SIZEB	20
	OG SIZEB	21
	ESS SIZEB	22
	TKFC SIZEB	23
	TKOG SIZEB	24
	EC SIZEB	25
	EBOY SIZEB	26
	TKEBOY SIZEB	27
	ST SIZEB	28
	TKST SIZEB	29
	STHP SIZEB	30
	HP SIZEB	31
	TKHP SIZEB	32
	GRID SIZEB	33
	TKCHP SIZEB	34
	ITCEL SIZE	35
	ITCTH SIZE	36

Table A.2 *Composition of the genotype of the CHP-MMG. The 38 genes (variables of the problem) are associated to the chromosome of siting (2 genes) and the chromosome of sizing (36 genes)*

APPENDIX B

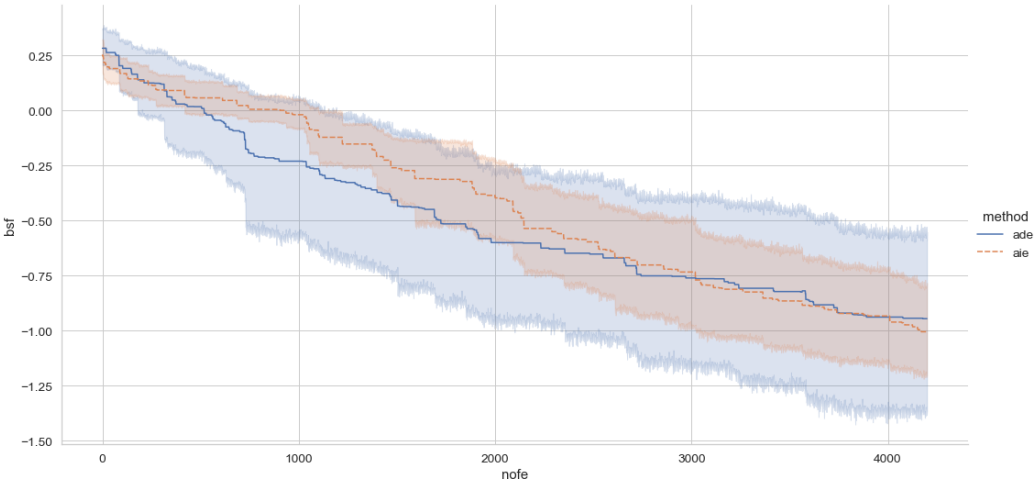

Figure B.1 *Comparison of the fitness spread, 350 generation, AIE and ADE with objective function based on ATE*

APPENDIX C

Within the FCH-JU European Project “Pembeyond” in 2014 [1] a primitive version of a SW tool was developed. The simulator was designed to execute technical-economic analysis of micro-electrical networks, powering telecom towers. The original version of the algorithm was set up in Microsoft Excel. The tool can be used to execute market analysis in different areas of the world for potential installations of PEMFC integrated with low-grade bioethanol processor units.

The algorithm was ported into python language [2] to extend the study from simulation to optimization of the most general problem concerning best design, siting, sizing of heat and power multi-microgrids.

The current algorithm includes now more than 25.000 lines of code. The main script is structured into separated and interrelated functions and libraries [3][4][5] embedding: the numerical models of DER, financial models, SLSQP objective, constraints (Chapter 2) the equations of ATE, AIE, DE (Chapter 4, 5).

The main script is also interrelated to a set of libraries, created to compute the MLR, NN, DNN, processing training datasets (Chapter 3) and finally to plot [6] and save the results.

Due to the large numbers of inputs for each DER, selection criteria for optimization, data-processing inputs and output, a Graphical User Interface (GUI) based on Python's de-facto standard package, Tkinter [7][8] it has been developed. In the upper part of Figure C.1 the popup’s pages (i.e., tabs) of the inputs are shown.

The first pages are used to input the information about the siting search, discount rate and modalities to manage the execution of the script (e.g., print/plot in real-time the trial solutions, best-so-far fitness, number of queries, replacement of random input variables with mean values).

The other pages concern the sizing bandwidth of the DER, the definition of their main features (i.e., characteristic curves, minimum of state of heaths, unit CAPEX, OPEX, REPEX, etc..).

The following DER are considered to configure two interconnected microgrids (MG_A, MG_B): electrical and thermal devices for microgrids’ interconnections, photovoltaic panels, wind turbines, electrical storage systems, inverters, fuel cells with

thermal and fuel tanks, electrolyzer, traditional gensets with fuel tanks, devices for main grids' interconnections, electric boilers with thermal storage, thermal solar collectors, combined with heat pumps and thermal storage, stand-alone heat pumps with thermal storage.

Two tabs are dedicated to sizing and the management of thermal and electric loads, grid demand profiles (e.g., load shedding, load shifting, peak shaving, period of peak loads), price policies (e.g., unit price energy of electric and thermal loads, remunerations and penalties for grid demand response, unit price for water generated by FC, unit price for carbon black produced by methane (TP).

The screenshot of Figure C.1 shows the page to setup the parameters concerning the optimization simulation: 1) SLSQP's objectives of each time-step (e.g., to maximize profit of energy generated, maximize states of health, maximize the buy or sell of energy from the main grid, maximize the energy generated by RES, FC, OG, EC, EBOY, ST, STHP, HP, maximize the efficiency of energy generated by FC, OG, EC); 2) minimum number of generation/query; 3) selection of EA optimization's method (e.g., AIE, ADE, DE); 4) EA's objectives (e.g., to maximize IRR, NPV, LCOE and their combination); 5) additional criteria for selections and fitness's cut-off values; 6) choice of the techno-economic model (e.g., analytical model, machine learning models) and type of data

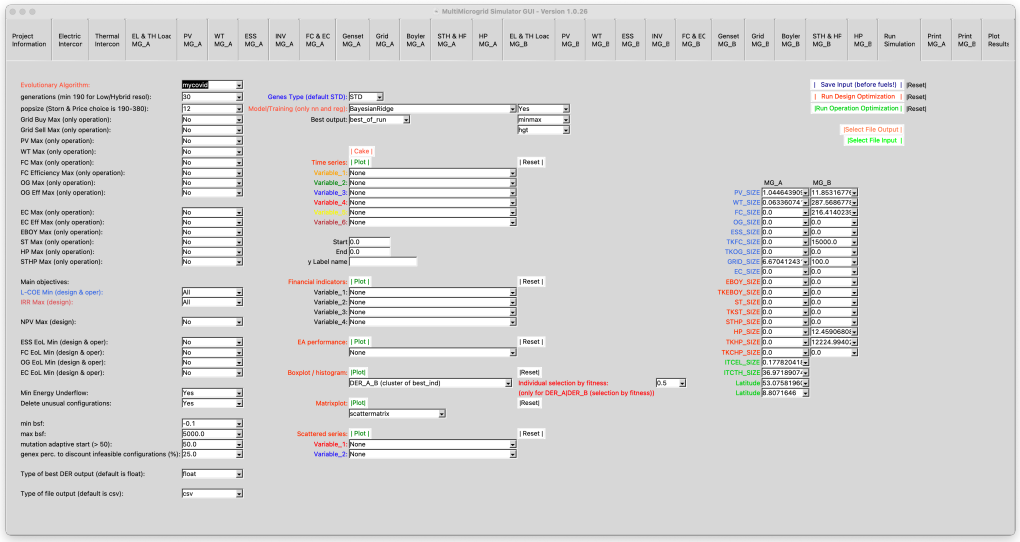

Figure C.1 *GUI of the optimization-simulation tools*

transformations; 7) plot the outputs (e.g., time-series, financial performances, key optimization's performance indicators); 8) launch the optimization 9) run the simulation of selected configurations.

The output/inputs are uploaded in a sole dataset and then saved in csv-format file which is marked with a serial number to univocally identify the run and query.

Despite the large number of configurable parameters and options, inputs' setting is defined in a way to prevent errors and override undesired conditions (e.g., if boundaries of DER are null, all the other correspondent parameters will be ignored and trial solutions associated to locations with vegetation or sea will be discarded).

Moreover, the tailored-made software based on the high-level programming language Python®, is intuitive to read and the vast open-source library support allows to write quickly further algorithms to enhance the features the comprehensions of the results.

C.1 References

[1] FCH-JU Project: PEMFC system and low-grade bioethanol processor unit development for back-up and off-grid power applications", European Union's Seventh Framework Programme, Grant Agreement no 621218: http://pembeyond.eu. May 2014.

[2] G. van Rossum, Python tutorial, Technical Report CS-R9526, Centrum voor Wiskunde en Informatica (CWI), Amsterdam, May 1995

[3] Harris, C.R., Millman, K.J., van der Walt, S.J. et al. Array programming with NumPy. Nature 585, 357–362 (2020). DOI: 0.1038/s41586-020-2649-2

[4] McKinney, W. & others, 2010. Data structures for statistical computing in python. In Proceedings of the 9th Python in Science Conference. pp. 51–56

[5] Pauli Virtanen, Ralf Gommers, Travis E. Oliphant, Matt Haberland, Tyler Reddy, David Cournapeau, Evgeni Burovski, Pearu Peterson, Warren Weckesser, Jonathan Bright, Stéfan J. van der Walt, Matthew Brett, Joshua Wilson, K. Jarrod Millman, Nikolay Mayorov, Andrew R. J. Nelson, Eric Jones, Robert Kern, Eric Larson, CJ Carey, İlhan Polat, Yu Feng, Eric W. Moore, Jake VanderPlas, Denis Laxalde, Josef Perktold, Robert Cimrman, Ian Henriksen, E.A. Quintero, Charles R Harris, Anne M. Archibald, Antônio H. Ribeiro, Fabian Pedregosa, Paul van Mulbregt, and SciPy 1.0 Contributors. (2020) SciPy 1.0: Fundamental Algorithms for Scientific Computing in Python. Nature Methods, 17(3), 261-272

[6] J. D. Hunter, "Matplotlib: A 2D Graphics Environment", Computing in Science & Engineering, vol. 9, no. 3, pp. 90-95, 2007

[7] Lundh, F., 1999. An introduction to Tkinter. URL: www. pythonware. com/library/ tkinter/introduction/index. htm.

[8] John W. Shipman, 2013, Tkinter 8.5 reference: a GUI for Python, https://reu.cct.lsu.edu/documents/Python_Course/tkinter.pdf

APPENDIX D

Tool	Simulation	Scenario	Equilibrium	Top-down	Bottom-up	Operation	Investment
AEOLIUS	Yes	–	–	–	Yes	–	–
BCHP	Yes	–	–	–	Yes	Yes	–
COMPOSE	–	–	–	–	Yes	Yes	Yes
E4cast	–	Yes	Yes	–	Yes	–	Yes
EMCAS	Yes	Yes	–	–	Yes	–	Yes
EMINENT	–	Yes	–	–	Yes	–	–
EnergyPLAN	Yes	Yes	–	–	Yes	Yes	Yes
energyPRO	Yes	Yes	–	–	–	Yes	Yes
ENPEP	–	Yes	Yes	Yes	–	–	–
GTMax	Yes	–	–	–	–	Yes	–
H2RES	Yes	Yes	–	–	Yes	Yes	–
HOMER	Yes	–	–	–	Yes	Yes	Yes
HYDROGEMS	–	Yes	–	–	–	–	–
IKARUS	–	Yes	–	–	Yes	–	Yes
INFORSE	–	Yes	–	–	–	–	–
Invert	Yes	Yes	–	–	Yes	–	Yes
LEAP	Yes	Yes	–	Yes	Yes	–	–
MARKAL/TIMES	–	Yes	Yes	Partly	Yes	–	Yes
MESSAGE	–	Yes	Partial	–	Yes	Yes	Yes
MiniCAM	Yes	Yes	Partial	Yes	Yes	–	–
NEMS	–	Yes	Yes	–	–	–	–
ORCED	Yes	Yes	Yes	–	Yes	Yes	Yes
PERSEUS	–	Yes	Yes	–	Yes	–	Yes
PRIMES	–	–	Yes	–	–	–	–
ProdRisk	Yes	–	–	–	–	Yes	Yes
RAMSES	Yes	–	–	–	Yes	Yes	–
RETScreen	–	Yes	–	–	Yes	–	Yes
STREAM	Yes	–	–	–	–	–	–
TRNSYS16	Yes	Yes	–	–	Yes	Yes	Yes
UniSyD3.0	–	Yes	Yes	–	Yes	–	–
WASP	Yes	–	–	–	–	–	Yes

Table D.1 *Guideline of the main tools developed since 2009 by application*

Model	Sectors	Math modeltype	Georesolution
AnyMOD	User-dependent	Optimization	User-dependent
Backbone	All	Optimization	Depends on user
Balmorel	electricity, heating	Optimization	Zonal
Calliope	User-dependent	Optimization	User-dependent
CAPOW	Electric power	Simulation	Zonal
DESSTinEE	All / Electricity	Simulation	National
DIETER	electricity, heating	Optimization	Germany
ELMOD	electricity, heating	Optimization	power plant block, transmission network node
EMLab-Generation	Electricity, carbon	Simulation	Zones
EMMA	Electricity	Optimization	Some countries
Energy Policy Simulator	electricity, heating	Simulation	single region
Energy Transition Model	All	Simulation	Country
EnergyNumbers	Electricity	Simulation	Country
FlexiGIS	Electricity	Optimization, Simulation	building, street, district, city
Genesys	Electricity	Optimization, Simulation	EUMENA, 21 regions
Oemof	electricity, heating	Optimization, Simulation	Depends on user
OSeMOSYS	all	Optimization	Country
POMATO	Electricity, heating	Optimization	Nodal resolution
PowNet	Electricity	Optimization, Simulation	High-voltage substation
PyLESA	electricity, heating	Simulation	Local/Community/District
PyPSA	Electricity, heating	Optimization, Simulation	User dependent
Region4FLEX	electricity, heating	Optimization	Administrative districts
Renpass	Electricity	Optimization, Simulation	Germany
SciGRID	Electricity	Simulation	nodal resolution
StELMOD	Electricity	Optimization	Nodal resolution
Switch	electricity, gas	Optimization	Building to continent

Table D.2 *Main open source optimization and simulation tools in the Wiki Workspace of "Openmod initiative"*

APPENDIX E

The techno-economic analysis that involves wind turbines is subjected to the prediction of wind speed. A large number of studies published in scientific literature proposed the use of a variety of probability density functions to approximate the uncertainty and intermittency of wind speed profiles and their frequency distribution. Weibull distributions and Normal distribution has been considered in several studies(e.g., [1-2]).

In this thesis, these distributions have been proposed with the aim to convert the wind speed daily mean into hourly mean datasets.

The approach based on Weibull distribution is formulated in Chapter 2, Eq. 2.21.

The normal distribution used in the simulations of this thesis is indicated in Eq. E.1:

$$W_s(t_s,\theta,\phi) = \begin{cases} N\left[w\left(t_s,\theta,\phi\right),\sigma_s\left(\theta,\phi\right)\right] \\ W_s(t_s,\theta,\phi) \quad \geq \quad 0 \end{cases} . \qquad [E.1]$$

Where the wind speed daily mean of each month, here is defined as $w\left(t_s,\theta,\phi\right)$, and θ,ϕ are respectively the latitude and longitude and t_s is the time-step of the hourly mean.

The optimal values of the standard deviation $\sigma_s\left(\theta,\phi\right)$ in Eq. E.1 has been computed by minimizing the MSE error between the result of Eq. E.1 and the profile for each geographic location, can be derived from the NASA Surface meteorology and Solar Energy database (https://power.larc.nasa.gov).

It has been observed that the Weibull distribution usually replicates the original profile issued by NASA with a MSE error lower than the normal distribution. E.g., in the city of Bremen, with Latitude: 53.0758196 and Longitude: 8.8071646, the normal distribution returns a MSE error: 0,4% while for the Weibull distribution the MSE error is 0,01% .

However, due to the high unpredictability of the wind speed variable (as discussed in the author's publication [3]) the use of both distributions has been considered valid for the purpose of the overall techno-economic analysis. Techno-economic optimization's trials executed with the both Normal and Weibull distributions have not influenced the final results. The simulations presented in this thesis are based on approximating the wind speed with the Normal distribution.

E.1 References

[1] J.A. Carta, P. Ramírez, S. Velázquez,2009, A review of wind speed probability distributions used in wind energy analysis: Case studies in the Canary Islands, Renewable and Sustainable Energy Reviews, Volume 13, Issue 5, Pages 933-955, ISSN 1364-0321, https://doi.org/10.1016/j.rser.2008.05.005.

[2] Arrabal-Campos, F. M., Montoya, F. G., Alcayde, A., Baños, R., & Martínez-Lao, J.,2020. Estimation of Weibull parameters in winds speed mixture using nonlinear optimization for wind energy applications. Renewable Energy and Power Quality Journal, 18. https://doi.org/10.24084/repqj18.327

[3] Fracas, P., Zondervan, E., 2019, Fast Fourier Transforms for Microgrid Climate Computing. Proceedings of the 29th European Symposium on Computer Aided Process Engineering, Eindhoven, The Netherlands, Elsevier 10.1016/B978-0-12-818634-3.50277-0

Biography

Paolo Fracas is the founder and chief executive officer of Genport, a company with headquarter in Italy and a subsidiary in California making hybrid fuel cells. He achieved a M.Sc. degree in Electrical Engineering at University of Genoa in 1989, post-graduate specialization in International Management at Stoà School of Management (IT), MIT (MA), Brooking Institutions (Washington, D.C.) in 1992. PhD researcher at Twente University and Bremen University. He held management roles in research, engineering, marketing, sales and business development in high-tech multinational companies bringing advanced technologies and products to global markets. He served in advisory boards of international research consortium and associations. He is an expert consultant of the Europe Commission and European governments. He received international awards in European venture business competitions. He is the author of patents, publications.

Author's patents

Automatic Machine for photoengraving screen printing plates for screen printing high quality compact discs. (US7017480, CN1648770)

Device for controlled production of hydrogen characterized by high energy density, zero impact.(Patent IT0000271919; PCT/IB2010/055947; WO 2011/073958)

Electronic adjusting device for electric energy storing apparatus of the type provided with batteries.(IT102016000002586, EP2017/050454, US11,031,791, CN2017800062620)

Ergonomic wearable case to transport a PEMFC. (Patent IT0000272516)

Highly efficient hybrid power supply to manage PEMFC-Battery subsystems. (IT001398058)

Method for covering the surface of technical fabric fibers, in particular for screen printing. (ITMI20050813, EP1676713)

Method for making components for fuel cells and fuel cells made thereby. (PCT/IT2005/000297, MI2004A001035, EP1769554, JP2008500706)

Method for processing polymeric yarns and textile materials for modifying their surface resistivity. (IT2006745321, PCT/IT2006/000311)

Telecom Tower embedding hydrogen storage. (IT LC20130003)

Transportable Electricity Generation Unit and Method for Generating electricity using said unit no other fuels required. (IT0001394308; US8,896,262; PCT/EP2010/056998)

Author's publications

Carbone, A., Saccà, A., Pedicini, R., Gatto, I., Fracas, P., Passalacqua, E., Preparation of reinforced membranes based on sulphonated PEEK for high temperature fuel cell application, (2008) ACS National Meeting Book of Abstracts, 1 p.

Fracas P., Edwin Zondervan, 2019, Fast Fourier Transforms for Microgrid Climate Computing, Computer Aided Chemical Engineering, Elsevier, Volume 46, Pages 1657-1662, ISSN 1570-7946, ISBN 9780128186343, https://doi.org/10.1016/B978-0-12-818634-3.50277-0 (http://www.sciencedirect.com/science/article/pii/B9780128186343502770)

P. Fracas, E. Zondervan, M. Franke, K. V. Camarda, 2021, Nature-inspired two-layer optimizations for interconnected heat and power multi-microgrids, 9th Global Conference on Global Warming, http://www.gcgw.org/gcgw2021/.

Fracas, Paolo, Camarda, Kyle V. and Zondervan, Edwin, Shaping the future energy markets with hybrid multimicrogrids by sequential least squares programming, Physical Sciences Reviews, vol. , no. , 2021. https://doi.org/10.1515/psr-2020-0050

Fracas, P., Grassini, P., Dotelli, G., Stampino, P.G., Brivio, D., 2008, Electrical characterization of GDL materials for polymer fuel cells (PEMFQ), ECS Transactions, 12 (1), pp. 51-57.

Koski, P., Pulkkinen, V., Auvinen, S., Ihonen, J., Karimaki, H., Keranen, T., Ryden, A., Tingelof, T., Limonta, S., Croci, D., Fracas, P., Wichert, M., Kolb, G., Magalhaes, R., Relvas, F., Boaventura, M., Mendes, A., Development of reformed ethanol fuel cell system for backup and off-grid applications - System design and integration, (2016) INTELEC, International Telecommunications Energy Conference (Proceedings), 2016-November, art. no. 7749097

L. Omati; T. Barni; G. Dotelli; P. Gallo Stampino; D. Brivio; P. Fracas; P. Grassini, 2008, Modellazione agli elementi finiti di una cella a combustibile a membrana polimerica, Atti del 9° Convegno Nazionale Aimat, Piano di Sorrento, 29-giugno – 2 luglio 2008, pp. 517-520

Saccà, A., Pedicini, R., Carbone, A., Gatto, I., Fracas, P., Passalacqua, E., A preliminary investigation on reinforced double layer Nafion membranes for high temperature PEFCs application, (2014) Chemical Physics Letters, 591, pp. 149-155

Stampino, P.G., Dotelli, G., Omati, L., Fracas, P., Brivio, D., Grassini, P., Carbon-based textiles as gas diffusion layers (GDL) for polymer fuel cells (2008) CIMTEC 2008 - Proceedings of the 3rd International Conference on Smart Materials, Structures and Systems - Smart Textiles, 60, pp. 128-133.

Abbreviations

AC	Alternating Current
ADE	Self-Adaptive Differential Evolution
AIE	Self-Adaptive Artificial Immune Evolutionary Algorithm
ATE	Analytical Techno-Economic model
BFGS	Broyden–Fletcher–Goldfarb–Shanno
BSF	Best-So-Far
C^A	Convergence of Antibody
CAPEX	Capital Expenditure
CCS	Carbon Capture and Storage
CHP-MG	Combined Heat and Power Microgrid
CHP-MMG	Combined Heat and Power Multi-Microgrid
CNT	Carbon Nanotube
COP	Coefficient of Performance
CPU	Central Processing Unit
DC	Direct Current
DE	Differential Evolution
DER	Distributed Energy Resource
DER-CAM	Distributed Energy Resources Customer Adoption Model
DG	Distributed Generation
DNA	Deoxyribonucleic Acid
DNN	Deep Neural Network
D^R	Diversity of Repertoire
EA	Evolutionary Algorithm
EBOY	Electric Boiler
EC	Electrolyzer
ECM	Evolutionary Computation Method
ECMWF	European Centre for Medium-Range Weather Forecasts
ED	Energy Demand
EMS	Energy Management System
EOM	Energy and Operation Management

EP	Evolutionary Programming
ES	Energy Storage
ESS	Electric Energy Storage
EV	Electric Vehicles
EVS	Evolution Strategies
FA	Firefly Algorithm
FC	Fuel Cell
FCEV	Fuel Cell Electric Vehicle
FF	Fitness Function
FFT	Fast Fourier Transform
FIFO	First Input First Output
G2V	Grid-to-Vehicle
GA	Genetic Algorithm
GHG	Greenhouse Gas
GP	Genetic Programming
GPU	Graphic Process unit
GRID	Utility (main) grid
GSIM	Grid Series Interconnected Microgrids
GUI	Graphical User Interface
HGT	Horizontal Gene Transfer
HM	Hybrid Mode
HP	Heat Pump
HSDE	Hybrid Differential Evolution and Harmony Search
IFFT	Inverse Fast Fourier Transform
IG	Information Gain
INV	Inverter
IRR	Internal Rate of Return
ITCEL	Electric Interconnection between microgrids
ITCTH	Thermal Interconnection between microgrids
LCOE	Levelized Cost of Energy
LDR	Load Dissatisfaction Rate

LR	Linear Regressor
LSOE	Levelized Sale of Energy
MACO	Two-layer Ant Colony Optimization
MCL	Maximum Contaminant Level
MG	Microgrids
MGCC	Microgrid Control Center
MILP	Mixed Integer Linear Programming
MLR	Multiple Linear Regression
MLTE	Machine Learning Techno-Economic Model
MMG	Multi Microgrid
MOP	Multi Objective Optimization Problem
MOSEA	Multi-Objective Self-adaptive Evolutionary Algorithms
MPPT	Maximum Power Point Tracking
MSE	Means Square Error
NASA	National Aeronautics and Space Administration
NLP	Non Linear Programming
NN	Neural Network
NOFE	Number Of Fitness Evaluation
NPV	Net Present Value
OF	Objective Function
OG	Diesel Genset
OP	Optimization Problem
OPEX	Operating Expenditure
P2P	Peer-to-peer
PCC	Point of Common Coupling
PCM	Parallel Connected Microgrids
PEMEC	Proton Exchange Membrane Electrolyzer
PEMFC	Proton Exchange Membrane Fuel Cell
PEMFC - CHP	Combined Heat and Power Proton Exchange Fuel Cell
PSO	Particle Swarm Optimization
PV	Photovoltaic Panel
R2H2	renewable-to-hydrogen

REPEX	Replacement Cost
RES	Renewable energy systems
RNA	Ribonucleic Acid
RUL	Remaining Useful Life
SLSQP	Sequential Least Squares Programming
SMR	Steam Methane Reforming
SOC	State of Charge
SoH	State of Health
SSA	Sample Average Approximation
SSE	Sum Squared Error
SSER	Small-Scale Energy Resources
ST	Solar Thermal Collector
STHP	Solar Thermal Heat Pump
TCO	Total Cost of Ownership
TE	Techno-economic (model)
TES	Thermal Energy Storage
TP	Thermal Plasma
TS	Thermal Storage
V2G	Vehicle-to-Grid
VGT	Vertical Gene Transfer
WT	Wind Turbine